Parameter's Limitation at Electron Cooling Facilities

V.V. Parkhomchuk
Budker Institute for Nuclear Physics
630090 Novosibirsk, Russian Federation

1 Magnetization electron cooling

1.1 The Friction Force

For a case of absence of the magnetic field at a cooling section the cooling force can be written down as follows [1]:

$$F = -\frac{4\pi e^4 L_C n}{m} \int \frac{\vec{V} - \vec{V_e}}{|V - V_e|^3} f(V_e) d^3 V_e, \tag{1}$$

where $L_C = ln(\rho_{max}/\rho_{min})$ is the Coulomb logarithm of interactions, $\rho_{max} = min(V/\omega_p, \tau V, a)$, $\rho_{min} = e^2/mV^2$, τ is the time of a particle's single path through the electron beam, V is the particle velocity, V_e is the electron velocity, ω_p is the electron plasma frequency.

The presence of the magnetic field generally results in the appearance of three different regions of impact parameters [2].

Small impact parameters, where the presence of the magnetic field is not essential:

$$\rho_a = \frac{V_A}{\omega_L} > \rho > \rho_{min} = \frac{e^2}{mv_e^2}, \tag{2}$$

where $\vec{V_A} = \vec{V} - \vec{V_{\|e}}$. Intermediate impact parameters, where a multiple repeated passing of the electron by the particle is essential:

$$\frac{V_e}{\omega_L} = \rho_L > \rho > \frac{V_A}{\omega_L}. \tag{3}$$

Large impact parameters, where the particle interacts practically with the Larmor circle moving along the magnetic field:

$$\rho_{max} > \rho > \rho_L. \tag{4}$$

The contribution of these three regions to the friction force, for a longitudinally "flat" electron distributions $V_{\perp e} >> V_{\|e} = \sqrt{2e^2 n^{1/3}/m}$ can be written as follows.

The contribution of the fast cooling is

$$\vec{F} = -\frac{4\pi e^4 n}{m} \frac{\vec{V}}{\sqrt{V_{\perp e}^2 + \mid \vec{V} \mid^2}^3} ln(\frac{\rho_a}{\rho_{min}}). \tag{5}$$

In a multiply repeated collision region we can estimate the friction force:

$$\vec{F} = -\frac{4e^4 n}{m} \frac{\vec{V}}{V^2 V_{\perp e}} ln(V_{\perp e}/V). \tag{6}$$

And for large impact parameters, i.e. the case of strong magnetization, the friction force is equal to:

$$\vec{F} = -\frac{2\pi e^4 n}{m} \frac{\vec{V}}{\sqrt{V^2 + V_{\parallel e}^2}^3} ln(\rho_{max}/\rho_L). \tag{7}$$

For a small V the friction force has its maximum near $V = V_{\parallel e}$, and maximum force is:

$$F_{max} = 2e^2 n^{2/3}. \tag{8}$$

For practical use we can make unification of all this equations in the simplest form:

$$\vec{F} = -\frac{4e^4 n}{m} \frac{\vec{V}}{\sqrt{V^2 + V_{effe}^2}^3} ln(\frac{\rho_{max} + \rho_L}{\rho_{min} + \rho_L}), \tag{9}$$

where $V_{effe} = \sqrt{V_{\parallel e}^2 + \Delta V_{\perp e}^2}$, $\Delta V_{\perp e}$-transverse motion of electron caused by transverse magnetic and electric fields. In the case $\rho_{max} << \rho_L$ we have partial magnetization when:

$$Ln_c \approx \frac{\Delta V_{\perp e} \tau_{max} * \omega_L}{V_L} \tag{10}$$

and cooling decrement versus with V as $\lambda \approx 1/V^2$ as it was founded at NAP-M cooling experiments [3].

2 The Limitation of the Ion Beam Intensity

Some effects making limitations for obtaining high ion currents are observed at interaction of an ion beam with an electron cooling beam. These effects so called electron heating are observed at the CELSIUS facility [4], and limitations of the proton beam intensity at the electron cooling ring at the Indiana University [5].

The most fundamental limitations are connected with the process of cooling by itself [6]. The ion moving in the electron beam excites an electron flow disturbance, creating a friction force. As a result an electric field braking the ion appears in its area. In a case when the ion moves slowly and the electron beam temperature is high enough, dimensions of this area are determined by a Debaye shielding radius. In a very cold electron beam the area dimensions depend on velocity of the ion and its transit time in a cooling section. Fig.1 and Fig.2 show example electron distribution and friction fields after passing the ion at the electron beam way equal 10 ρ_{min}.

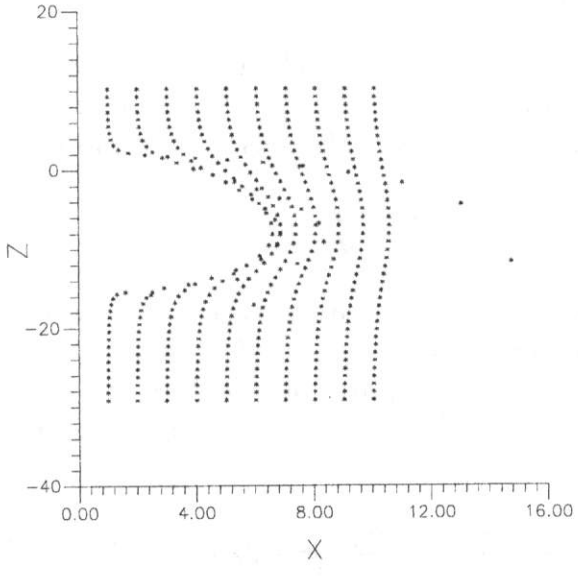

Figure 1: The distribution of electrons after interaction with an ion.

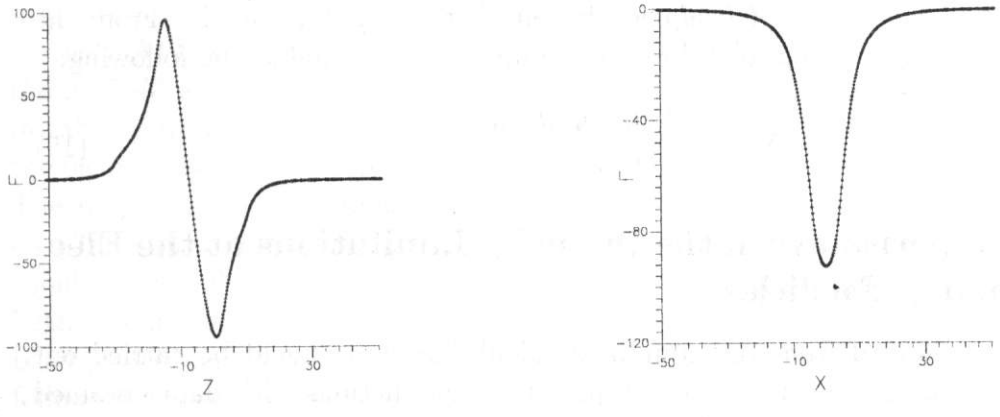

Figure 2: The friction force along and transverse an ion motion.

In a case of the intensive ion beam there are a lot of ions in the interaction area at the same time, and the electrical field E is determined by a total effect of all the ions:

$$E = -\frac{\lambda}{Ze} M \sum_{i}^{N_s} v_i, \tag{11}$$

where λ is a cooling decrement, Ze is an ion charge with a mass M and velocity v_i. N_s is a number of ions being in the interaction area. A transit time for each ion inside this area is determined by a velocity spread of the ions relative movements:

$$\tau = \frac{a}{\sqrt{< v^2 >}}, \tag{12}$$

where a is a radius of the mutual influence sphere, $\sqrt{< v^2 >}$ is a mean square spread of the ion velocities. Hereinafter we shall suppose that the relative movement of the ions is determined only by a longitudinal spread of velocities considering special features of movement in a storage ring magnetic system. Equations for the particular ion movement have the following form:

$$\frac{dp^2}{dt} = \frac{(p + ZeE * \tau)^2 - p^2}{\tau} = -2\lambda p^2 + N_s \lambda^2 \tau < p_i^2 > . \tag{13}$$

For this equation it is supposed that there are no correlations in the movement of particles $< v_i v_k >= 0$ for $i \neq k$. It is obvious that heating from adjacent ions prevent from damping with a decrement λ . A threshold number of ions, allowed in the interaction area, equals:

$$N_{sth} = \frac{2}{\lambda \tau}. \tag{14}$$

For the condition of stability the coherent decrement should be small in comparison with an inverse transit time in the interaction area (time of existing fluctuation). If we take a cross-section of the ion beam interaction area to estimate a dimension of the coherent area, the transit time is $\tau = a/\gamma/(\beta c \eta dp/p)$ (Hereinafter $\eta = pdf/(fdp)$!!). From the condition (14) $\lambda < 2/\tau$ the cooled ions threshold number is estimated as the following:

$$N_{th} < \frac{\gamma^7 \beta^4 a l_b R \eta dp/p}{2 n_e r_e r_i l^4}. \tag{15}$$

2.1 The Comparison with the Intensity Limitations at the Electron Cooling Facilities

This estimation is obtained from the simplified calculation and should be carried out more exactly. Nevertheless, let us try to compare these predictions with data obtained at the Indiana University cooling facility [5]. There was observed the proton current limitation of 6 mA at the following cooler parameters: 0.3 A electron current, 2.5 cm beam diameter, 45 MeV proton energy, 2.5 m cooling section length, size of the cooled beam a=0.1 cm, momentum spread $\Delta p/p = 0.510^{-4}$ $\eta = 0.86$ (Fig.3). From the formula (15) we obtain $N_{th} = 5.710^{10}$, this is in compliance with a current of 8.0 mA, presenting

the best agreement with the experiment (6 mA)! At the CELSIUS facility [4] high losses in a beam were observed at proton currents from 4 to 25 mA, this is in correspondence with coasting currents without RF 25-300 mA. It is obvious that this value is much higher than the limit and is attended with the beam heating, but not cooling. An experiment on the helium ions cooling was carried out at the CELSIUS facility in December 1992. High losses were observed at 60 mA electron current as long as the ion current dropped below 0.04 mA. After that the ion losses sharply stopped and the beam life time became very long. They observed an injection under which only 0.02 mA was injected in the ring as a result of an error in the injector, under this situation no losses at cooling were observed. Fig.4 (upper picture) shows a pickup signal when the current quickly decreases at 3mA injection, and one at 0.02mA injection when the signal slightly increases, this is connected with a decrease of the bunch length under cooling. Fig.4 (lower picture) clearly shows losses at repeated injections in the storage ring, and absolute absence of losses at a signal less than 41dB, this corresponds to 0.04 mA ion current. At the accelerating voltage switched off the beam extended over the whole orbit (coasting beam), and the threshold current increased to 0.52 mA, corresponding to a grouping factor about 13. When the electron current decreased to 30 mA, the ion current increased up to 1.6mA. As this took place the cross-section dimension of the ion beam was not measured because of absence of a profilometer, so it makes more difficult to compare with theoretical predictions. But it is possible to use a well-known fact that under electron cooling of an intensive ion beam the cross-section dimensions are limited by a Laslet displacement value of betatron tune 0.2-0.3:

$$\Delta\nu = \frac{Nr_i\beta_r R}{2a^2 l_b \beta^2\gamma^3}, \tag{16}$$

where β_r is an aperture function. So for the above-stated parameters of IUCF $\Delta\nu = 0.27$. Under, this the momentum spread value depends on interbeam scattering, and the balance sets in when longitudinal and transverse temperatures are equal in the beam reference system. As a result of these self-consistent calculations we obtain the following estimation for parameters of the cooled ion beam: at I_e=60mA a=0.09 $\Delta p/p = 0.510^{-4}$ and 0.52 mA threshold current, and at I_e=30mA a=0.12 $\Delta p/p = 0.710^{-4}$ and 2.0 mA threshold current. As it is seen, the estimations are in good agreement with the observations. At the NAP-M accumulator the maximal cooled current was 50 mkA and only allusions to instability were observed [3]. Under currents of about 50 mkA spontaneous flashes of the beam bunching accompanied by enlargement of transverse dimensions were observed. The beam cooling was going on at the proton energy of 65MeV and electron current of 0.3A after acceleration of the beam, and an accumulation mode was impossible. It should be noted that a small length of the cooler (1 m) is compensated by a very small beam momentum spread and unique small transverse dimension of the cooled proton beam a=0.01cm. A threshold momentum spread for NAP-M depends on the current and follows from the equation (14): $\Delta p/p = I(mkA) * 6.7610^{-8}$. It is seen that this instability possibly limited the beam momentum spread at NAP-M under high proton currents.

The Table 1 collected data from the different coolers.

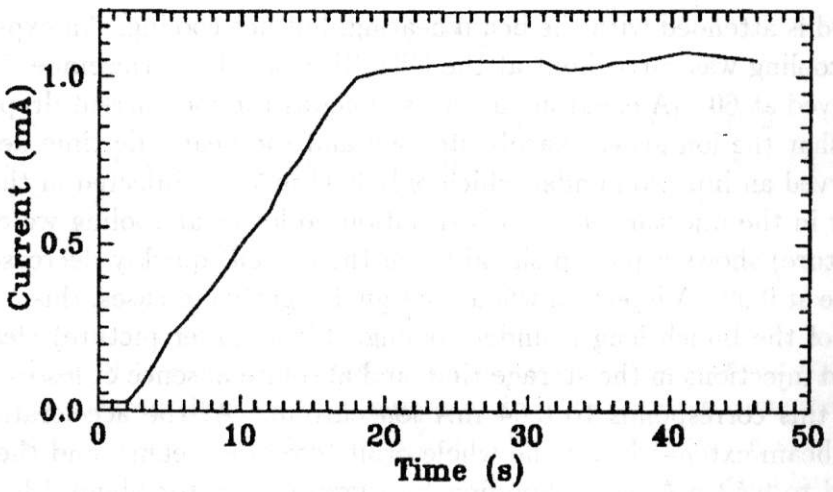

Figure 3: The injection beam at Indian cooler. Beam current as a function of time during continious stripping injection with cooling accumulation. $V_{rt} = 10V$.

Cooler ring	Indian	NAP-M	CELSIUS
Energy of electron beam (keV)	26	35	6
Electron beam current ()	300	300	60
Radius of electron beam (cm)	1.2	.5	1.2
Ion beam current (mA)	5	.05	1
Radius of ion beam for Ii=0mA(cm)	.07	.01	.1
Ion charge (Z)	1	1	2
Ion mass (A)	1	1	4
Maximal Laslet turn (dQmax)	.25	.15	.25
Beta function x (m)	13	13	13
df/f/(dp/p)	.7	.1	.8
Circumference (m)	84	50	84
Bunch length (m)	84	50	84
Length of cooling section (m)	2.5	1	2.5
Radius of ion beam (cm)	.14	.014	.2
Momentum spread dp/p	4.010^{-5}	$.510^{-5}$	5.010^{-5}
Threshold ion current (mA)	6.62	.094	1.54
Maximal cooling beam (mA)	6	0.06	0.52

Table 1: The data from the different coolers.

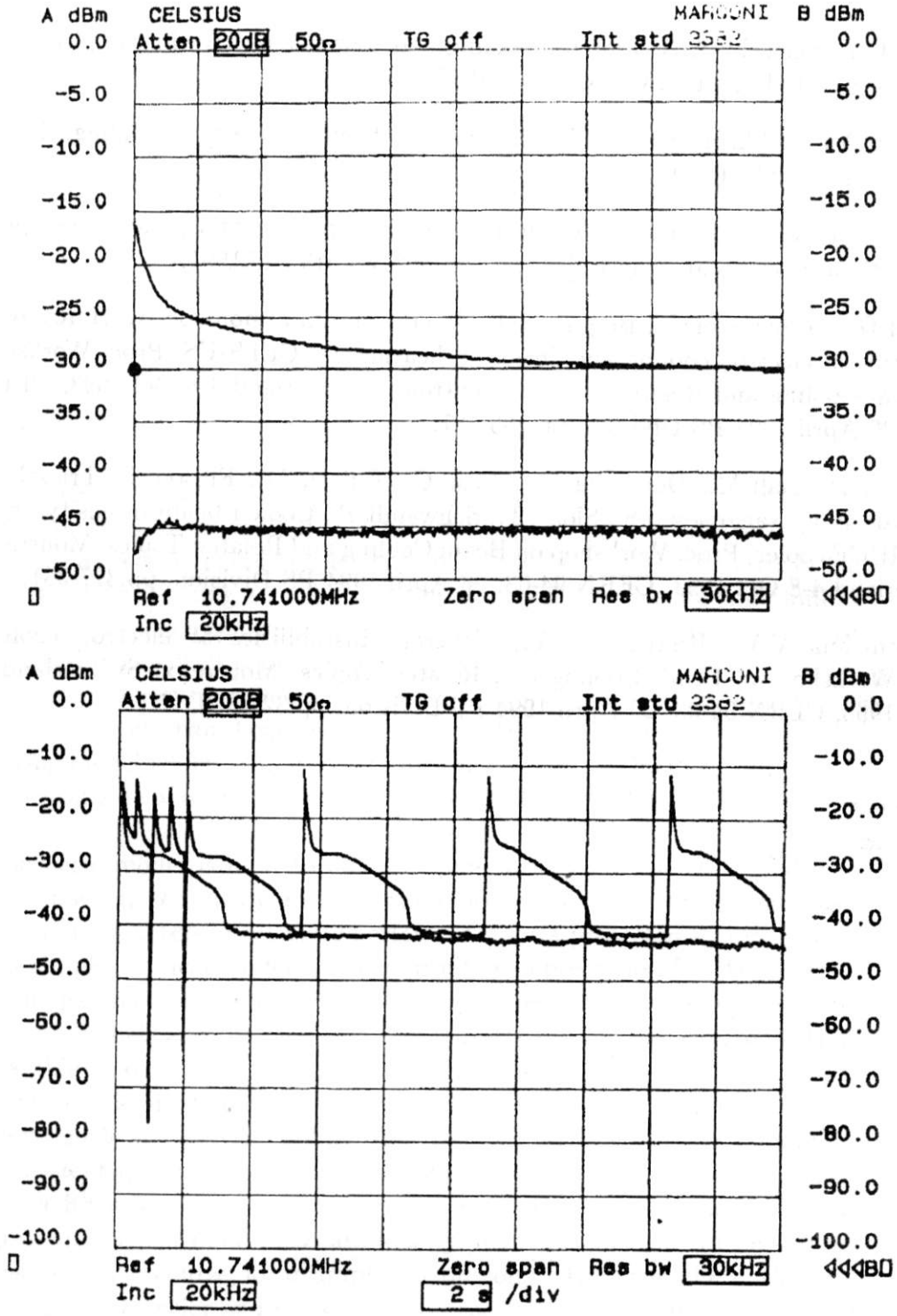

Figure 4: The result of injection helium ions at CELSIUS. Upper fig 1sec/div injection large current 3mA and very small current 0.02mA. And the lower fig. demonstrate multi-injection (time scale 2sec/div) when current losses just after injection and losses at process of cooling.

References

[1] Budker G.I., Skrinsky A.N. Electron cooling and new perspective in the physics of elementary particles, UFN, v.124, p.561, 1978.

[2] Derbenev Ya.S., Skrinsky A.N. Magnetization effects in electron cooling, Fizika Plasmy, v.4. pp.492-500, 1978.

[3] Parkhomchuk V.V., Skrinsky A.N. Electron cooling: physics and prospective application , Report on Progress in Phisics, v. 54, n. 7 pp.919-946,1991.

[4] Reistad D., Hermansson L., Bergmark T., Johansson O., Simonsson A., Burov A.V. Measuring of electron cooling and "electron heating" at CELSIUS, Proc. Workshop on Beam Cooling and Related Topics, Montreux, Switzerland 4-8 Oct.1993, CERN 94-03, 26 April 1994 PS Division, pp.183-187.

[5] Anderson D., Ball M., Derenchuk V., East G., Ellison M., Ellison T., Friesel D., Hamilton B.J., Nagaitsev S.S., Sloan T., Schwandt P., Cooled beam intensity limits in the IUCF cooler, Proc. Workshop on Beam Cooling and Related Topics, Montreux, Switzerland 4-8 Oct.1993, CERN 94-03, 26 April 1994 PS Division, pp.377-381.

[6] Parkhomchuk V.V., Pestrikov D.V., Coherent instabilities at electron cooling, Proc. Workshop on Beam Cooling and Related Topics, Montreux, Switzerland 4-8 Oct.1993, CERN 94-03, 26 April 1994 PS Division, pp.327-329.

Damping of Betatron Coherent Modes in Coasting Beams due to Non-hamiltonian Interactions Between Particles

D.V. Pestrikov
Budker Institute for Nuclear Physics
630090 Novosibirsk, Russian Federation

Abstract

In this paper we study the stability of the transverse coherent oscillations of a coasting beam using a simplified model, where the forces between particles are presented by sums of the cooling forces of the interacting particles. Within the framework of this model no unstable coherent modes are found.

1 Introduction

Recently, a model explaining the so-called electron heating of ion beams (see in Ref.[1]) was suggested in Ref.[2]. In this model, the interaction of the cooled particles through the electron cooling device could result in the beam heating, when the number of ions in the beam exceeds some critical value. The interactions of ions in Ref.[2] were described by the following non-hamiltonian forces

$$F_{z,a} = -\lambda \sum_{b=1}^{N_i} p_{z,b}, \quad a = 1 \ldots N_i. \tag{1}$$

Here, λ is the cooling decrement of a particle, N_i is the number of the interacting particles.

Previously, the model with the forces given in Eq.(1) was used to study the intensity limitation on the cooling rate in the so-called stochastic cooling systems, where the limitation occurred due to the instability of coherent oscillations of the cooled beam (see, for example, in Ref.[3]). In the case of stochastic cooling, the instability is caused by the delay between the measurement of the coherent signal of the beam and the correction of deviations, producing that signal, and by the necessity of too strong corrections.

In electron cooling devices ions are cooled due to their radiation of the plasma waves in the cooling electron beam. The measurement and the correction of the particle deviation occur here quasi-permanently. That results in the difference in the stability conditions for coherent oscillations of ion beams, interacting with the electron, or stochastic cooling devices.

In this note we show that for particles interacting through the forces, given in Eq.(1), a direct solution of the linearized Vlasov equation predicts no unstable betatron modes of a monochromatic coasting beam.

2 Dispersion Equations

In a coasting beam, the motion of a particle with the momentum $p = Mv$ is described using the following formulae

$$\begin{aligned} z &= a_z \cos\psi_z, \quad p_z = -M\omega_z a_z \sin\psi_z, \\ \dot{\psi}_z &= \omega_z = \omega_0\nu_z, \quad \theta = \omega_0 t + \phi, \quad \dot{\phi} = \alpha_p\omega_0\frac{\Delta p}{p}, \\ \Delta p &= p - p_0, \quad I_z = \frac{M\omega_z a_z^2}{2}. \end{aligned} \tag{2}$$

Here, I_z and ψ_z are the action-phase variables of unperturbed betatron oscillations, $\alpha_p = 1/\gamma^2 - 1/\gamma_{tr}^2$ is the slip factor of the ring, p_0 is the momentum of the particle moving along the reference orbit.

If $f = f(I_z, \psi_z, \Delta p, \theta, t)$ is the distribution function in ion beam, the force in Eq.(1) can be presented using the following expression

$$F_z = -\frac{\pi\lambda}{\theta_0} g(\theta) \int dI_z d\psi_z d\Delta p d\theta' g(\theta') p_z f(I_z, \psi_z, \Delta p, \theta', t), \tag{3}$$

where $g(\theta)$ is the function describing the correlations in the particle cooling. For the sake of simplicity we assume that g is a step function

$$g(\theta) = \begin{cases} 1, & |\theta| \le \theta_0 \\ 0, & |\theta| > \theta_0 \end{cases},$$

where $\theta_0 = l_c/(2\Pi)$, l_c is the correlation length. If we replace the smooth distribution function f by the beam microscopic density in the phase space

$$f \to \sum_{a=1}^{N} \delta(p_z - p_{az}(t))\delta(z - z_a(t))\delta(\Delta p - \Delta p_a)\delta(\theta - \theta_a(t)),$$

then Eq.(3) yields

$$F_z = -\frac{\pi\lambda}{\theta_0} g(\theta) \sum_{a=1}^{N} p_{az}(t) g(\theta_a(t)),$$

and therefore,

$$\dot{p}_{za} = -M\omega_z^2 z - \frac{\pi\lambda}{\theta_0} g(\theta_a(t)) \sum_{b=1}^{N} p_{bz}(t) g(\theta_b(t)).$$

If for all particles in the beam $|\theta_a - \theta_b| > 2\theta_0$, the averaging of the last equation over the rotation period results in

$$\dot{p}_{za} = -M\omega_z^2 z - \lambda p_{az}.$$

Hence, the constant λ in Eq.(3) coincides with the single particle cooling decrement.

If

$$Nf_0 = Nf_0(I_z, \Delta p), \quad \int dI_z d\psi_z d\Delta p d\theta' f_0 = 1$$

is the distribution function of the unperturbed beam, the vertical coherent oscillations of the beam are described by a small addend δf to f_0

$$f = f_0 + \delta f = Nf_0 + \sum_{m,n} f_{m,n}(I_z, \Delta p) e^{im\psi_z + in\theta - i\omega t}. \tag{4}$$

The amplitudes $f_{m,n}$ obey the linearized Vlasov equation

$$-i(\omega - \omega_{mn}) f_{mn} + N \left(\frac{\partial z}{\partial \psi_z} F_z \right)_{m,n} \frac{\partial f_0}{\partial I_z} = 0. \tag{5}$$

Here, N is the number of particles in the beam and $\omega_{mn} = m\omega_z + n\omega_0$. Now, we note that

$$\left(\frac{\partial z}{\partial \psi_z} \right)_m = \int_0^{2\pi} \frac{d\psi_z}{2\pi} \frac{\partial z}{\partial \psi_z} e^{-im\psi_z} = im \frac{a_z}{2}, \quad m = \pm 1$$

and hence

$$(F_z)_n = i \frac{M\omega_z \lambda g_n \pi}{\theta_0} \sum_n g_{-n} \int d\Delta p \int dI_z \frac{a_z}{2} [f_{1,n} - f_{-1,n}],$$

where

$$g_n = \int_0^{2\pi} \frac{d\theta}{2\pi} g(\theta) e^{-in\theta} = \frac{\sin(n\theta_0)}{\pi n}.$$

Substituting these expressions in Eq.(5), we find ($m = \pm 1$)

$$f_{m,n} = \frac{\pi a_z}{2\theta_0} \cdot \frac{Nm\partial f_0 / \partial I_z}{\omega - \omega_{mn}} (iM\omega_z \lambda g_n) \sum_n g_{-n} \int d\Delta p \int dI_z' \frac{a_z'}{2} [f_{1,n} - f_{-1,n}], \tag{6}$$

and

$$1 = \frac{i\pi N\lambda}{2\theta_0} \sum_n |g_n|^2 \int d\Delta p \int dI_z I_z \frac{\partial f_0}{\partial I_z} \left[\frac{1}{\omega - n\omega_0(\Delta p) - \omega_z} + \frac{1}{\omega - n\omega_0(\Delta p) + \omega_z} \right]. \tag{7}$$

In our calculations, we shall neglect the effects of the frequency spreads in the beam. Generally, this assumption results in the worst stability conditions. For such a monochromatic beam the dispersion equation Eq.(7) can be written in the following form

$$1 = \frac{-i\pi N\lambda}{2\theta_0\omega_0}\sum_n |g_n|^2\left[\frac{1}{x-n-\nu_z}+\frac{1}{x-n+\nu_z}\right], \quad x=\frac{\omega}{\omega_0}, \tag{8}$$

or

$$1 = \frac{-i\pi N\lambda}{2\theta_0\omega_0}[\Phi(x-\nu_z)+\Phi(x+\nu_z)], \tag{9}$$

where (see, for example, in Appendix A)

$$\Phi(x) = \sum_{n=-\infty}^{\infty}\frac{|g_n|^2}{x-n} \tag{10}$$

$$= \frac{\theta_0}{\pi x}-\frac{\sin(2x\theta_0)}{2\pi x^2}+\frac{\sin^2 x\theta_0}{\pi x^2}\cot(\pi x). \tag{11}$$

3 Stability Conditions

Since the right-hand side in Eq.(8) presents a rather complicated function, we consider several cases, when the evaluation of the roots of the dispersion equation can be simplified. Simplest solutions can be found in the region, where $N^*\lambda \ll \omega_0$ ($N^* = N\theta_0/\pi$) and where the decrements of the coherent modes ($\delta = -\mathrm{Im}x$) are small as compared to the distance in the unperturbed spectrum ($x = \pm\upsilon_z + n$). For that reason, the roots in Eq.(8) can be calculated using

$$x_{mn} = m\nu_z + n - i\delta_{mn}, \quad m=\pm 1, \quad |\delta_{mn}| \ll 1 \tag{12}$$

and

$$1 = \frac{-iN\pi\lambda}{2\theta_0\omega_0}\left(\frac{|g_n|^2}{-i\delta_{mn}}+\sum_{k\neq n}|g_k|^2\left[\frac{1}{x-k-\nu_z}+\frac{1}{x-k+\nu_z}\right]\right) \simeq \frac{N\pi\lambda|g_n|^2}{2\theta_0\omega_0\delta_{mn}},$$

which yields

$$\delta_{mn} \simeq \frac{N\pi\lambda|g_n|^2}{2\theta_0\omega_0}. \tag{13}$$

In this region, all betatron coherent modes decay with decrements δ_{mn}. The sum of decrements of all modes

$$\sum_{m,n}\delta_{mn} = \frac{N\pi\lambda}{\theta_0\omega_0}\sum_{n=-\infty}^{\infty}|g_n|^2 = \frac{N\lambda}{\omega_0} \tag{14}$$

coincides with the sum of the cooling decrements of individual particles (see, for example, in Ref.[3]). For the low-frequency modes ($\theta_0|n| \ll 1$), we may replace g_n for $g_n \simeq \theta_0/\pi$, which yields

$$\delta_{mn} \simeq N^*\frac{\lambda}{2\omega_0}, \quad N^* = N\frac{\theta_0}{\pi}. \tag{15}$$

Prior to discuss others possible solutions of Eq.(8) we have to note a significant difference of the obtained expressions for decrements in Eq.(13) and analogous decrements, calculated for the case, when the beam wakes are expressed in terms of the hamiltonian forces. In the last case, the calculations are based on the evaluation the Green function of the induced fields(see, for example, in Ref.[3]). In the region, where coherent frequency shifts (and decrements) are small as compared to the distance in the unperturbed spectrum, the decrements of the coasting beam coherent modes are proportional to the product $m\mathrm{Im}G(n+m\nu_z)$, where $G(\omega)$ is the Fourier amplitude of the Green function (see in Ref.[3] for more details). Since $\mathrm{Im}G(x)$ is an odd function of its argument, depending on the sign of $\mathrm{Im}G(x)/x$ the stability conditions for coherent modes of the monochromatic coasting beam may read $m(n+m\nu_z)>0$, or $m(n+m\nu_z)<0$. Although the sum of these decrements can be positive, only the modes with $|n|<|m|\nu_z$ (or, $|n|>|m|\nu_z$) will be stable. On the contrary, the non-hamiltonian interaction of particles described by Eq.(3) stabilize all betatron coherent modes (provided that their decrements are small). That could be a defect of the considered model.

We note that the non-hamiltonian forces in Eqs (1) and (3) contain the single particle cooling decrements λ, which already are the sums of decrements of coherent modes, calculated microscopically [3]. For that reason, the forces in the model do not obey, for example, the causality conditions.

Another region of parameters, which provides simple expressions for the roots of Eq.(8), is given by the following conditions

$$\nu_z\theta_0 \ll 1, \quad |x|\theta_0 \ll 1. \tag{16}$$

Since θ_0 presents the correlation length, for realistic tunes the first condition holds automatically. In such a region, the leading terms of the Taylor expansion of $\Phi(x\pm\nu_z)$ in the power series in $x\theta_0$ and $\nu_z\theta_0$ yield

$$\Phi(x) \simeq \frac{\theta_0^2}{\pi}\cot(\pi x), \tag{17}$$

and

$$\begin{aligned} 1 &= \frac{-iN\theta_0\lambda}{2\omega_0}[\cot\pi(x+\nu_z)+\cot\pi(x-\nu_z)] \\ &= -i\chi[\cot\pi(x+\nu_z)+\cot\pi(x-\nu_z)]/2 \\ &= \frac{-i\chi\sin 2\pi x}{\cos 2\pi\nu_z-\cos 2\pi x}, \quad \chi=\pi N^*\lambda/\omega_0. \end{aligned} \tag{18}$$

Substituting here $q=\exp(-2\pi i x)$, we obtain

$$q^2-\frac{2\cos(2\pi\nu_z)}{1+\chi}q+\frac{1-\chi}{1+\chi}=0, \tag{19}$$

or

$$q_\pm=\frac{\cos(2\pi\nu_z)\pm\sqrt{\chi^2-\sin^2(2\pi\nu_z)}}{1+\chi}. \tag{20}$$

The oscillations are stable, if $|q_\pm| \leq 1$. In the region, where $\chi^2 \leq \sin^2(2\pi\nu_z)$, we write

$$q = \sqrt{\frac{1-\chi}{1+\chi}} e^{\pm i\mu}, \quad \mu = \arctan\left(\tan[\mu_z]\sqrt{1-\frac{\chi^2}{\sin^2\mu_z}}\right). \tag{21}$$

Since $|q_\pm| \leq 1$, these roots correspond to stable solutions. If $\chi \ll 1$, these expressions result in

$$\delta = -\mathrm{Im}x \simeq \frac{\chi}{2\pi} = N^* \frac{\lambda}{2\omega_0}$$

and ($\nu = \mathrm{Re}x$)

$$\nu_k \simeq \pm\nu_z + k \mp \frac{\chi^2}{\cos(2\mu_z)}, \quad k = 0, \pm 1, \ldots \pm k_{\max}, \quad k_{\max}\theta_0 \ll 1.$$

In this region, in agreement with Eqs (12) and (15) the tune shifts of coherent modes are small as compared to their decrements.

In the region, where $\chi^2 \geq \sin^2(2\pi\nu_z)$, we have $\mathrm{Im}q = 0$. It means that here the coherent tune shifts are so big that $\mu = 0$ (or $\mu = \pi$, if $q < 0$). In order to find the stability conditions we write

$$\begin{aligned} 1 + \chi - \cos(2\pi\nu_z) &> \sqrt{\chi^2 - \sin^2(2\pi\nu_z)}, \\ [1 + \chi - \cos(2\pi\nu_z)]^2 &> \chi^2 - \sin^2(2\pi\nu_z), \\ 2 + 2\chi - 2(1+\chi)\cos(2\pi\nu_z) &= 2(1+\chi)[1 - \cos(2\pi\nu_z)] \geq 0. \end{aligned}$$

The last inequality holds automatically. Hence, both roots in Eq.(20) describe stable solutions for all χ. Simple expressions for decrements can be obtained in the region $\chi \gg 1$, or

$$N \gg N_c = \frac{2}{\lambda\tau}, \quad \tau = 2\theta_0/\omega_0.$$

Using Eq(20) we find that in this region the values of decrements are small

$$\delta \simeq \frac{1}{2\pi\chi} = \frac{1}{\pi}\frac{N_c}{N} = \frac{\omega_0}{2\pi N\theta_0\lambda} \ll 1 \tag{22}$$

According to Eq.(19), if χ approaches 1, one of the roots of the dispersion equation (q_+ or q_-) tends to zero. Since $|q| \propto \exp(2\pi\mathrm{Im}x)$, in this region coherent modes may vary so fast that the condition $|x|\theta_0 \ll 1$ will be violated. For such roots the right-hand side in the dispersion equation Eq.(9) can be rewritten as follows (still $\nu_z\theta_0 \ll 1$)

$$1 = -i\chi F(x, \nu_z), \quad \mu = x\theta_0, \tag{23}$$

$$F = \frac{1}{\mu} - \frac{\sin 2\mu}{2\mu^2} + \frac{\sin^2\mu}{\mu^2}\frac{\sin\left(\frac{\pi\mu}{\theta_0}\right)}{\cos\mu_z - \cos\left(\frac{\pi\mu}{\theta_0}\right)}. \tag{24}$$

This equation shows that in the region, where $\chi \gg 1$, in addition to the roots in Eq.(22) the dispersion equation (23) has the root $x = -i\delta$ with

$$\delta \simeq \frac{\chi}{\theta_0} = N\frac{\lambda}{\omega_0}. \tag{25}$$

The total sum of decrements in this region ($\chi \gg 1$) again is equal to the sum of decrements of individual particles

$$\sum \delta \simeq N\frac{\lambda}{\omega_0}, \quad \chi \gg 1.$$

4 Conclusion

Non-hamiltonian interactions of the cooled particles which are described by forces in Eq.(1) do not result in the instability of betatron coherent oscillations in a monochromatic coasting beam. Meanwhile, in the region, where $\chi \gg 1$, the decrements of coherent modes in such a beam can be very small. Without frequency spreads that circumstance may result in an increase in the power of the Schottky noise of the beam. On its turn, the collisions of particles and coherent fluctuations of the beam could significantly contribute in the beam kinetics resulting in additional blow up of the beam [3].

In more realistic cases, the damping of such slowly decaying modes will occur due to the beam frequency spreads. In the coasting beam, the frequency spread due to the longitudinal temperature of particles can be very small. Important contribution to the frequency spread of betatron oscillations in the deeply cooled beam gives the nonlinearity of the space charge forces. Such a frequency spread can be small only for the so-called crystalline coasting beams. However, for the last case the forces in Eq.(5) must be strongly modified.

A Calculation of the rhs in Eq.(10)

The function

$$\Phi(x) = \sum_{n=-\infty}^{\infty} \frac{|g_n|^2}{x-n} \tag{A.1}$$

in the right-hand side of Eq.(10) can be calculated directly. We write

$$\Phi(x) = \frac{\theta_0^2}{\pi^2 x} + \frac{2x}{\pi^2}\sum_{n=1}^{\infty} \frac{\sin^2 n\theta_0}{n^2(x^2-n^2)}.$$

and

$$\sum_{n=1}^{\infty} \frac{\sin^2 n\theta_0}{n^2(x^2-n^2)} = \frac{1}{x^2}\sum_{n=1}^{\infty}\left(\frac{\sin^2 n\theta_0}{n^2} + \frac{\sin^2 n\theta_0}{x^2-n^2}\right). \tag{A.2}$$

Now, we use (see, for example, in Ref.[4])

$$\sum_{n=1}^{\infty} \frac{\sin^2 n\theta_0}{n^2} = \frac{\theta_0(\pi - \theta_0)}{2} \tag{A.3}$$

and

$$\sum_{n=1}^{\infty} \frac{\sin^2 n\theta_0}{x^2 - n^2} = \frac{\pi}{4x} \{\cot(\pi x)[1 - \cos(2\theta_0 x)] - \sin(2\theta_0 x)\} . \tag{A.4}$$

Substituting Eqs (A.3) and (A.4) in Eq.(A.2) , we find Eq.(11).

References

[1] D. Reistad, L. Hermansson, T. Bergmark, et al. In Proc. of the Workshop on beam cooling and related topics. Montreux 4-5 October 1993, CERN 94-03, p.183, 1994.

[2] V.V. Parkhomchuk. Limitation of Intensities of Ion Beams at Electron Cooling Devices. ENC, 240996. http://www.gsi.de, 1996.

[3] N.S. Dikansky, D.V. Pestrikov. Physics of Intense Beams and Storage Rings. AIP PRESS, New York, 1994.

[4] I.S. Gradstein, I.M. Ryjik. Tables of Integrals, Sums and Products. Academic Press, New York, 1965.

Electron Cooler Impedances

A. V. Burov*
Budker INP, 630090, Novosibirsk, Russia

April 10, 1997

Abstract

A cooling electron beam can be considered as a medium which responds to fields generated by a cooled ion beam. Electron density perturbations are awaken by ion fluctuations at an entrance of the cooler; due to cooler extent, this causes a retardation in the electron response, giving rise to stabilization or destabilization of the ion motion. This reaction is described in terms of an impedance introduced in the ring by the electron beam. The transverse impedance of the electron cooler is found , increment (decrement) rates introduced in the ion coherent modes are calculated. The cooled beam is shown normally to be stabilized by the cooling one.

1 Introduction

An electron cooling [1, 2] is proved to be one of efficient methods for a storage of dens ion beams. Hot ions collide with cold electrons of an accompanying electron beam inside a cooling part of the storage ring. In the result, an ion thermal energy is transferred to electrons, and ion phase density increases (details and referencies concerning electron cooling can be found e.g. in [3]). However, long-range Coulomb forces cause a coherent ion-electron interaction also. This interaction introduces decrements (increments) in various coherent modes of the ion beam, these rates are proportional to the electron current. This problem revealed its importance especially after experiments at an ion storage ring CELSIUS, Uppsala, where a decrease of an ion beam life-time with an increase of the electron current was observed [4]; the phenomenon is referred to as an 'electron heating'. The intensity-dependent phenomena were also observed at NAP-M [2], IUCF [5] and TARN II [6]. These effects are not well-understood. It is not clear, in a particular, could the coherent ion-electron interaction be responsible for some of them, as it was suggested in [7].

Here, an analytical study of the coherent ion-electron interaction is presented. An expression for the electrostatic potential of an arbitrary multipolarity is derived in the next section on a base of the hydrodynamic approximation for the electron medium. Then, transverse impedance introduced by the electron beam is obtained, the coherent stability is considered, the conclusions are formulated.

*e-mail address: Burov@inp.nsk.su

2 Main Equations

Density perturbations of a cooled ion beam excites coherent motion in a cooling electron beam. Electrostatic fields induced in the electron medium can give rise to coherent instabilities of the ions themselves [8, 7, 9]. If the electron beam is good enough, it can be considered as a cold plasma, with the Debye radius r_D much less than the beam radius a. In this case, the electron temperature does not influence the coherent ion-electron interaction, their thermal motion can be neglected and a hydrodynamic model [10] be applied.

In a reference frame, the dynamics of the magnetized electron medium excited by fluctuations of the cooled ion beam can be described by the following set of equations:

$$\begin{aligned} \frac{\partial \tilde{n_e}}{\partial t} + \bar{n_e}\frac{\partial \tilde{v_e}}{\partial z} &= 0 \\ \frac{\partial \tilde{v_e}}{\partial t} - \frac{e}{m}\frac{\partial \Phi}{\partial z} &= 0 \\ \frac{1}{r}\frac{\partial}{\partial r}\left(r\frac{\partial \Phi}{\partial r}\right) + \frac{\partial^2 \Phi}{\partial z^2} + \frac{1}{r^2}\frac{\partial^2 \Phi}{\partial \phi^2} &= 4\pi e(\tilde{n_e} - \tilde{n_i}) \end{aligned} \tag{1}$$

Here $\bar{n_e}$ is a bulk electron density, $\tilde{n_e}, \tilde{n_i}$ are electron and ion density perturbations, $\tilde{v_e}$ is a perturbation of electron velocity, Φ is an electrostatic potential. A magnetic field implied here to be directed along the longitudinal axis z, which neglects an influence of a bended entrance part of the cooler. The electron medium integrates the influence of ion perturbations for plasma time $\simeq \omega_e^{-1}$, $\omega_e = \sqrt{4\pi \bar{n_e} e^2/m}$; a contribution of the bended part can be neglected if a phase advance $\omega_e \tau_{bend} \ll 1$, which is normally satisfied.

The equations of motion (1) have to be supplemented by zero initial conditions imposed on the electron perturbations at the ion entrance in the electron beam:

$$\tilde{n_e}|_{z=-vt} = 0, \quad \tilde{v_e}|_{z=-vt} = 0 \tag{2}$$

The solution of the problem with the initial conditions (Eq.2) can be presented as a sum of a particular solution of Eqs.(1) and a general solution of the homogeneous set, with $\tilde{n_i} = 0$. The arbitrary constants of the general solution are found from the boundary conditions.

Looking for the general solution as $\propto \exp(iqz - i\omega t)\cos(l\phi)$, the result writes

$$\Phi(r) = \begin{cases} AJ_l(\kappa r), & r \le a \\ BK_l(qr) + CI_l(qr), & r \ge a \end{cases}, \tag{3}$$

$$\tilde{v_e} = -\frac{e}{m}\frac{q}{\omega}\Phi, \quad \tilde{n_e} = -\frac{\bar{n_e} e}{m}\frac{q^2}{\omega^2}\Phi, \quad \omega = \omega_\pm = \pm q\omega_e \,/\!/\sqrt{q^2 + \kappa^2},$$

where J_l is the Bessel function, K_l, I_l are modified Bessel functions. The constants B, C are specified by the constant A : due to electric field continuity,

$$\Phi|_{r=a-0} = \Phi|_{r=a+0}, \quad \frac{\partial\Phi}{\partial r}|_{r=a-0} = \frac{\partial\Phi}{\partial r}|_{r=a+0} \tag{4}$$

The requirement for the potential to be zero on the vacuum chamber surface

$$\Phi(b) = 0 \tag{5}$$

gives a sequence of eigennumbers $\kappa = \kappa_{l\mu}(q)$ with $\mu = 1, 2, 3, ...$ as a radial mode counter.

The eigenfrequencies are described by the dispersion equation (3):

$$\omega_{l\mu\pm}(q) = \pm\omega_{l\mu}(q) = \pm q u_{l\mu}(q), \quad u_{l\mu}(q) = \omega_e/\sqrt{q^2 + \kappa_{l\mu}^2} \tag{6}$$

The solution of the problem is simplified for two opposite cases. The first corresponds to the vacuum chamber to be radially remote from the electron beam: $b \gg a, q^{-1}$; the second – almost to touch it: $b - a \ll b$. In the first case, when the vacuum chamber is wide, the eigennumbers $\kappa_{l\mu}$ are found from $C = 0$. This condition together with Eqs.(4) is satisfied when the transverse wave number κ is a zero of the Bessel function J_{l-1}:

$$\begin{aligned} J_{l-1}(\kappa_{l\mu}a) = &\ 0, \quad (l,\mu) \neq (0,1) \\ \kappa_{01} = &\ a^{-1}\sqrt{2/(\ln(1/(qa)) + 1/2)}, \qquad 1/b \ll q < 1/a. \end{aligned} \tag{7}$$

If the metal surface of the vacuum chamber adjoins the electron beam, the eigennumbers are zeroes of the Bessel function J_l:

$$J_l(\kappa_{l\mu}) = 0, \quad b - a \ll a. \tag{8}$$

In a general case, the transverse wave numbers $\kappa_{l\mu} \doteq \kappa_{l\mu}(q)$ have to found from the following equation:

$$\begin{aligned} &K_l(qb)\left[qI_l'(qa)\,J_l(\kappa_{l\mu}a) - \kappa_{l\mu}I_l(qa)\,J_l'(\kappa_{l\mu}a)\right] - \\ &-I_l(qb)\left[qK_l'(qa)\,J_l(\kappa_{l\mu}a) - \kappa_{l\mu}K_l(qa)\,J_l'(\kappa_{l\mu}a)\right] = 0, \end{aligned} \tag{9}$$

gives for a given longitudinal wave number q; the primes denote derivatives over arguments. The solutions of the homogeneous problem form a complete orthogonal set, the orthogonality relations

$$\int_0^a J_l(\kappa_{l\mu}r)J_l(\kappa_{l\nu}r)rdr = \delta_{\mu\nu}\frac{a^2}{2}F_{l\mu}^2 \cdot \tag{10}$$

are satisfied; in the limit cases

$$F_{l\mu} = \begin{cases} J_l(\kappa_{l\mu}a) & \text{if } qb \gg 1 \\ J_l'(\kappa_{l\mu}a) & \text{if } b - a \ll b \end{cases} \cdot$$

Thus, the basic set of solutions for the homogeneous problem (Eqs.1 with $\tilde{n}_i = 0$) is found; at $r \leq a$

$$\begin{aligned}
\Phi = &\quad A_{l\mu\pm} J_l(\kappa_{l\mu} r)\cos(l\phi)\exp(iqz \mp i\omega_{l\mu} t) \\
\tilde{v_e} = &-\pm \frac{e}{m}\frac{A_{l\mu\pm}}{u_{l\mu}} J_l(\kappa_{l\mu} r)\cos(l\phi)\exp(iqz \mp i\omega_{l\mu} t) \\
\tilde{n_e} = &-\frac{\omega_e^2}{4\pi e}\frac{A_{l\mu\pm}}{u_{l\mu}^2} J_l(\kappa_{l\mu} r)\cos(l\phi)\exp(iqz \mp i\omega_{l\mu} t)
\end{aligned} \tag{11}$$

Turning to the particular solution, let us present the ion density perturbation as expanded over this basis:

$$\tilde{n}_i = \tilde{n}_{il\mu} J_l(\kappa_{l\mu} r)\cos(l\phi)\exp(ikz - i\omega_i t), \quad \omega_i = l\omega_b t + k\delta v t, \tag{12}$$

$$\tilde{n}_{il\mu} = \frac{2}{a^2 F_{l\mu}^2}\int_0^a \tilde{n}_{il}(r)\, J_l(\kappa_{l\mu} r) r dr; \quad \tilde{n}_{il}(r) = \frac{1}{\pi(1+\delta_{l0})}\int_0^{2\pi} \tilde{n}_i(r,\phi)\cos(l\phi) d\phi$$

where ω_b is a betatron frequency and $\delta v = v_i - v_e \ll v$ is an ion-electron velocity detuning. For this driving term, the particular solution has the same space-time structure:

$$\Phi = (1-g_\mu)\frac{4\pi e\tilde{n}_i}{k^2+\kappa^2}, \quad \tilde{n}_e = g_\mu \tilde{n}_i, \quad \tilde{v_e} = g_\mu \frac{\omega_i}{k}\frac{\tilde{n}_i}{\overline{n}_e}, \tag{13}$$

where

$$g_\mu = \frac{\omega_\mu^2(k)}{\omega_\mu^2(k) - \omega_i^2} \tag{14}$$

is a screening factor describing the reaction of the electron medium on external perturbations at the frequency ω_i.

The solution of the problem (1) consists of the particular solution (13) and a certain solution of the homogeneous problem, such that the initial conditions (2) are satisfied.

A time dependence of the electron perturbation $\propto \exp(iqz - i\omega t)$ at the ion entrance $z = -vt$ has to be the same as a time dependence of the ion exciting perturbation $\propto \exp(-ikvt - i\omega_i t) = \exp(-iqvt \mp i\omega_{l\mu} t)$, hence,

$$q = q_{l\mu\pm} = k + \omega_i/v \mp \omega_{l\mu}(q)/v. \tag{15}$$

This requirement determines the (Doppler) connection between the electron and ion longitudinal wave numbers. Normally, the electron beam is rather diluted,

$$\alpha \equiv \omega/kv = u/v \ll 1, \tag{16}$$

the $(\pm)$ wave numbers are almost equal: $q_- \approx q_+, \quad \omega_- \approx -\omega_+,$

$$(q_- - q_+)/k = 2\alpha; \quad (\omega_- + \omega_+)/(ku) = -2\alpha\kappa^2/\left(\kappa^2 + q^2\right), \tag{17}$$

the subscripts l, μ are implied. Retention of the small terms $\propto \alpha$ is caused by a mutual cancellation of leading $(\pm)$ terms in a total electron response (see below). The wave amplitudes corresponding to the zero initial conditions (2) follows:

$$\frac{A_{\mu\pm}}{u_{\mu\pm}} = 2\pi e\tilde{n}_{i\mu}\frac{u_\mu(k)}{\omega_e^2}\frac{\omega_\mu(k)}{\omega_\mu(k)\mp\omega_i}. \tag{18}$$

When the wave amplitudes are found, the particular solution (13) can be forgotten. This part of the total solution describes an instant reaction of the electron medium on the external perturbation, it does not cause energy losses and instabilities and is responsible for small frequency shifts only. On the contrary, the wave part of the total electron reaction (11) is concerned with the energy losses and can give rise to the instabilities of the ion beam.

The action of the electron waves on the ions is time-dependent and have to be integrated (averaged) over time of a pass through the cooler τ. Taking into account the small velocity detuning δv and the ion betatron motion, this averaging reduces to a change of time-dependent exponents in (11) on a time-transit factor:

$$\langle\exp(iq\delta vt - i\omega t + il\omega_b t)\rangle = \frac{1}{\tau}\int_0^\tau \exp(-i\omega t + i\omega_i t)\,dt \to -iT(\Delta\psi) \tag{19}$$

$$T(\Delta\psi) = \frac{1-\cos\Delta\psi}{\Delta\psi}, \quad \Delta\psi = (\omega-\omega_i)\tau.$$

Here an insignificant real part of the integral is omitted.

Summing up, the averaged wave potential writes

$$\langle\Phi\rangle = -i\frac{2\pi e}{\omega_e^2}\cos(l\phi)\sum_\mu J_l(\kappa_{l\mu}r)u_\mu(k)\,\tilde{n}_{il\mu}\times \tag{20}$$

$$\left[\frac{u_{\mu+}\omega_\mu(k)}{\omega_\mu(k)-\omega_i}T(\Delta\psi_{\mu+})\exp(iq_{\mu+}z) + \frac{u_{\mu-}\omega_\mu(k)}{\omega_\mu(k)+\omega_i}T(\Delta\psi_{\mu-})\exp(iq_{\mu-}z)\right] \tag{21}$$

$$\Delta\psi_{\mu\pm} = \psi_{\mu\pm} - \psi_i = (\omega_{\mu\pm}-\omega_i)\tau; \quad \omega_{\mu-} \approx -\omega_{\mu+}$$

In the following calculations of the spectral response functions (impedances), the longitudinal coordinate $z \to 0$, and the transverse radial dependence is finally averaged over the ion beam radial distribution.

Normally, the longitudinal impedance of the electron cooler is small in the comparision with the space-charge one [10, 13]. That is why it does not influence the stability (Keil-Schnell) condition which is determined by the dominated space charge contribution.

3 Transverse Impedance

According to a conventional concept, a back action of induced fields on a beam density perturbation can be described in terms of impedances. For a dipole mode, the transverse impedance $Z^\perp$ is introduced as a kick response function on an oscillating dipole moment:

$$-\frac{\partial\langle\Phi\rangle}{\partial x}\tau = ie\gamma\bar{\rho}_i x_i Z^\perp, \tag{22}$$

where $\bar{\rho}_i$ is a linear density of the ion beam in the reference frame, x_i is an amplitude of its deviation along the $x-$direction, $\tau = \ell/(\gamma v)$ is a time of pass through the cooler in the reference frame, ℓ is the cooler length in the laboratory frame. The potential $\langle\Phi\rangle$ is given by Eq.(21) with $l = 1$:

$$\langle\Phi\rangle = -i\frac{2\pi e}{\omega_e^2}\cos\phi J_1(\kappa_\mu r)u_\mu(k)\,\tilde{n}_{i\mu}\left[\frac{u_{\mu+}\omega_\mu(k)}{\omega_\mu(k)\,2-\omega_i}T(\Delta\psi_{\mu+}) + \frac{u_{\mu-}\omega_\mu(k)}{\omega_\mu(k)+\omega_i}T(\Delta\psi_{\mu-})\right] \tag{23}$$

Assuming terms $\propto \alpha$ to be small enough to be neglected, it gives

$$\mathrm{Re}Z^\perp(k) = \frac{Z_0}{4\pi\beta\gamma a}\frac{\ell}{\gamma a}\sum_\mu \frac{\mathcal{K}_\mu\kappa_\mu^2\psi_\mu}{\kappa_\mu^2+q^2}\left[\frac{1-\cos(\psi_\mu-\psi_i)}{(\psi_\mu-\psi_i)^2} - \frac{1-\cos(\psi_\mu+\psi_i)}{(\psi_\mu+\psi_i)^2}\right], \quad q = k/\gamma, \tag{24}$$

$$\psi_\mu = \omega_\mu\tau, \quad \psi_i = q\delta v\tau + \omega_b\tau$$

The most important here is the dependence of the impedance on the betatron phase; assuming $\psi_b = \omega_b\tau < 1$ and extracting a first-order term (24) over this small parameter, the corresponding impedance component follows:

$$\mathrm{Re}Z^\perp(k) = \frac{Z_0\psi_b}{2\pi\beta\gamma a}\frac{\ell}{\gamma a}S_2^\perp(q); \quad S_2^\perp(q) = \sum_\mu \frac{\mathcal{K}_\mu\kappa_\mu^2\psi_\mu}{\kappa_\mu^2+q^2}\frac{d}{d\psi_\mu}\frac{\cos\psi_\mu-1}{\psi_\mu^2}; \quad \psi_i < 1 \tag{25}$$

$$\mathrm{Re}Z^\perp(k) = \frac{Z_0\psi_b}{2\pi\beta\gamma a}\frac{\ell}{\gamma a}\frac{d^2}{d\bar{\psi}_i^2}\left(\frac{\cos\bar{\psi}_i-1}{\bar{\psi}_i^2}\right)S_3^\perp(q);$$

$$S_3^\perp(q) = \sum_\mu \frac{\mathcal{K}_\mu\kappa_\mu^2\psi_\mu^2}{\kappa_\mu^2+q^2}; \quad \bar{\psi}_i = q\delta v\tau, \quad \psi_\mu < 1.$$

The plots of the mode sums are presented on Figs.1,2 for a particular case $\psi_e = 3.5$ and variable sizes ratio a_i/a. For $\psi_\mu \ll \pi$, the sums differ on a constant factor: $S_2^\perp = S_3^\perp/12$.

In fact, the term $\mathrm{Re}Z^\perp \propto \psi_b$ corresponds to a dissipative contribution in the force applied on the ion beam. According to the definition (22), this force is proportional to the ion transverse velocity, actually $\propto i\mathrm{Re}Z^\perp x_i \propto i\omega_b x_i \propto \dot{x}_i$ A sign of a derivative $(\partial/\partial\psi_b)\,\mathrm{Re}Z^\perp$ determines a sign of decrements introduced in synchrobetatron ion modes by the considered interaction. The sign is positive, when the phase advances ψ_e, ψ_i are not too high: $\psi_e \le 2\pi$, $\psi_i \le 2.6$.

The sum factor $S_3^\perp$ is independent on the plasma frequency; the dependence of the factor $S_2^\perp$ on the plasma phase advance ψ_e is shown on Fig.3. The impedance reaches the maximum at $q \simeq 2\pi\kappa_1/\psi_e$, which is almost the same for the various phase advances ψ_e.

4 Transverse Stability

Real part of the transverse impedance is responsible for damping (antidamping) of the beam dipole motion. Assuming the interaction discussed to be weak enough, $\Lambda_m < \Omega_s$,

the synchrotron modes of the bunched ion beam are well-defined. The growth rate of the $m-$th mode calculated for an air-bag distribution reads [12]

$$\Lambda_m = -\frac{2Nr_i c\beta_x}{\gamma\Pi}\int\limits_0^\infty dk\frac{\mathrm{Re}Z^\perp(k)}{Z_0}J_m^2(kl_b) \approx -\frac{2Nr_i c}{\pi\gamma l_b}\frac{\ell}{\Pi\psi_b}\int\limits_{q_m}^\infty \frac{dq}{q}\frac{\mathrm{Re}Z^\perp}{Z_0}, \quad q_m = \frac{m}{\gamma l_b} \tag{26}$$

where $\beta_x = \ell/\psi_b$ is a beta-function in the location of the impedance. The real part of the impedance (24) $\mathrm{Re}Z^\perp(k) \propto \psi_b = \omega_b\tau$ means a dissipative force $F^\perp \propto ixZ^\perp \propto i\omega_b x = -\dot{x}$ applied to the ion oscillations (22). If the integral (26) is positive, the collective ion motion decays due to the coherent interaction with electrons; otherwise an instability take place. The impedance (24) is positive when the phase advances $\psi_e \leq 2\pi$, $\psi_i \leq 2.6$. However, even if $\psi_e > 2\pi$, an integral contribution of the intervals with the negative impedance cannot compete with the dominated positive contribution, which is demonstrated on Fig. 3. Therefore, the plasma phase advance ψ_e does not restrict the stability area. Substituting in the integral (26) $Z^\perp \propto S_3^\perp$ (Eq.25), the transverse growth rate can be presented in the following way:

$$\Lambda_m = \frac{Nr_i c\psi_e^2}{\pi^2\beta\gamma l_b\Pi}\left(\frac{\ell}{\gamma a}\right)^2\tilde{\Lambda}; \quad \tilde{\Lambda} = -\int\limits_{q_m}^\infty \frac{dq}{q}h''(\psi_i)\,S_3^\perp(q); \tag{27}$$

$$\psi_i = qa\delta, \quad \delta = (\delta p/p)(\ell/\gamma a), \quad h''(\psi) = \frac{d^2}{d\psi^2}\left(\frac{\cos\psi - 1}{\psi^2}\right)$$

The increment rates (27) for the systematic detuning are presented in Figs.4,5. The integral (26) with $Z^\perp \propto S_3^\perp$ converges at $q = k/\gamma \simeq 1/a_i$; the sufficient conditions of stability can be estimated as $\delta = (\delta p/p)(\ell/\gamma a) \leq 2 \cdot 2.6 a_i/a \approx 5a_i/a$. According to the plots in Figs.4,5

$$\delta_{th} = \frac{\delta p_{th}}{p}\frac{\ell}{\gamma a} = (5 \pm 1)\, a_i/a \qquad for\, a_i/a = 0.1 - 0.4. \tag{28}$$

The increment (27) as a function of the detuning parameter δ reaches a maximum $\Lambda_{\max}$ at $\delta \simeq 2\delta_{th}$. Taking into account that $S_3^\perp \sim (a/a_i)^2$ the maximum growth rate is found to be independent on the electron beam radius when $a/a_i \gg 1$, $\Lambda_{\max} \sim a_i^{-2} \propto (\delta p_{th}/p)^{-2}$.

The growth rate of this 'blow-wind' instability has been found in Ref.[8] for an infinite electron beam and flat ion beam; the result written in terms of (27) reads

$$\tilde{\Lambda} \simeq 0.07/\delta^2, \quad \delta v \gg \Delta_e. \tag{29}$$

The growth rates (27) and (29) are compared in Fig.5. The latter is seen to cross the former ones close to their maxima, coinciding asymptotically with the case of equal r. m. s. dimensions, $a_i/a = 0.4$. According to (29), the motion is unstable when the detuning exceeds the width of electron distribution, which differs from the conclusion (28) about stability at $\delta < \delta_{th}$. This threshold absence for zero-temperature electron beam in the result of Ref.[8] can be caused by the flat ion distribution assumed there. According to (28), $\delta_{th} \to 0$ when $a_i \to 0$.

The increments (27) do not depend on the longitudinal mode number m when $m < \gamma l_b/a_i$; thus, the instability taken place at $\delta \geq \delta_{th}$ cannot be damped due to the longitudinal frequencies dispersion. Also, it means a coherent damping below the threshold (28), with the same decrement for all the modes $m < \gamma l_b/a_i$, including $m = 0$. This effect can be used for stabilizing single- and multi-bunch modes.

The 'blow-wind' instability could be an explanation for a particular phenomenon observed at CELSIUS. According to ([4]), a decrease of an ion lifetime with increase of electron current, or 'electron heating', observed at this ring looks to be caused by nonlinearity of an electric field of the electron beam beyond the beam radius, $r > a$. However, a fast dying out of the ion beam was also observed when it was deeply inside of the electron beam and detuned from it with $\delta p/p = 0.02$. Substituting $\ell/a = 200$, $\gamma = 1$, $a_i/a = 0.2$ in Eq.(28), it gives the threshold $\delta p_{th}/p = 0.005$, which means that the blow-wind instability have to take place for the detuning applied.

A comparison of the increments obtained (27) with the result of Dikansky and Pestrikov (29) is shown in Fig. 5.

The increment (29) is seen to cross the lines (27) close to their maxima; asymptotically it looks to coincide with the growth rate for $a_i/a = 0.4$.

Thus, the transverse oscillations are unstable, first, when the ion-electron velocity detuning is too high. A reason for this detuning could be the space charge of the ion beam, changing the electron momentums proportionally to a local ion current [16]. This effect could be dangerous for future long relativistic coolers. Second, the instability takes place in the vicinity of the critical energy, where the Landau damping of the microwave motion does not work. In all other cases, the electron cooler introduces the coherent damping in all the synchrobetatron modes, stabilizing single- and coupled-bunch motion.

5 Conclusions

According to the analysis above, the coherent ion-electron interaction normally does not deteriorate ion beam parameters. On the contrary, this interaction introduces coherent decrements in low-order longitudinal and transverse modes of the cooled ion beam.

The electron cooler introduces increments in high-order longitudinal beam modes. These microwave modes are stable when the Keil-Schnell condition with the ion space-charge impedance is satisfied, which is necessary with as well as without the electron cooler.

Transverse instabilities are entailed, when the detuning of the average ion velocity from the electron one is too high. Another reason for the transverse instability could be a vicinity to the critical energy. For both cases, the stability conditions do not include the electron current and are usually satisfied. Thus, the electron cooler introduces normally the coherent damping in the synchrobetatron motion.

This conclusion agrees with experimentally-based ones of [4, 5] that the coherent ion-electron interaction cannot be responsible for the intensity phenomena observed at CELSIUS and IUCF. However, the coherent ion-electron instabilities could be dangerous for long relativistic coolers.

6 Acknowledgments

The author is thankful to N. S. Dikansky, V. V. Parkhomchuk, D. V. Pestrikov, D. Reistad, L. Tecchio, V. Vaccaro for fruitful discussions.

References

[1] G. I. Budker, Atomnaja Energiya, **22**, p.346 (1967)

[2] G. I. Budker et al., Part. Acc., **7** p.197 (1976).

[3] I. N. Meshkov, Particles & Nuclei, **25**, No 6, p.1487 (1994).

[4] D. Reistad et al, in *Proc. of the Workshop on Beam Cooling and Related Topics,* p. 327, Montreux, 1993.

[5] T. Ellison et al., *ibid,* p. 377.

[6] T. Tanabe et al. *ibid,* p. 312.

[7] V. V. Parkhomchuk, D. V. Pestrikov, in *ibid,* p. 327, Montreux, 1993.

[8] N. S. Dikansky, D. V. Pestrikov, *The Physics of Intense Beams and Storage Rings,* AIP Press, New York, 1994.

[9] A. V. Burov, in *Proc. of the Workshop on Beam Cooling and Related Topics,* p. 230, Montreux, 1993.

[10] A. V. Burov, in *Proc. PAC-95*, Dallas 1995.

[11] A. Sessler and V. Vaccaro, CERN Report ISR-RF/67-2 (1967)

[12] A. W. Chao, *Physics of Collective Beam Instabilities in High Energy Accelerators,* J. Wiley & Sons, Inc., New York, 1993.

[13] A. V. Burov, V. Vaccaro, in *Proc. of the Workshop on the Crystalline Beams*, Erice, Italy, 1995.

[14] L. Tecchio et. al. *CRYSTAL. A Storage Ring for Beam Crystallization,* Legnaro, Italy, 1995.

[15] N. S. Dikansky, D. V. Pestrikov, Preprint INP 76-40, Novosibirsk, 1976.

[16] N. S. Dikansky, *private communication.*

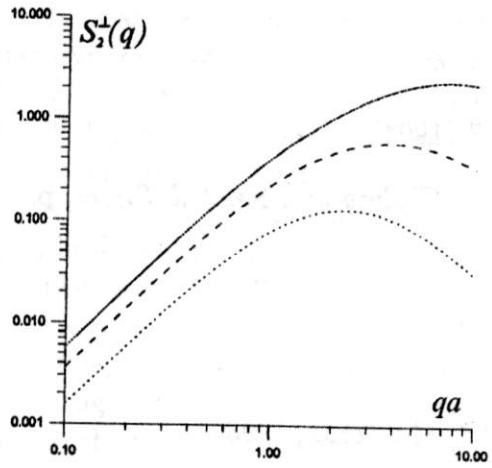

Figure 1: The transverse mode sum $S_2^{\perp}$ calculated for different beam sizes $a_i/a = 0.1$, 0.2 and 0.4 (the solid, dash and dot lines correspondingly). The Lengmuir phase advance $\psi_e = 2.7$.

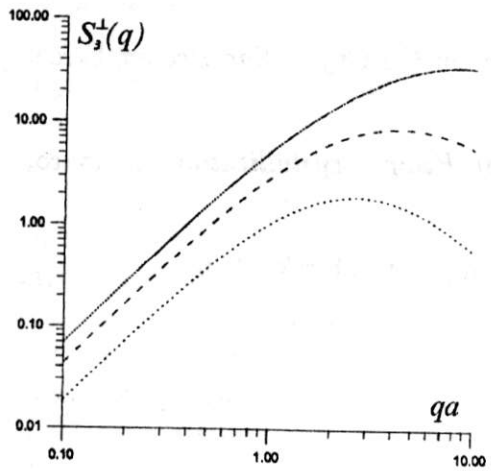

Figure 2: The mode sum $S_3^{\perp}$ at the same conditions as $S_2^{\perp}$ in a previous figure.

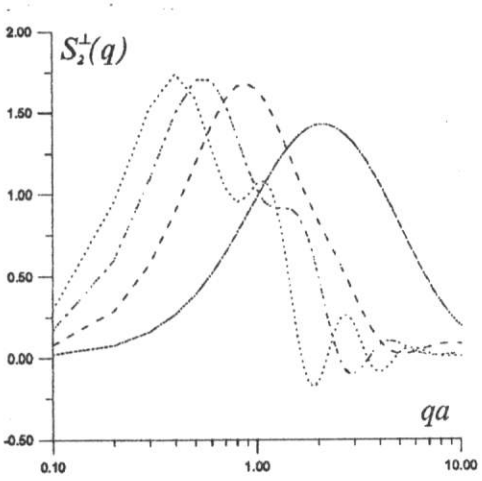

Figure 3: The mode sum $S_2^{\perp}$ for different plasma phase advances: $\psi_e/2\pi = 1, 2, 3$ and 4 (solid, dash, dash-dot and dot lines). The sizes ratio $a_i/a = 0.2$.

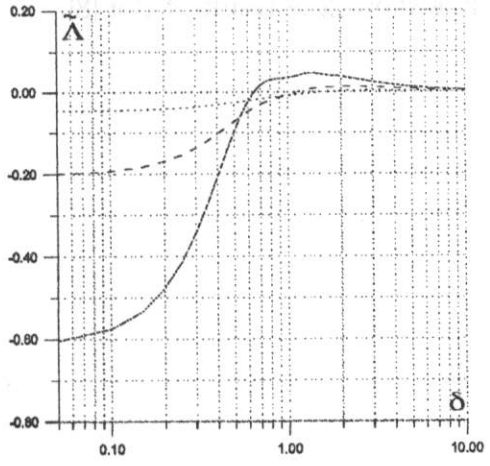

Figure 4: Factor $\tilde{\Lambda}$ specifies a growth rate of a transverse instability for a time-independent velocity detuning. When the wind factor δ is small enough, all the synchrotron modes are damped; otherwise the blow-wind instability takes place. The solid, dash and dot lines correspond to $a_i/a = 0.1$, 0.2 and 0.4.

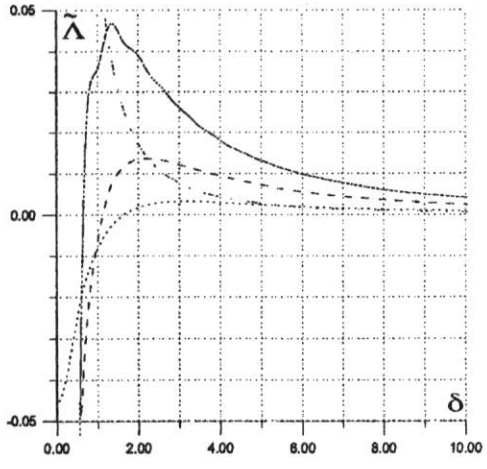

Figure 5: Solid, dash and dot lines are the same as in previous Figure, a dash-dot line shows the result of Ref.[8].

Conceptual Design Study of the GSI Electron – Nucleon Collider *

K. Blasche, J. Struckmeier
Gesellschaft für Schwerionenforschung mbH (GSI),
Planckstrasse 1, 64291 Darmstadt, Germany
and
N.S. Dikansky, A.A Didenko, Yu.I. Eidelman,
I.K. Kuksanov, P.V. Logachev, A.V. Malinin,
P.I. Nemyitov, V.V. Parkhomchuk, D.V. Pestrikov,
V.I. Ptitsin, R.A. Salimov, B.A. Skarbo,
A.N. Skrinsky, M.E. Weis, V.E. Yakimenko.
Budker Institute for Nuclear Physics,
630090 Novosibirsk, Russian Federation

1 Introduction

Here we briefly report a feasibility study for the construction of the Electron – Nucleon Collider (ENC), which could provide the luminosity of electron-nucleon collisions $L = 10^{33}$ $1/[\mathrm{cm}^2\mathrm{s}]$ for the center of mass energies in the range of $\sqrt{s} = 10 \div 30$ GeV/u. The envisaged operational modes of such a collider should enable the collisions of electron against bare ion bunches from protons till U^{92}_{238}. Two interaction points are foreseen. The colliding bunches may have at the interaction points the longitudinal polarization. More extended description of the project can be found in Ref. [1]

The main interaction region contains the detector solenoid ($\int Bdl = 5$ Tm) surrounded by two spectrometer dipoles ($\int Bdl = 1.7$ Tm). The optical scheme of the main interaction region provides the observations of both the large angle ($\theta > 10°$) and the small angle ($\theta < 3°$) collisions. For that reason, the optical elements in the main IR should be placed inside the cones between $3° < \theta < 10°$. (see in Fig.1).

In this report we focus discussion on limitations on the high luminosity performance, which are specific for electron – ion colliders. More detailed technical study is left for the future designing of such a collider. This task will be partially simplified by the fact that many requirements for ENC are similar, or close to those, which are specific for the future

*This work was supported in parts by the contract RU/03533872/60220.

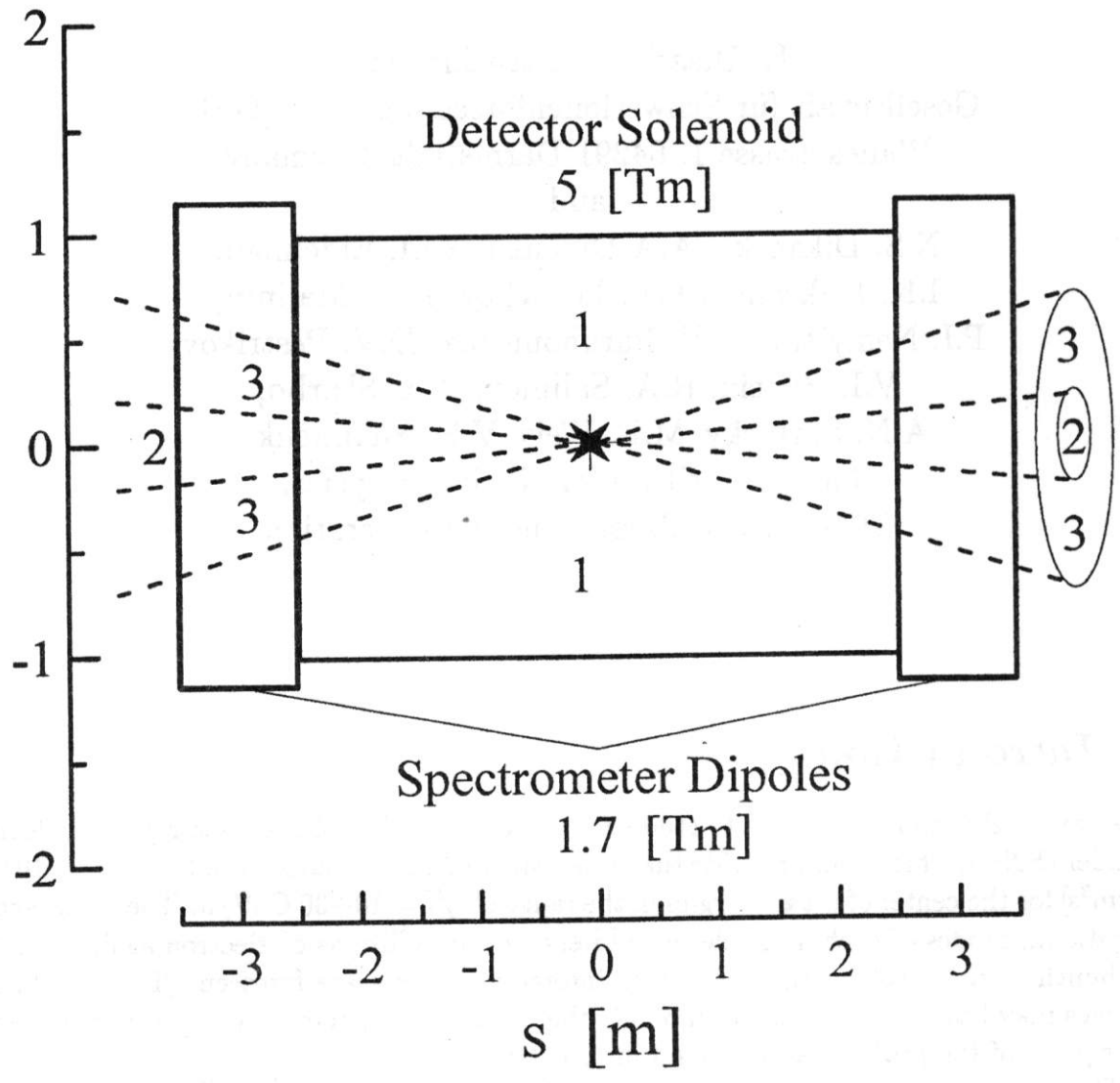

Figure 1: Schematic layout of the main interaction region. Transverse dimensions are measured in meters, 1 – large collision angle zones, 2 – small collision angle zones, 3 – equipment zones.

electron – positron factories. For that reason, we assume that relevant technical solutions, which will be developed for B (or C-τ)–factories, can be used in the future design of ENC.

2 Design concepts

The ENC parameter sets are chosen analyzing the limitations on the luminosity performance. For the bunches with round cross sections and with the rms bunch lengths σ_s approximately equal to the β-function at the interaction point (IP) the luminosity of nucleon-electron collisions reads

$$L \simeq 0.75 A f_b \frac{N_i N_e}{2\pi\beta(\epsilon_i + \epsilon_e)}. \tag{1}$$

Here, suffixes i and e mark the values related to ion and electron bunches, N_i and N_e are the numbers of particles in bunches, $\epsilon_{i,e}$ are their emittances, β is the value of the β-function at the interaction point, A is the atomic number of the ion.

In the case of ENC, the value of the luminosity is limited due to both beam-beam interaction of the colliding bunches and the space charge repulsion in ion bunches. The strengths of the beam-beam instabilities are specified by the beam-beam parameters

$$\xi_e = \frac{N_i Z r_e}{4\pi\gamma_e\epsilon_i}, \quad r_e = \frac{e^2}{m_e c^2}, \tag{2}$$

and

$$\xi_i = \frac{N_e Z r_p}{4\pi A\gamma_i\epsilon_e}, \quad r_p = \frac{e^2}{m_p c^2}, \tag{3}$$

while the strength of the ion space charge instability is specified by the so-called Laslett tune shift

$$\Delta\nu_L \simeq \frac{Z^2}{A} \cdot \frac{N_i r_p}{4\pi\gamma_i^3\epsilon_i} \cdot \frac{\Pi}{\sigma_s\sqrt{2\pi}}. \tag{4}$$

The thresholds for $\xi_{i,e}$ and $\Delta\nu_L$ limit the ratios N_i/ϵ_i, or N_e/ϵ_e and, hence, the values of the specific luminosities (either L/N_e, or L/N_i). Due to the synchrotron radiation damping the threshold value for ξ_e can be rather high. The world average value is about 0.05. Ion bunches must be cooled artificially. Although the threshold value for ξ_i is less definite, we expect same threshold for equivalent cooling conditions of ion bunches $[(\xi_e)_{th} = (\xi_i)_{th} = \xi]$. The estimations show that in the case of ENC, stochastic cooling does not work satisfactory. Required cooling times can be obtained using electron cooling of ion bunches.

For long colliding bunches ($\sigma_s \simeq \beta$), the beam-beam instability thresholds are strongly affected by synchro-betatron resonances. The strengths of these resonances for flat colliding bunches ($\sigma_x \gg \sigma_z$, $\sigma_{x,z}$ are the rms horizontal and vertical bunch sizes) generally increase with an increase in the bunch length and in the amplitude of synchrotron oscillations. On the contrary, for the bunches with round cross section at IP ($\sigma_x = \sigma_z$) the strengths of synchro-betatron resonances asymptotically do not exceed the strengths of betatron resonances for short bunches. In both cases, the strengths of the beam-beam

resonances are strongly suppressed for the particles inside the bunch core. For these reasons, the round bunch geometry at IP seems to be more preferable. The β-functions of the colliding bunches at IP should be set equal.

If the horizontal and vertical β-functions at IP are equal and especially in the case of the strong cooling, the round ion bunch geometry holds automatically. The natural geometry of electron bunches in storage rings is flat. Hence, special tools must be foreseen in the lattice of electron ring of ENC to equalize the vertical and horizontal emittances of electron bunches.

An analysis of the betatron tune shifts due to beam-beam interaction and due to space charge repulsion of ions shows that the frequency distributions in ion bunches are better, if the emittances of electron and ion bunches are set to be equal. Then, a requirement of the common stability of the coherent and incoherent beam-beam oscillations demands that in the case of ENC the Laslett tune shift of ion bunches must be some safe fraction of ξ_i. Taking as a possible threshold value $\Delta\nu_L \simeq \xi_i$ (two interaction points), we find that for given $\sqrt{s}$ the specific luminosity of ENC reaches a maximum value

$$(L/N_e)_{\max} \simeq 0.75 f_b \left(\frac{A}{Z}\right)^{5/4} \left(\frac{\sigma_s\sqrt{2\pi}}{\Pi}\right)^{1/4} \frac{\xi(\gamma_s/2)^{3/2}}{\beta r_p}, \tag{5}$$

when

$$\gamma_i = (\gamma_i)_{\max} \simeq \left\{\frac{Z\Pi}{4A\sigma_s\sqrt{2\pi}}\right\}^{1/4} \sqrt{\gamma_s}, \quad \frac{\gamma_s^2}{4} \simeq \frac{m_p}{m_e}\gamma_i\gamma_e \quad \gamma_s = \frac{\sqrt{s}}{m_p c^2}. \tag{6}$$

If either ion, or electron energies deviate from the optimum value, the specific luminosity decreases according to

$$(L/N_e) = (L/N_e)_{\max} \begin{cases} \gamma_i^3/\gamma_{i,\max}^3, & \gamma_i \le \gamma_{i,\max}, \\ \gamma_{i,\max}/\gamma_i, & \gamma_i \ge \gamma_{i,\max}. \end{cases} \tag{7}$$

Described facts and equations were used for the calculations of the parameter sets enabling the luminosity of electron-nucleon collisions $L = 10^{33}$ 1/[cm^{2}s] in the energy range 10 [GeV/u] $\le \sqrt{s} \le$ 30 [GeV/u]. In our estimations we considered as limiting cases the electron-proton and electron-U^{92}_{238} operational modes of ENC. General parameters of ion and electron rings of ENC for these estimations are listed in the Table 1. For particles with the optimum energies the magnetic rigidity of electron ring does not exceed 30 Tm, while the rigidity of ion ring should be in the range $(BR)_i \le 100$ Tm for electron-proton mode of ENC and in the range $(BR)_i = 100 \div 200$ Tm for electron-ion modes. The assumed perimeters of the rings ($\simeq$1 km) are more relevant to the electron-proton mode with 30 GeV protons ($BR = 100$ Tm). With the maximum specific luminosity, such a magnetic rigidity of the ion ring enables the operation of ENC in the electron-ion mode with $A/Z = 2$ only at low energies ($\sqrt{s} \simeq 10$ GeV/u). Wider ion energy ranges are possible, if the ion energy is shifted down the energy, corresponding to the maximum specific luminosity. In such a case, the suppression of the specific luminosity ($L/N_e \propto \gamma_i^3$) and the requirement to maintain the designed luminosity demands higher electron beam currents and higher energies of electrons. On its turn, those result in the increase of the necessary power of the RF-system of the electron ring.

In the desired interval of the center of mass energies more relevant magnetic rigidity of the ion ring is $BR = 200$ Tm. For the case, when the magnetic system of the ion ring of ENC is performed using the normal-conducting elements, the perimeters of the closed orbit must be enlarged till approximately 2 km. A limitation of the perimeters of the ENC rings by the values $\simeq 1$ km, will make necessary to use for the magnetic system of the ion ring the super-conducting elements.

Table 1: General parameter list

Closed orbit perimeter	1 km
Collision frequency	60 MHz
$\chi = \epsilon_e/\epsilon_i$	1
Curvature radius in bending magnets	60 m
β-function at IP	10 cm
Rms bunch length	10 cm
β_{av}	12 m
$D_{x,av}$	1.6 m
Momentum compaction factor	0.006
β-function in cooling section	200 m
Length of the cooling region	50 m
Cathode temperature	0.1 eV
Longitudinal magnetic field in cooling region	0.5 T
$\xi_e = \xi_i$	0.05

Without special devices, the equilibrium emittance of electron bunch is formed in arcs due to fluctuations of the synchrotron radiation losses. If the bending angle in a single dipole is small ($\phi_B \ll 1$), the equilibrium beam emittance varies proportionally to $\gamma_e^2\phi_B^3$ (for a given $\sqrt{s}$, $\epsilon_x \propto \gamma_s^3\phi_B^3$). On the contrary, the requirement to maintain the luminosity at a given level demands a decrease in the beam emittance proportionally to $\gamma_s^{-1/2}$. Present lattice scheme enables small emittance at higher energy of the electron ring. An increase in the beam emittance at lower electron energies can be provided using, for example, wigglers placed in an insertion with the increased value of the dispersion function. Such an insertion can be placed in the straight section, which in ion ring is occupied by the cooling area.

In the ion ring, a demand to decrease the intrabeam scattering grows rates also requires to decrease a combination $\gamma_i^2\phi_B^2$. For these reasons, the lattices of both rings should contain increased number of cells. On its turn, that increases the ring perimeter, the focusing strength and the ring chromaticity. Careful compensation of this chromaticity is necessary to provide the single beam collective stability as well as to maintain the ring dynamic apertures.

The results of the calculations (see in Table 2) show that in the considered limiting cases the high luminosity performance in ENC is feasible, although may encounter various problems. For example, in the electron-proton operational mode of ENC the required cooling beam densities are rather high. In the beam rest frame system these densities are

Table 2: Parameter sets for the electron-proton and electron-bare uranium colliders, calculated assuming the luminosity 10^{33} 1/[cm^{2}s] per nucleon, $(\Delta\nu_L)_{th} = \xi_i$ (two IP) and $\xi_i = \xi_e = 0.05$; RF-voltage in the ion ring 50 kV.

	Protons			Bare uranium		
$\sqrt{s}$ [GeV/u]	10	20	30	10	20	30
Specific luminosity/10^{21} [1/cm^{2}s]	2.3	6.5	12	7.6	21.4	39.4
Ion Ring	Protons			Bare uranium		
Bunch intensity/10^9	36	26	21	.075	.053	.043
Beam current [mA]	350	250	200	66.5	47	38.4
Energy [Gev/u]	17.2	24.3	29.8	13.57	19.19	23.51
Emittance [nm]	57.3	14.3	6.4	8.6	2.1	1
$(Z/n)_{th}$ [Ohm]	1.8	3.3	4.5	11.5	23	33
IBS growth time [s]	6.5	1.9	1	.06	.014	.07
Cooling time [ms]	700	170	76	22.45	5.5	2.6
Rad. recomb. lifetime [h]	87	61	50	0.21	0.15	0.12
Electron Ring	Protons			Bare uranium		
Bunch intensity/10^{10}	43.	15.	8.3	13.2	4.7	2.5
Beam current [A]	4.2	1.5	0.8	1.27	0.45	0.24
Energy [GeV]	1.45	4.1	7.55	1.8	5.2	9.6
Emittance [nm]	57.3	14.3	6.4	8.56	2.14	0.95
Energy loss/turn [MeV]	0.007	0.43	4.9	0.02	1.1	12.6
RF-Power [MW]	0.03	0.6	4	0.02	0.5	3.0
$(Z/n)_{th}$ [Ohm]	0.03	1.0	8.5	0.16	6	51
Bremsstrahlung lifetime [h]	50	22	15	0.5	0.2	0.14

about 3×10^8 1/cm^3 so that those do not limit, for example, desired beam temperatures, or cooling times. Technically the beams with the current densities in the range 50 – 100 A/cm^2 (see in Table 3) can be produced using the beam compression.

The colliding electron bunch intensities, which are necessary to ensure $L = 10^{33}$ 1/[cm^{2}s], are rather high. That may result in embarrassments due to collective interactions of these bunches with surrounding electrodes. The low energy operation of electron ring requires a serious R&D study of the necessary damping feedback systems.

In the electron-U^{92}_{238} operational mode the main limitation on the luminosity performance occurs due to short lifetime of electron and uranium bunches. Since $(L/N_e)_{max} \propto (A/Z)^{5/4}$ and $\sigma_R \propto Z^2$, the lifetime of electrons due to their bremsstrahlung on the bare ions varies according to

$$\tau_{br} \propto \frac{1}{A^{1/4}Z^{3/4}} \propto \frac{1}{Z}.$$

This problem is specific for electron-heavy ion modes of ENC. Scaling the electron beam lifetime from U^{92}_{238} (500 s) to lighter ions we find that it approaches to one hour only for $Z \simeq 15$. For all intermediate cases, it is short enough to demand the preparation of electron bunches in additional booster synchrotron prior to their injection in ENC.

The radiative recombination lifetime of bare uranium bunches can be made longer using artificial excitation of the Larmour motion of electrons prior they enter the cooling region. The radius of the Larmour circle, corresponding to the cathode temperature 0.1 eV is $r_L = 1.5$ μm, while the minimum value from the maximal impact parameters of adiabatic collisions varies in the range 260 μm – 90 μm. An increase in the electron Larmour velocities by a factor, for example, 3 decreases the value of the Coulomb logarithm for about 20%, while the lifetime increases 3 times.

3 Electron cooling device

The main goal for the cooling system in ENC is the suppression of the higher order beam-beam resonances in order to enable desirable high threshold for the ion beam-beam parameter. As is seen from the Table 2, for ion bunches the desired cooling rates about 10 times exceed the emittance growth rates due to intrabeam scattering. In practice, so short cooling times can be achieved only in the case, when the magnetized cooling predominates. The required parameters of the electron beam, which ensure these cooling times are listed in the Table 3.

Since the magnetized electron cooling rates strongly depend on the temperature of electron Larmour circles, special care requires the suppression of the sources of the increase in the electron beam longitudinal temperature. The main source for this blow-up provides the intrabeam scattering. Since the densities of ion bunches in the cooling section are in the range $10^8 \div 10^{10}$ 1/cm^3, the densities in the cooling electron beam must exceed these values. Small temperature of the electron beam can be then maintained, if it is transported along the cooling section in a strong magnetic field. In the case of ENC, the magnetic field $B_{sol} \simeq 0.5$ T is sufficient to enable the cooling times in the millisecond region. The angular divergency spread of the magnetic force lines in the cooling section $(B_\perp/B_{sol})$ should not exceed the angular divergency spread in the ion bunch [$\simeq 1$ μrad].

Table 3: Parameter set requirements for the electron cooling device.

	Protons			Bare uranium		
$\sqrt{s}$ [GeV/u]	10	20	30	10	20	30
Cooling time [ms]	700	170	76	22.45	5.5	2.6
Beam density/10^9 [1/cm^3]	4	11	21	.056	.16	.3
Beam current [A]	14	9.9	8	.03	.02	.017
Rms beam radius [cm]	0.3	0.17	0.11	0.13	0.06	0.04
Current density [A/cm^2]	19.4	55	101	0.27	0.76	1.4
$B_\perp/B_{sol}$ [μrad]	17	8.4	5.6	6.5	3.2	2.2
Longitudinal temperature $[e^2(n_e/\gamma_i)^{1/3}$; K]	1	1.2	1.4	0.24	0.3	0.36

Up to date, most studies were focused on the employment as a cooling device a DC-acceleration facility. Schematic layout of such a cooling device and general parameters of the acceleration facility are shown in Fig.2). Simulations of the acceleration of the electron beam from the cathode along the acceleration tube have enabled to find a scenario, when electrons are produced on the cathode in the field 0.5 T, then the electron beam radius is adiabatically increased to accelerate electrons in the field 0.1 T and prior the entering the cooling section the magnetic field increased till 0.5 T. This scenario enables sufficient decrease of the power consumption of the solenoids on the acceleration section.

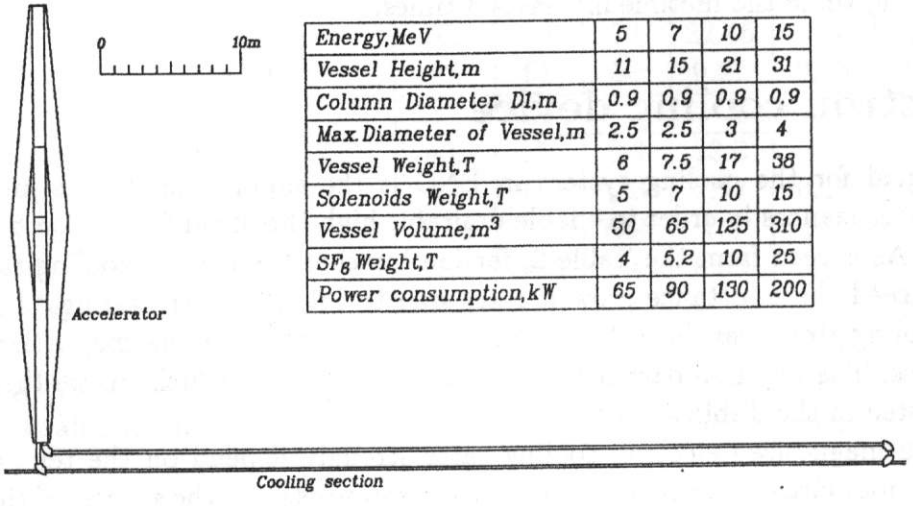

Energy, MeV	*5*	*7*	*10*	*15*
Vessel Height, m	*11*	*15*	*21*	*31*
Column Diameter D1, m	*0.9*	*0.9*	*0.9*	*0.9*
Max. Diameter of Vessel, m	*2.5*	*2.5*	*3*	*4*
Vessel Weight, T	*6*	*7.5*	*17*	*38*
Solenoids Weight, T	*5*	*7*	*10*	*15*
Vessel Volume, m^3	*50*	*65*	*125*	*310*
SF_6 Weight, T	*4*	*5.2*	*10*	*25*
Power consumption, kW	*65*	*90*	*130*	*200*

Figure 2: The general view of cooling facility.

4 Lattice design

In order to provide the desired luminosities of ENC, the lattices of the electron and ion storage rings must enable the following operational options:

1. final focusing of the colliding bunches at two interaction points;
2. longitudinal polarization of the colliding particles at the main IP;
3. maintenance of the necessary and equal emittances of colliding bunches;
4. cooling of the ion bunches;
5. synchronization of the revolution frequencies of electron and ion bunches;

The simplest scheme of a storage ring, which provides these functions is a racetrack with four 90° arcs and four straight sections. Two straight sections must be foreseen for the interaction regions, one – for injection and for RF-systems and another one for the emittance control of electron and ion bunches. The injection straight sections and the cooling section in ion ring are dispersion free. In the straight sections containing the interaction regions the dispersion function and its first derivative vanish at the entrance to the detector solenoid.

The functions of the arc optics in the ion and electron rings are different. In the ion storage ring the main goal for the arc lattice is the transporting of the beam between the straight sections, containing special insertions and synchronization of the ion and electron bunch revolution frequencies. In order to avoid additional blow-ups of the beam due to intrabeam scattering and due to the space charge instability, its optical functions should be as smooth as possible. That can be done using a separated functions FODO lattice.

The arc lattice in electron ring significantly contributes to the producing of the horizontal beam emittance. After examining different schemes an antisymmetrical FODO structure was chosen as the standard lattice cell for both rings. Each arc contains 27 cells, the length of a cell 5.55 m, the bending radius of the cell magnet 53.2 m ($\phi_B \simeq 0.03$), the quadrupole gradient is ±20 T/m. Presently, for the sake of simplicity, we design the

Table 4: Optical parameters of the ENC arc cells.

ring		electron		proton	
motion		horizontal	vertical	horizontal	vertical
Betatron tune ν	cell	.345298	.346222	.071847	.071442
	total	37.292	37.392	7.759	7.716
β_{max},	m	12.03	12.07	15.34	15.43
$<\beta>$,	m	6.5	6.5	12.7	12.7
D_{xmax},	m	.147	0	1.781	0
Chromaticity of the arcs	cell	−.599	−.603	−.0694	−.0705
	total	−64.68	−65.106	−7.495	−7.611
Momentum compaction		.0009904		.0167982	
Energy spread		0.00088			
Transition Energy	GeV	.016		7.239	

electron and ion rings arcs as consisting of identical items (dipoles and quadrupoles). The

field strengths are certainly different for both rings due to different values of the designed BR. An optimization of the arc lattice and improvements in the strategy of obtaining of the required electron beam emittances can be done during the future work.

An inspection of the Table 4 shows that the obtained arc lattices are very rigid ($\nu_{x,y} \approx 37$ for electrons and $\nu_{x,y} \approx 8$ for protons) and are characterized by large natural chromaticities. That is a payment for small electron bunch emittance at high energy. The compensation of these chromaticities will be done using special families of sextupoles. Evaluations of the parameters of these families will be more relevant during final ENC lattice design. The chosen arc lattices enable the equilibrium electron beam emittance 4 nm at electron energy 7.5 Gev ($\sqrt{s} = 30$ GeV).

The optics in the interaction region straight section enables the head-on collisions; equal $\beta-$functions (≈ 10 cm) at IP; longitudinal polarizations of the bunches at IP. For the closed orbit perimeter $\Pi = 1000$ m and for the collision frequency 60 MHz the bunch to bunch distance is exactly equal to the length of the detector solenoid (5 m). It means that the distance between the main IP and the first parasitic IP is 2.5 m. The chosen scheme provides the beams separation in the horizontal plane $(5 - 7)\sigma_x$ at the parasitic IP. The final focusing elements and deflecting magnets inside the detector solenoid are placed within the equipment cones with polar angles between $3° \div 10°$.

Additional embarrassments for the final focus system occur due to the spectrometer dipoles (1 m long). It can be cured, if a spectrometer dipole is divided into two parts, while the second lens of the final focus system is placed between these dipoles (Fig.3). Such a scheme may also enhance the energy resolution of the spectrometer. An inspection of the main parameters of the elements around IP (Table 5) shows that the required magnets although must be performed as superconducting, are not very tight. The places for the

Table 5: Parameters of the elements around IP for ENC with $\beta^* = 10$ cm.

placement	inside solenoid		spectrometer with $\int Hds = 1.7$ Tm	
element	1st magnet	1st lens	total L, cm	100
dist. from IP, cm	48.70	130.35	L_{B1}, cm	77.48
L, cm	81.64	36.49	lens L, cm	36.49
α (for e^-), mrad	32.66	14.60	(inside) G, T/cm	$-.2576$
H, T	1.00		beams separation, cm	
G, T/cm	–	.0806	5.77 after solenoid and 10.93 after B1	

spin rotators are foreseen in the electron and proton interaction regions; besides, the places for the emittance control wigglers are foreseen in the electron ring.

Identical rotation frequencies of electron and ion bunches in the energy range $\sqrt{s} = 10 \div 30$ GeV/u will be set varying the perimeter of the ion ring within 0.12%. Presently, 8 orbit bumps are foreseen for this purpose at the ends of arcs. Each bump (see in Fig.4) provides same bending angle as the replaced arc cells. The Table 6 shows that the chosen scheme with 8 bumps enables the lowest required radial displacement of the ion orbit. An employment of this system demands a tool enabling the radial displacement of about 1 m of the bump segments. The fields in the bump magnets are reasonable. The magnets do not violate the symmetry of the ring.

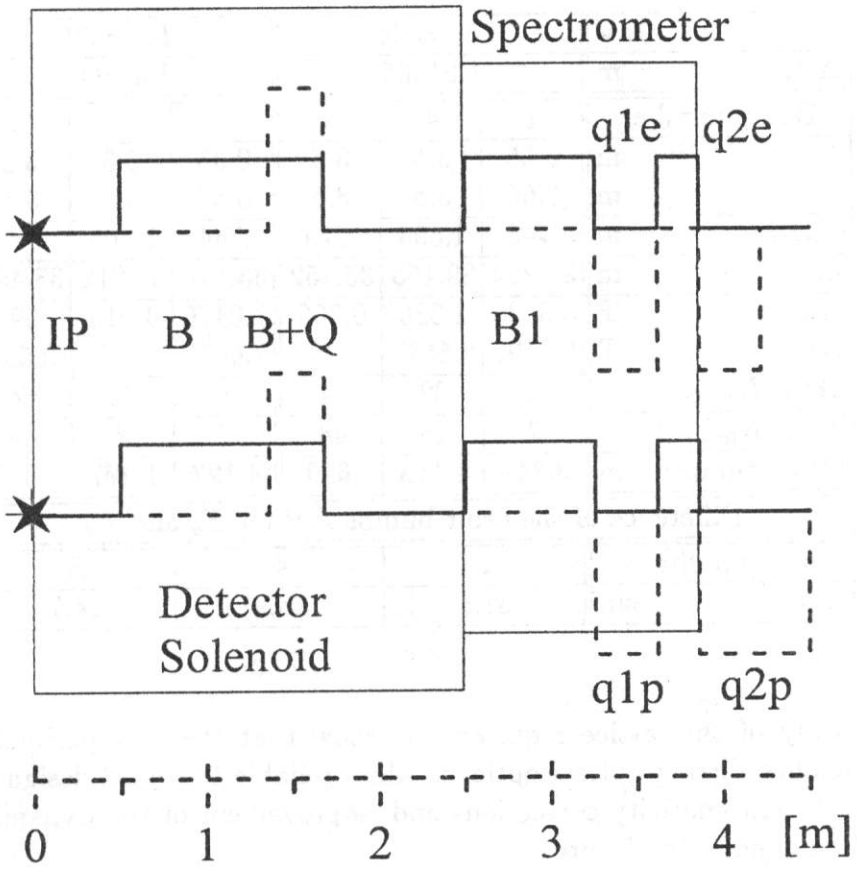

Figure 3: Schematic layout of the interaction region around IP for both rings; upper graph – electrons.

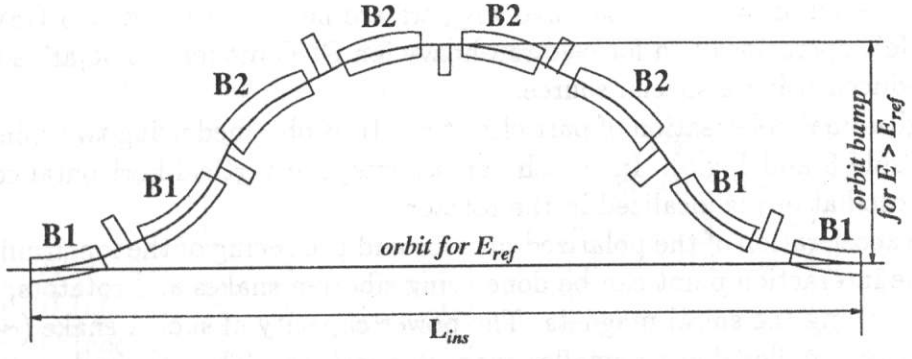

Figure 4: The principle scheme of the element of the adjustment system.

Table 6: Characteristics of the adjustment systems for $E_{ref} = 16$ GeV and $\Pi = 1200$ m.

GeV	$E_d = 25$			$E_u = 30$		
$\Delta\Pi$, m	1.21965			1.47800		
Bump number	1	4	8	1	4	8
L_{B1} m	0.35	3.5	3.5	0.35	3.5	3.5
L_{B2} m	6.65	3.5	3.5	6.65	3.5	3.5
L_{drift}, m	.746	1.593	.779	.784	1.603	.784
L_{ins}, m	33.220	39.155	33.452	33.478	39.212	33.485
H_{B1} T	5.3596	1.336	0.706	7.0476	4.016	0.0974
H_{B2} T	5.3596	2.5577	2	7.0476	3.31	2.591
Total N_{bend}, m	8	32	64	8	32	64
Total N_{lens}, m	7	16	48	7	16	48
Orbit bump, m	3.749	1.118	.690	4.127	1.277	.837

Difference of the orbit bumps ΔR for E_u and E_d			
bump number	1	4	8
ΔR, cm	37.8	16.9	14.7

Present study of the lattice requirements show that the ring perimeter 1 km is a bit tight to enable all ring optical options. More reliable technical design including the elements for the chromaticity corrections and improvement of the dynamic aperture of the ring will be done in the future.

5 Polarization control

For electron-proton (light ion) operational ENC modes the radiation polarization time of electrons can be done shorter than 30 min using special wiggler magnets [1] (see in Table 7). Two wigglers provide the required polarization time ($\leq$ 30 min.) for $E = 7.5$ GeV, three wigglers – for $E = 4$ GeV and five wigglers are necessary for $E = 3$ GeV. For the energy 1.6 GeV operations and for electron-heavy ion ENC modes the polarized electrons must be produced using a special source.

The longitudinal polarization of particles at the IP is obtained using two spin rotations [1] (see in Table 8 and Fig.5). In the chosen scheme, the vertical-horizontal coupling of the particle oscillations is localized in the rotator.

Both the acceleration of the polarized protons and producing of the longitudinal polarization at the interaction point can be done using siberian snakes and rotators, which are manufactured using the spiral magnets. The power capacity of such a snake ($\sim \int H^2 dV$) turns out to be smaller due to smaller magnet aperture. The required parameters of necessary snakes (see in Table 9 and Ref. [1]) indicate that their manufacturing and operation are quite feasible.

Table 7: Wiggler characteristics.

The basic pole,	T · cm	7.097 · 12
Compensating poles,	T · cm	2 × 1.581 · 35
Magnet length,	cm	82
$< \|B\|^3 >$ [1)]	T^3	0.0375
$\oint B^2 ds$ [1)]	T^2·cm	780
$\oint \|B\|^3 ds$ [1)]	T^3·cm	$4.5 \cdot 10^3$
Equilibrium polarization	%	81.2

[1)] If one considers the variants with a different beam energy, the wiggler field H does not change.

Table 8: Main parameters of the solenoid spin rotator (e–ring).

element	name	number	L, m	G, T/cm	sign(α_{tilt})
lenses	q1	2	0.2	.4335	−, +
	q2	2	0.2	−.4441	−, +
	q5	1	0.4	−.3358	no
solenoid		2	3.2	$H = 6.629$ T	

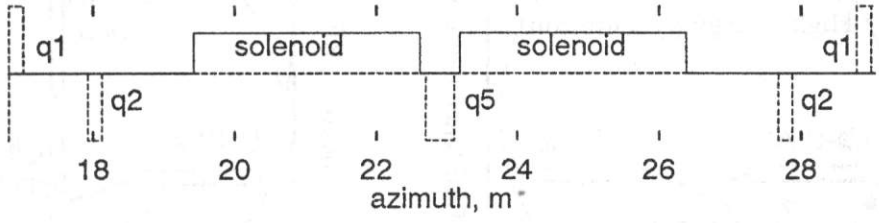

Figure 5: Solenoid spin rotator insertion (e–ring).

Table 9: Parameters of the snakes for acceleration of polarized protons (accel.) and their longitudinal polarization (long.p.) at the IP.

type of snake	number of magnets	$\int H dl$, Tm	orbit deviation (cm) for different energies (GeV)		
			30	25	16
A (accel.)	4	25.5	2.6	3.1	4.8
B (accel.)	4	24.5	2.0	2.4	3.8
C (accel.)	4	30.9	2.0	2.4	3.7
C (long.p.)	4	22.9	1.7	2.0	3.2
D (long.p.)	3	19.9	2.2	2.7	4.2

6 Injection chain

The electron and ion bunches are delivered to the collider experiment energy in a sequence of accelerators providing the bunches with the parameters which are necessary for the experiments. As far as the planed experiments are going to use the polarized bunches, the accelerators in the injection chain must be capable to preserve the polarization of the accelerated bunches.

Although the bunch particle losses are not very high (for example, for electron ring it varies from 2×10^6 to 4×10^7 particles per second) the short life times of electron and heavy ion bunches (about 500 s) demand the full energy injection in ENC, when after the first filling-up of the rings the bunches are replaced one by one about each 100 s (electron-U^{92}_{238} mode).

The injection accelerator chain (see, for example in Figs 6 and 7) for electrons contains 540 MeV linac, low energy booster (possible SIS) and the high energy synchrotron (up to 10 GeV). Corresponding chain for ions can use already existing accelerators UNILAC and SIS.The high energy synchrotron (till at least 30 GeV) must be constructed. This synchrotron can be used for final acceleration of both ion and electron bunches. In order to decrease the injection period it is very desirable to precool ion bunches prior extraction from SIS, or just after injection in the high energy synchrotron.

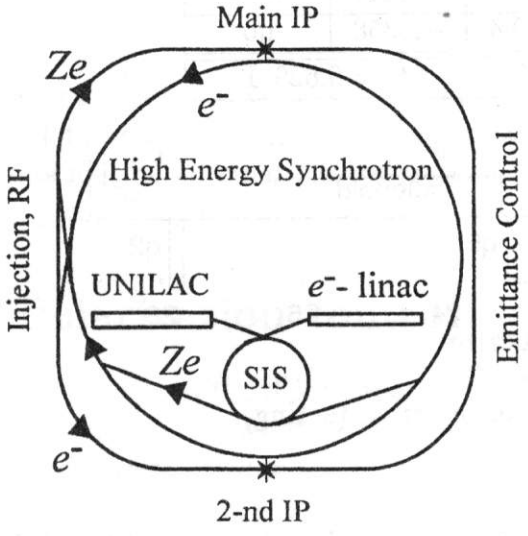

Figure 6: ENC injection scheme using SIS as an electron booster

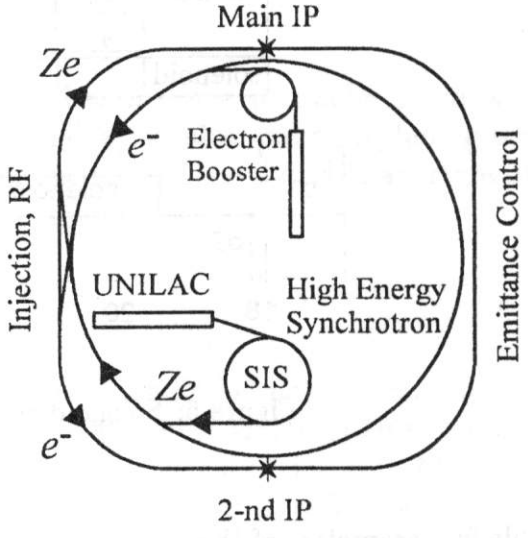

Figure 7: ENC injection scheme using additional electron booster

7 Conclusion

The performed study shows that the construction of the electron-nucleon collider for the energy range $\sqrt{s} = 10 \div 30$ GeV/u and with the luminosity 10^{33} $1/[\mathrm{cm}^2\mathrm{s}]$ is feasible. The total cost of such a collider including costs of injector accelerators (but excluding the building constructions) could be within 904 MDM.

A possibility to reach necessary damping times was demonstrated in the experiments at the installations NAP-M (BINP) and ESR (GSI) as well as at other electron cooling storage rings in US and in the Western Europe. However, an extrapolation of data obtained in the energy range of hundred MeV to that of several tens of GeV still leaves some concern. For that reason, the experiments on ion and proton cooling in an energy range of 1-5 GeV using conventional electron cooling devices could be very useful. Relevant test facility could be created in a period of 2.5 years.

An alternative possibility is to accelerate the cooling beam using a linear accelerator. As far as such a suggestion is very new, it requires a detailed theoretical and experimental study. In this case, the construction of the test cooling device and the cooling tests are even more necessary. The required time interval for these studies could be estimated as about 3 years. Both for the first and the second cases the result of tests could be obtained in 2001-2002 years, after which it will be possible to manufacture a full-scale electron cooling device.

Preliminary studies show that in the case of ENC, the beam dynamics issues should be inspected in more detail. It is clear that the codes, developed to study the beam–beam interaction for the e^+e^- and for conventional hadron colliders will not work for ENC conditions due to strong effect on the beam-beam instabilities from the ion beam space charge, electron cooling and intrabeam scattering. The population of the tails in electron bunches colliding with heavy ion bunches will be also more intensive in ENC.

Existing experiments indicate effects of the ion beam intensity on the efficiency of electron cooling. Although this subject is under attack for already more than 20 years, the theory of these phenomena still is far from its completion. A comprehensive design of ENC demands more efforts in this direction.

References

[1] Conceptual Design Study of the GSI Electron – Nucleon Collider. GSI, March, 1997, http://www.gsi.de/~struck/concepts.html.

Limitation on the Luminosity Performance in Electron-Nucleon Colliders

D.V. Pestrikov
Budker Institute for Nuclear Physics
630090 Novosibirsk, Russian Federation

1 Introduction

It is well known that the luminosity of a collider can be limited by the beam-beam instability of the colliding bunches. The strengths of these instabilities are usually described in terms of the so-called beam-beam strength parameters (ξ), which are the tune shifts of small betatron oscillations of a particle per one interaction region and which are produced by the fields of the counter-moving bunch. For the electron-nucleon colliders (ENC; see, for example, in Ref.[1]), which employ strong ion beam cooling, on more limitation on the luminosity performance may occur due to space charge forces in ion bunches. In this report we discuss limitations on the ion bunch density and, hence, on the collider luminosity due to ion bunch space charge. For the sake of simplicity, we assume colliding bunches with round cross section and Gaussian distributions. Then, the beam-beam parameters for electron and ion bunches read

$$\xi_e = \frac{N_i Z r_e}{4\pi\gamma_e\epsilon_i}, \quad r_e = e^2/m_e c^2, \quad v_e \simeq c, \tag{1}$$

$$\xi_i = \frac{N_e Z r_p}{4\pi A\gamma_i\epsilon_e}, \quad r_p = e^2/m_p c^2, \quad v_i \simeq c. \tag{2}$$

Here, the suffixes i and e mark the values related to ion and electron bunch correspondingly, $N_{i,e}$ are the numbers of particles in the colliding bunches, $\epsilon_{i,e}$ denote the r.m.s. emittances of the ion and electron bunches respectively, Ze and A are the charge and the atomic mass number of the ion, m_p is the proton mass and c is the speed of light. For the counter-charged particles the beam-beam force increases the focusing of particles and, correspondingly, increases the tunes of particles

$$\Delta\nu_b = n_{IP}\xi > 0, \tag{3}$$

where n_{IP} is the number of interaction points.

A possibility to reach in ENC the luminosity in the range of 10^{33} 1/[cm^{2}s] per nucleon is strongly based on the employment of a strong cooling of the ion bunches. Mainly, such a

cooling is necessary to ensure a possibility to reach as high as possible the threshold value of the beam-beam parameter for ion bunches. We remind the reader that in the case, when the bunch intensities are limited by the beam-beam interactions, the luminosity of a collider:

$$L = f_b A \frac{N_i N_e}{2\pi\beta^*[\epsilon_i + \epsilon_e]} \tag{4}$$

can be written in the following form

$$L = f_b \left(\frac{A}{Z}\right)^2 \frac{4\pi\xi_i\xi_e\gamma_i\gamma_e}{\beta^* r_e r_p} \cdot \frac{2\epsilon_e\epsilon_i}{\epsilon_i + \epsilon_e}. \tag{5}$$

Here, f_b is the bunch collision frequency, β^* is the value of β-function at the interaction point and for the sake of simplicity we assume that the r.m.s. bunch lengths σ_s are small compared to β^* ($\sigma_s \leq \beta^*$). According to Eq.(5), for given bunch emittances, a strong decrease in the threshold value of ξ_i will result in a corresponding decrease in the luminosity of the collider. For example, in conventional hadron colliders, which do not use beam cooling, the typical threshold value of ξ is about 0.001, which is approximately two orders of magnitude less than that, achieved for e^+e^- colliders. In these conditions an essential increase in the luminosity of hadron colliders without the beam cooling can be done only by stacking of huge ion currents.

Strong cooling of ions with energies in the range up to several tens of GeV/nucleon increases the influence of the Coulomb repulsions of ions on the stability of oscillations in ion bunches. The strengths of these perturbations are usually described in terms of the so-called Laslett tune shift

$$\Delta\nu_b = -\Delta\nu_L, \tag{6}$$

which is the tune shift of small betatron oscillations due to the space charge fields of the ion bunch. For a bunch with Gaussian distributions in all coordinates $\Delta\nu_L$ reads

$$\Delta\nu_L = \left(\frac{Z^2}{A}\right) \frac{N_i r_p}{4\pi\gamma_i^3\epsilon_i} \cdot \frac{\Pi}{\sigma_s\sqrt{2\pi}}. \tag{7}$$

Here, Π is the perimeter of the closed orbit. Similar to the case of the beam-beam interaction, limitations on $\Delta\nu_L$ occur due to the fact that both tune shifts and strengths of resonances produced by the space charge of the ion bunch, are proportional to that parameter. In a single beam ion storage ring, the threshold value of $\Delta\nu_L$ apart from the beam density is determined by the modulation of the lattice functions and by the lattice periodicity, but never strongly exceeds the value of about 0.1.

2 Working Point for Ion Ring

The limitations due to both the beam-beam and the space charge instability are mainly caused by non-linear dependences of relevant deflecting forces on the particle offsets from the equilibrium position in the bunch (see, for example, in Fig.1). Non-linear behaviors of these forces result in the dependences of relevant tune shifts on the particle amplitudes of oscillations (an example of such dependence for the case of the beam-beam interaction is

shown in Fig.2) and in an excitations of various non-linear resonances, when the particle oscillations tunes approach the resonant values. For example, for betatron oscillations such resonant conditions read

$$m_x\nu_x + m_z\nu_z = n, \tag{8}$$

where $m_{x,z}$ and n are integer numbers.

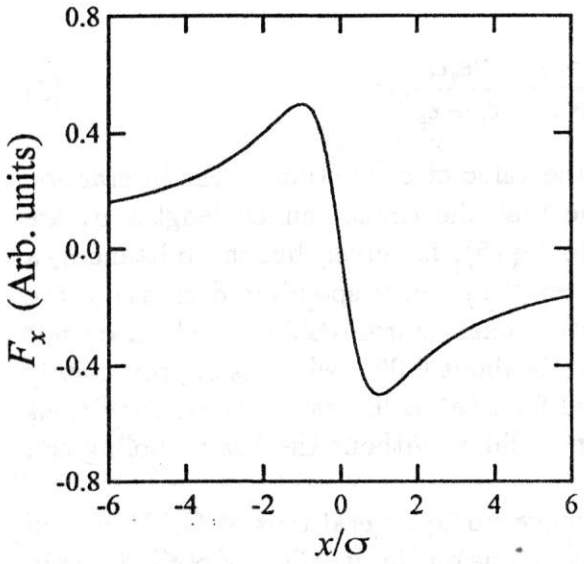

Figure 1: Schematic dependence of the beam-beam force on the horizontal offset of a particle.

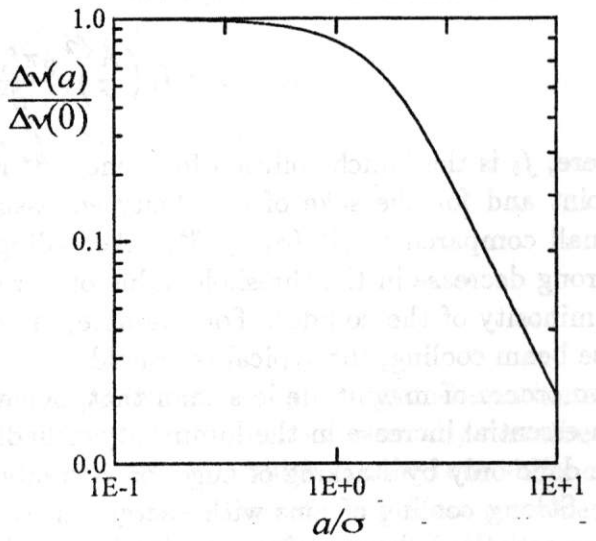

Figure 2: Schematic dependence of the beam-beam tune shift of betatron oscillations on the amplitude.

Below, for the sake of simplicity we consider the case of one-dimensional resonance standing ν_b for any of ν_x and ν_z. Due to dependences of tune shifts on amplitudes (a) a resonant condition

$$\nu_b(a) = \nu_b + \Delta\nu_b(a_s) = n/m, \tag{9}$$

holds for definite amplitude of the particle oscillations $a = a_s$. The value $\Delta\nu_b(a_s)$ determines the center of the resonance in the ν-space. The particles with amplitudes deviating form a_s by small amount $\Delta a = a - a_s$ execute the oscillations around a_s within the region (the bucket) with the width, depending on the value of the resonant harmonic of the perturbing force F and on the tune spread $\Delta\nu_b(a)$. In particular, if such a spread in tunes vanishes, the excited amplitudes infinitely grow. The widths of the corresponding regions in the ν-space (the width of the stopband of the resonance) generally decrease with an increase in the order of the resonances m.

In the discussed cases, the tune shifts are decreasing functions of the amplitudes. For instance, for the beam-beam interaction $\Delta\nu_b(a)$ has the following asymptotes

$$\Delta\nu_b \sim n_{IP}\xi \begin{cases} 1, & a \ll \sigma, \\ \sigma^2/a^2, & a \gg \sigma. \end{cases} \tag{10}$$

Equations (9) and (10) show that the positions of the resonances in the tune space relative to the lines $\nu_b = n/m$ depend on the sign of the tune shift of small oscillations. If, for

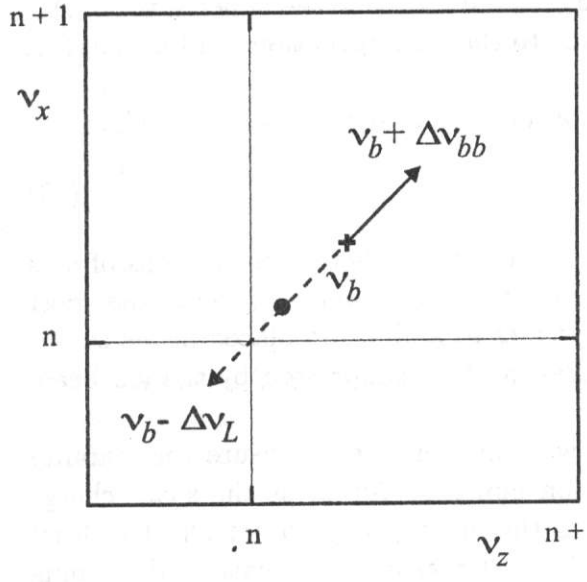

Figure 3: Schematic variation of the working point of betatron oscillations due to beam-beam interaction (solid line) and due to the space charge field (dashed line). Full cross shows the position of the unperturbed working point; full dot – its position due to common effect of the beam-beam and space charge perturbations.

example, $\Delta\nu_b(0)$ is positive, Eq.(9) holds only in the case, when $\nu_b < n/m$. So that the resonance stopband occurs below the resonance $\nu_b = n/m$. On the contrary, if $\Delta\nu_b(0)$ is negative, the stopbands of resonances n/m occur above the resonant value $\nu_b = n/m$. Such simple reasons become crucial for evaluation of the threshold value of the Laslett tune shift of ion bunches in the case of ENC.

For relativistic electron bunches the tune shifts of betatron oscillations are determined by the beam-beam interaction only. Since these tune shifts are positive (see in Fig.3), the stopbands for resonant perturbations of the electron bunches are placed above the resonances $\nu_b = n/m$. It means that the oscillations of electrons will be more stable, if the working point of the ring in ν-space is tuned as close as possible to $\nu_{x,z} \simeq 1$. In such a case, ν_b can be removed form strong lower order resonances like $\nu_b = 1, 1/2, 1/3, 1/4$, while the perturbations due to resonances of the higher order can be suppressed by the synchrotron radiation damping. A choice of the working point in the corner close to some integer is a common for electron-positron collider.

The values of the tune shifts for betatron oscillations of ions due to beam-beam interaction and due to space charge repulsion compensate each other (see in Fig.3):

$$\Delta\nu_i = n_{IP}\xi_i - \Delta\nu_L. \tag{11}$$

Depending on the ratio of the tune shift due to beam-beam interaction to $\Delta\nu_L$, the quantities $\Delta\nu_i$ can take both positive and negative values so that the Laslett tune shift compensates the beam-beam tune shift. Generally, due to different spectra of the beam-beam and ion beam space charge perturbations such a compensation does not takes place for the strengths of relevant non-linear resonances.

In the case, when $n_{IP}\xi > \Delta\nu_L$, the total tune shift $\Delta\nu_i > 0$. As was already discussed, in this case the most preferable is to place the working point slightly above integers. It occurs, if the value of $\Delta\nu_L$ is equal to some fraction of the beam-beam tune shift ($n_{IP}\xi_i$):

$$\Delta\nu_{L,th} = C n_{IP}\xi_i, \quad C < 1. \tag{12}$$

We also note, that since the particles oscillations are stabilized due the dependence of $\Delta\nu_i$ on a, the blow-up of the ion bunch emittances due to these perturbations will be smaller, if C does not approach 1.

Let us now consider the stability conditions of ion oscillations for the case, when

$$\Delta\nu_L > n_{IP}\xi. \tag{13}$$

Since $\Delta\nu_i$ is now negative, the stopbands of resonances of incoherent oscillations of ions are placed above the resonant values $\nu_b = n/m$. From this point of view, the most preferable become the working points, where the tunes ν_x and ν_z are placed in the corner below integers. Again, the higher order resonances must be suppressed by the ion beam cooling.

On the other hand, a correct choice of the working point must ensure the stability of both incoherent and coherent oscillations of ion bunches. As far as the space charge forces depend only on relative positions of ions in the bunch, they do not affect at least the dipole coherent oscillation of ion bunches. For that reason, the equations describing dipole beam-beam oscillations in ENC will not contain the Laslett tune shift of ions. Hence, the stability conditions of these coherent modes will have the same form like that for electron-positron bunches. Namely, independent of the value of the Laslett tune shift the stopband for the dipole coherent beam-beam oscillations always occurs below the integers. It means that in the case, when Eq.(13) holds, the stability conditions for dipole coherent beam-beam oscillations contradict to the stability conditions for incoherent ion oscillations. Since the instability of the dipole beam-beam mode is very strong, practically, such a contradiction means that the ion ring of ENC can never reach the region of the parameters, where the Laslett tune shift exceeds the beam-beam tune shift.

3 Conclusion

The described contradiction between the stability conditions of incoherent oscillations of ions and dipole coherent oscillations of the colliding ion and electron bunches eliminates a possibility for the Laslett tune shift of ion bunches to exceed the beam-beam tune shift. Moreover, to prevent abnormal blow-up of ion bunches the beam-beam tune shifts must significantly exceed the ion bunch Laslett tune shifts. Say, if the collider has two interaction points so that $\Delta\nu_{bb} = 2\xi$, it seems that a safe value for $\Delta\nu_L$ could be $\Delta\nu_L \leq \xi$. In this case, in an analogy with electron-positron colliders the working points for electron and ion rings can be places in a corner slightly above integers.

The requirement to reach in ENC the highest possible luminosity demands to maintain ξ_i as high as possible. In that case, the reachable values of the Laslett tune shifts also will be high. Since the position of the working point in the colliding beams operational mode contradicts to the stability conditions of a single ion beam, it is very likely that there will be necessary to develop a special scenario for the initial filling up of the ion ring.

The mentioned problems are avoided in the positron-ion collider, when the beam-beam interaction decreases the tunes of colliding particles. In this case, the threshold value of the Laslett tune shift is not limited anymore by its comparison with the beam-beam tune shift. Since both tune shifts are negative, the working points of both positron

and ion ring can be chosen in a corner below integers (like for proton-proton, or electron-electron collider). An employment of positrons as the ion colliding partners eliminates the limitations due to accumulation in electron beam of the ions, produced by the ionization of the atoms of the residual gas by electron bunches.

K. Blasche, N. Dikansky, V. Parkomchuk, A.Skrinsky and J. Strukmeier are acknowledged for their valuable comments.

References

[1] N.S. Dikansky, V.V. Parkhomchuk, D.V. Pestrikov, A.N. Skrinsky, V.E. Yakimenko. Physics Aspects of Electron–Ion Collider. ENC 220396, http://www.gsi.de, Novosibirsk, 1996.

Cooling Rates in ENC

D.V. Pestrikov
Budker Institute for Nuclear Physics
630090 Novosibirsk, Russian Federation

1 Introduction

In this note we examine transverse and longitudinal electron cooling rates for two model expressions for the cooling force. This analysis shows that simplified expressions for the cooling decrement

$$\lambda = \frac{K}{\left(\frac{\epsilon}{\beta} + \frac{\delta^2}{\gamma^2}\right)^{3/2}}, \quad K = \frac{Z^2}{A}\frac{4\pi n_e e^4 L}{\gamma^5 m M c^3}\frac{l}{\Pi} \tag{1}$$

overestimates the betatron and underestimates the longitudinal cooling rates. Here, ϵ is the ion beam emittance, β is the β-function at the cooling section, δ is the relative ion beam rms momentum spread, $p = \gamma Mc$ is the ion momentum, Ze is the ion charge, A is its atomic number, n_e is the density of the cooling electron beam, m is the electron mass, L is the so-called Coulomb logarithm, l/Π is the fraction of the cooling section length in the closed orbit perimeter.

We shall calculate the rates of the ion bunch betatron emittance (ϵ) and of its relative rms momentum spread (δ) assuming a Gaussian distribution in the ion bunch, zero dispersion at the cooling section. For the sake of simplicity, we neglect the variations of the betatron functions of ion ring along the cooling section.

2 Non-magnetized betatron cooling

Let us first calculate the cooling rate of, for example, vertical betatron emittance (ϵ_z) assuming that the cooling force is determined by the following simplified expression (all values are calculated in the beam rest frame system)

$$F_z = -\frac{4\pi n_e Z^2 e^4 L}{m}\frac{v_z}{(v_0^2 + v^2)^{3/2}}. \tag{2}$$

Such an expression for the cooling force simulates the case, when the cooling electrons are not magnetized.

We take that betatron oscillations in cooling section are described using (and similar equations for x-oscillations)

$$z = \sqrt{J_z \beta_z} c \cos \psi_z, \quad p_z = p \frac{dz}{ds} \tag{3}$$

so that the action variable is $I_z = pJ_z/2$, while

$$J_z = \frac{z^2}{\beta_z} + \beta_z \left(\theta_z - \frac{\beta_z'}{2\beta_z} z \right)^2, \quad \theta_z = \frac{p_z}{p}. \tag{4}$$

If the particles are distributed in the bunch according to a Gaussian function so that the bunch distribution function reads (Δp is the deviation of the ion momentum from the synchronous value p)

$$f. = \frac{e^{-\Sigma}}{(2\pi)^3 \epsilon_x \epsilon_z \sigma_s \delta}, \quad \Sigma = \frac{J_z}{2\epsilon_z} + \frac{J_x}{2\epsilon_x} + \frac{[s-ct]^2}{2\sigma_s^2} + \frac{[\Delta p/p]^2}{2\delta^2}, \tag{5}$$

then

$$\epsilon_z = \int d\Gamma (I_z/p) f, \quad d\Gamma = d^3\theta dx dz ds, \quad \theta_{||} = \frac{\Delta p}{p},$$

while

$$\frac{d\epsilon_z}{dt} = \frac{1}{p} \int d\Gamma \frac{dI_z}{dt} f = \frac{1}{p} \int d\Gamma \frac{\partial I_z}{\partial p_z} F_z f = \frac{1}{p} \int d\Gamma \frac{\partial z}{\partial \psi_z} F_z f.$$

Now, using

$$\frac{\partial z}{\partial \psi_z} = -\sqrt{J_z \beta_z} \sin \psi_z = \beta_z \left(\theta_z - \frac{\beta_z'}{2\beta_z} z \right),$$

we write

$$\frac{d\epsilon_z}{dt} = \frac{1}{p} \int d\Gamma \beta_z \left(\theta_z - \frac{\beta_z'}{2\beta_z} z \right) F_z f. \tag{6}$$

To select the systematic variation of ϵ_z this expression must be averaged over the closed orbit perimeter. As we mentioned, below we simplify calculations neglecting the variations of β-functions along the cooling section ($\beta' = 0$). For more simplicity, we also assume equal vertical and horizontal β-functions in the cooling section ($\beta_z = \beta_x = \beta$) and equal vertical and horizontal bunch emittances ($\epsilon_z = \epsilon_x = \epsilon$). Using that in the beam rest frame system $n_e \to n_e/\gamma$, $\mathbf{v}_\perp \to \gamma c(\mathbf{p}_\perp/p)$, $v_{||} \to c\theta_{||}$, we write

$$\dot{\epsilon}_z = -\frac{K\beta}{(2\pi)^3 \epsilon^2 \sigma_s \delta} \int d\Gamma \frac{\exp(-\Sigma)\theta_z^2}{\left(a^2 + \theta_\perp^2 + \theta_{||}^2/\gamma^2\right)^{3/2}}, \quad a = \frac{v_0}{c\gamma}. \tag{7}$$

The integration over coordinates (x, z, s) yields $(2\pi)^{3/2} \beta \epsilon \sigma_s$ so that

$$\dot{\epsilon}_z = -\frac{K\beta^2\gamma}{(2\pi)^{3/2} \epsilon \delta} \int \frac{d^3\theta \theta_z^2}{(a^2 + \theta^2)^{3/2}} \exp\left(-\frac{\beta\theta_\perp^2}{2\epsilon} - \frac{\gamma^2}{2\delta^2} \theta_{||}^2 \right). \tag{8}$$

Substituting

$$\frac{1}{w^{3/2}} = \frac{2}{\sqrt{\pi}} \int_0^\infty ds\sqrt{s}\exp(-sw),$$

and calculating Gaussian integrals, we find

$$-\frac{\dot{\epsilon}_z}{\epsilon_z} = \frac{K}{\sqrt{2\pi}} \int_0^\infty \frac{du\sqrt{u}\exp(-a^2u/2)}{(1+\epsilon u/\beta)^2\sqrt{1+\delta^2 u/\gamma^2}}. \tag{9}$$

Simple expressions for the cooling rates ($\Lambda = -\dot{\epsilon}_z/\epsilon_z$) can be obtained in regions, where $a^2 \gg (\epsilon/\beta)$, (δ/γ) and hence

$$\Lambda = \frac{K}{\sqrt{2\pi}} \frac{\sqrt{\pi}}{2} \frac{2^{3/2}}{a^3} = \frac{Z^2}{A} \frac{4\pi n_e e^4 L}{\gamma^2 m M v_0^3} \frac{l}{\Pi}, \tag{10}$$

and where $a^2 \ll (\epsilon/\beta)$, (δ/γ) so that

$$\Lambda = \frac{K}{\sqrt{2\pi}} \int_0^\infty \frac{du\sqrt{u}}{(1+\epsilon u/\beta)^2\sqrt{1+\delta^2 u/\gamma^2}}.$$

After simple transformations the integral in the r.h.s. in this formula is expressed in terms of elementary functions

$$\Lambda = \frac{\Lambda_0}{\sqrt{2\pi}} \begin{cases} \dfrac{\arcsin\sqrt{1-z^2}}{(1-z^2)^{3/2}} - \dfrac{z}{1-z^2}, & z \le 1, \\ \dfrac{z}{z^2-1} - \dfrac{\ln[z+\sqrt{z^2-1}]}{(z^2-1)^{3/2}}, & z \ge 1, \end{cases} \tag{11}$$

where $z = (\delta/\gamma)\sqrt{\beta/\epsilon}$ and

$$\Lambda_0 = \frac{K}{(\epsilon/\beta)^{3/2}} = \frac{Z^2}{A} \frac{4\pi n_e e^4 L}{\gamma^5 m M c^3 (\epsilon/\beta)^{3/2}} \frac{l}{\Pi} \tag{12}$$

is the emittance cooling decrement of the monochromatic bunch. It is interesting to note that in the asymptotic region $z \gg 1$ (or, $\delta \gg \gamma\sqrt{\epsilon/\beta}$) the cooling decrement in Eq.(11) decrease proportionally to γ/δ only

$$\Lambda \simeq \frac{K\gamma}{(\epsilon/\beta)\delta} = \frac{Z^2}{A} \frac{4\pi n_e e^4 L}{\gamma^4 m M c^3 (\epsilon/\beta)\delta} \frac{l}{\Pi}, \quad \delta \gg \gamma\sqrt{\epsilon/\beta} \gg v_0/c. \tag{13}$$

3 Magnetized electron cooling

If the contributions of the adiabatic collisions in the cooling force predominate, the vertical cooling force is determined by the following expression (see, for example, in Ref.[1])

$$F_z = -\frac{2\pi n_e Z^2 e^4 L}{m} \frac{v_z(v_\perp^2 - 2v_\parallel^2)}{(v_\perp^2 + v_\parallel^2)^{5/2}}. \tag{14}$$

Here, we neglect the temperature velocities of the cooling electron Larmour circles as compared to ion velocities. Substituting this expression in Eq.(6) we obtain (again $\beta' = 0$)

$$\dot{\epsilon}_z = \frac{K}{2(2\pi)^{3/2}} \frac{\beta^2\gamma}{\epsilon\delta} \int \frac{d^3\theta\theta_z^2[\theta_\perp^2 - 2\theta_{||}^2]}{\theta^5} \exp\left(-\frac{\beta\theta_\perp^2}{2\epsilon} - \frac{\gamma^2}{2\delta^2}\theta_{||}^2\right). \tag{15}$$

The integral in this expression is calculated in the spherical coordinates $(\theta, \alpha, \varphi)$ with the polar axes directed along $\theta_{||}$, so that

$$\theta_z = \theta \sin\alpha \cos\varphi, \quad \theta_x = \theta \sin\alpha \sin\varphi, \quad \theta_{||} = \theta \cos\alpha.$$

The integrations over φ and θ yield

$$\Lambda = -\frac{\dot{\epsilon}_z}{\epsilon_z} = \frac{K}{2\sqrt{2\pi}} \frac{\beta\gamma}{\epsilon\delta} \int_0^1 du \frac{(1-u^2)(1-3u^2)}{1-qu^2}, \quad q = 1 - \frac{\gamma^2\epsilon}{\beta\delta^2}. \tag{16}$$

Simple calculations result in

$$\Lambda = \frac{\Lambda_0}{2\sqrt{2\pi}} \Phi_x(z) \tag{17}$$

where

$$\Phi_x(z) = \begin{cases} \dfrac{1+2z^2}{(1-z^2)^{5/2}} \arcsin\sqrt{1-z^2} - \dfrac{3z}{(1-z^2)^2}, & z \le 1, \\ \dfrac{1+2z^2}{(z^2-1)^{5/2}} \ln\left[z + \sqrt{z^2-1}\right] - \dfrac{3z}{(z^2-1)^2}, & z \ge 1. \end{cases} \tag{18}$$

Note, that although the cooling force change the sign when $v_\perp \le \sqrt{2}v_{||}$, the emittance cooling decrement is positive for all ratios between the betatron angular divergency (ϵ/β) and the bunch momentum spread (δ). The effect of the local instability results only in a more sharp decrease in the cooling decrement with an increase in δ

$$\Lambda \simeq \frac{\Lambda_0}{\sqrt{2\pi}} \frac{\ln(2z) - 3/2}{z^3}, \quad z \gg 1. \tag{19}$$

A comparison of the calculated cooling rates with predicted by the simplified formula in Eq.(1) shows (Fig.1) that for most bunch momentum spreads the cooling decrements due to magnetized cooling are substantially lower than predicted by Eq.(1).

4 Magnetized momentum cooling

The magnetized momentum cooling force is determined by the following expression (in the beam rest frame system; [1])

$$F_{||} = -3\frac{2\pi n_e Z^2 e^4 L}{m} \frac{v_\perp^2 v_{||}}{v^5}. \tag{20}$$

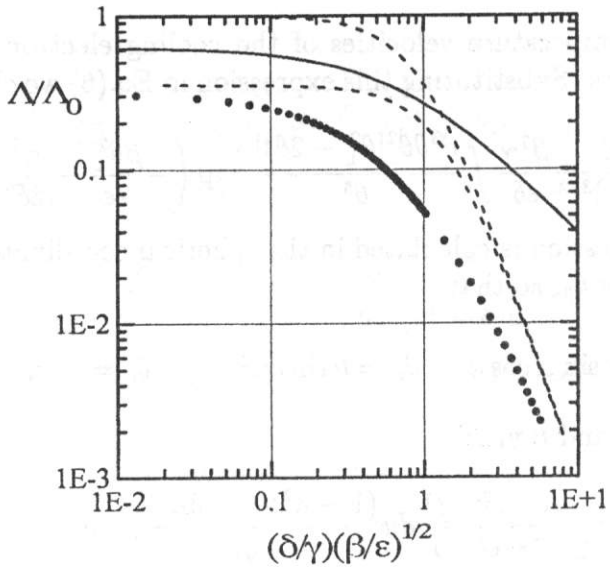

Figure 1: Dependence of the betatron cooling decrement (Λ/Λ_0) on the momentum spread. Solid line – non-magnetized case, full dots – magnetized cooling, upper dashed line – Eq.(1), lower dashed line – $\lambda_\perp = K/[2(\epsilon/\beta) + (\delta/\gamma)^2]^{3/2}$.

Then, for a Gaussian distribution in the ion bunch, the variation of the rms bunch momentum spread (δ) reads

$$\frac{d\delta^2}{dt} = \frac{2}{p}\int d\Gamma \frac{\Delta p}{p} F_\parallel f,$$

or

$$\begin{aligned}
\frac{d\delta^2}{dt} &= -\frac{3}{(2\pi)^{3/2}}\frac{\beta}{\epsilon\delta}\frac{4\pi n_e Z^2 e^4 L}{m\gamma^4 c^2 p}\int d^3\theta \frac{\theta_\perp^2\theta_\parallel^2}{(\theta_\perp^2+\theta_\parallel^2/\gamma^2)^{5/2}}\exp\left(-\frac{\beta\theta_\perp^2}{2\epsilon}-\frac{\theta_\parallel^2}{2\delta^2}\right) \qquad (21)\\
&= -\frac{3K}{(2\pi)^{3/2}}\frac{\beta}{\epsilon\delta}\gamma^3\int d^3\theta\frac{\theta_\perp^2\theta_\parallel^2}{\theta^5}\exp\left(-\frac{\beta\theta_\perp^2}{2\epsilon}-\frac{\gamma^2\theta_\parallel^2}{2\delta^2}\right)\\
&= -\frac{3K}{(2\pi)^{1/2}}\frac{\gamma^3}{\delta}2\int_0^1 du\frac{u^2(1-u^2)}{1-qu^2}, \quad q = 1-\frac{\gamma^2\epsilon}{\beta\delta^2}.
\end{aligned}$$

The calculation of the integral in the rhs of Eq.(21) results in

$$\int_0^1 du\frac{u^2(1-u^2)}{1-qu^2} = \begin{cases} \dfrac{3-2q}{3q^2} - \dfrac{1-q}{q^{5/2}}\ln\dfrac{(1+\sqrt{q})^2}{1-q}, & q \geq 0;\\ \dfrac{3-2q}{3q^2} - \dfrac{1-q}{(-q)^{5/2}}\arcsin\dfrac{\sqrt{-q}}{1-q}, & q \leq 0. \end{cases}$$

Substituting this expression in Eq.(21), we find

$$\frac{d\delta^2}{dt} = -\frac{2K}{\sqrt{2\pi}}\gamma^2\sqrt{\frac{\beta}{\epsilon}}z\Phi(z), \quad z = \frac{\delta}{\gamma}\sqrt{\frac{\beta}{\epsilon}}, \qquad (22)$$

where

$$\Phi(z) = \begin{cases} \dfrac{2+z^2}{(1-z^2)^2} - \dfrac{3z\arcsin(\sqrt{1-z^2})}{(1-z^2)^{5/2}}, & z \le 1, \\ \dfrac{2+z^2}{(z^2-1)^2} - \dfrac{3z\ln(z+\sqrt{z^2-1})}{(z^2-1)^{5/2}}, & z \ge 1. \end{cases} \tag{23}$$

The momentum cooling decrement is obtained dividing $\dot{\delta^2}$ by δ^2, which yields

$$\Lambda_{\|} = -\frac{\dot{\delta^2}}{\delta^2} = \frac{2\Lambda_0}{\sqrt{2\pi}}\frac{\Phi(z)}{z}, \tag{24}$$

where Λ_0 is defined in Eq.(12). Since $\Phi(0) = 2$, the momentum cooling decrement in Eq.(24) diverges for small momentum spreads ($\delta \ll \gamma\sqrt{\epsilon/\beta}$). In the region $\delta \ll \gamma\sqrt{\epsilon/\beta}$ the momentum cooling decrements substantially exceed the betatron ones (see in Fig.2).

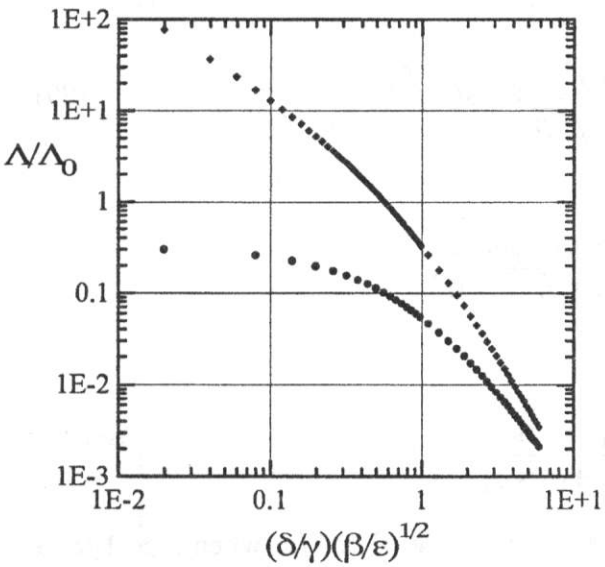

Figure 2: Dependence of the longitudinal (full diamonds) and of the betatron (full dots) cooling decrements on the bunch momentum spread.

A balance between the momentum cooling rate in Eq.(22) and the bunch momentum heating rate due to intrabeam scattering yields the equilibrium bunch momentum spread. In the smoothed focusing approximation ($\beta_{x,z}(s) \to \overline{\beta_{x,z}}$; $D_x(s) \to \overline{D}$) and for the bunch with a "round" cross section ($\overline{\beta_x} = \overline{\beta_z} = \overline{\beta}$, $\epsilon_x = \epsilon_z = \epsilon$) and assuming that the bunch length (σ_s) in maintained to be a constant, we write (see, for example, in Ref.[2])

$$\left(\frac{d\delta^2}{dt}\right)_{IBS} = \frac{K_{IBS}\gamma^2}{\overline{\beta}\epsilon\sigma_s\delta}\int_0^1 du \frac{1-3u^2}{1+[(\gamma/\gamma_c)^2 - q]u^2}. \tag{25}$$

Here, $\gamma_c = \overline{\beta}/\overline{D}$, σ_s is the bunch length and

$$K_{IBS} = \left(\frac{Z^2}{A}\right)^2 \frac{N_i r_p^2 c L_{IBS}}{2\pi\gamma^4}, \quad r_p = \frac{e^2}{Mc^2}, \tag{26}$$

N_i is the number of ions in the bunch, L_{IBS} is the Coulomb logarithm corresponding to the intrabeam scattering. Calculating the integral in Eq.(25), we find

$$\left(\frac{d\delta^2}{dt}\right)_{IBS} = \frac{K_{IBS}\gamma}{\sigma_s\sqrt{\overline{\beta}}\epsilon^{3/2}}\Phi_{IBS}(z\sqrt{\overline{\beta}/\beta}), \tag{27}$$

where $(g = \gamma^2/\gamma_c^2)$

$$\Phi_{IBS}(z) = \frac{1}{1+(g-1)z^2}\left\{\frac{(2+g)z^2+1}{\sqrt{1+(g-1)z^2}}\arcsin\sqrt{\frac{1+(g-1)z^2}{1+gz^2}} - 3z\right\}. \tag{28}$$

Total variation of the bunch momentum spread reads

$$\frac{d\delta^2}{dt} = -\frac{2K}{\sqrt{2\pi}}\gamma^2\sqrt{\frac{\beta}{\epsilon}}z\Phi(z) + \frac{K_{IBS}\gamma}{\sigma_s\sqrt{\overline{\beta}}\epsilon^{3/2}}\Phi_{IBS}(z\sqrt{\overline{\beta}/\beta}),$$

or

$$\frac{d\delta^2}{dt} = -Q\left[z\Phi(z) - \frac{\Delta\nu_L\gamma^3}{2n_e r_e l\sqrt{\beta\overline{\beta}}}\Phi_{IBS}(z\sqrt{\overline{\beta}/\beta})\right], \tag{29}$$

where

$$Q = \left(\frac{Z^2}{A}\right)\sqrt{\frac{2}{\pi}}\frac{4\pi n_e r_e r_p cL}{\gamma^3\sqrt{\epsilon/\beta}}\frac{l}{\Pi},$$

and $\Delta\nu_L$ is the ion bunch Laslett tune shift

$$\Delta\nu_L = \frac{Z^2}{A}\frac{N_i}{4\pi\gamma^3\epsilon}\frac{\Pi}{\sqrt{2\pi}\sigma_s}.$$

Since $z\Phi(z) \simeq 2z$, when $z \ll 1$, and $\Phi_{IBS}(0) = \pi/2$, while $z\Phi(z) \simeq 1/z$, when $z \gg 1$, and

$$\Phi_{IBS}(z) \simeq \frac{1}{z(g-1)}\left[\frac{g+2}{\sqrt{g-1}}\arcsin\sqrt{\frac{g-1}{g}} - 3\right],$$

Eq.(29) may have a stable fixed point ($\delta = \delta_{st}$, see in Fig.3), if

$$n_e > (n_e)_{th} = \frac{\Delta\nu_L\gamma^3}{2r_e l\overline{\beta}}\frac{1}{g-1}\left[\frac{g+2}{\sqrt{g-1}}\arcsin\sqrt{\frac{g-1}{g}} - 3\right]. \tag{30}$$

A comparison of $(n_e)_{th}$ and the ion bunch density (in the cooling section), which is required to reach the necessary luminosity in ENC, shows that in the optimum luminosity conditions ($\Delta\nu_L = \xi_i$, two interaction points) the momentum heating due to intrabeam scattering of ions does not eliminate a possibility for bunches to reach an equilibrium (see in Fig.4). Moreover, the calculation of the stationary momentum spreads (z_{st}) for the bare uranium ion bunches in ENC ($\overline{\beta} \simeq 12$ m, $\overline{D} \simeq 1.6$ m, $\beta \simeq 200$ m, $\sigma_s = 10$ cm see also in

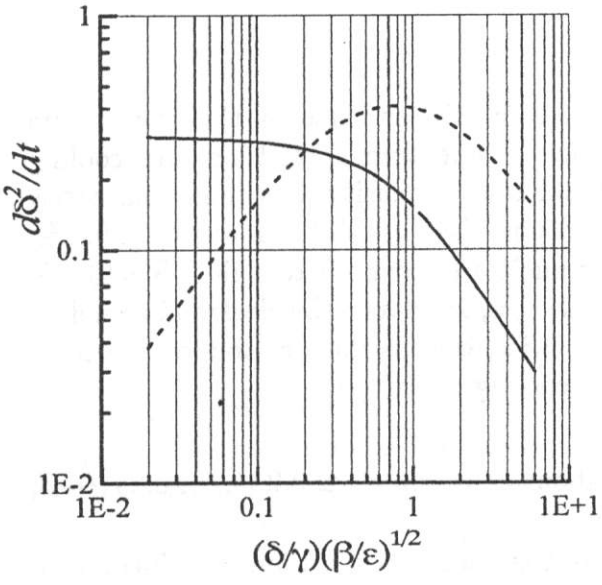

Figure 3: Dependence of the IBS momentum heating rate (solid line) and the momentum cooling rate (dashed line) on the relative momentum spread in the bunch $[(\delta/\gamma)\sqrt{\beta/\epsilon}]$. Electron-$U^{92}_{238}$ ENC mode, $\sqrt{s} = 20$ GeV/u, $N_i \simeq 5.3 \times 10^7$, $n_e = 1.6 \times 10^8$ 1/cm^3.

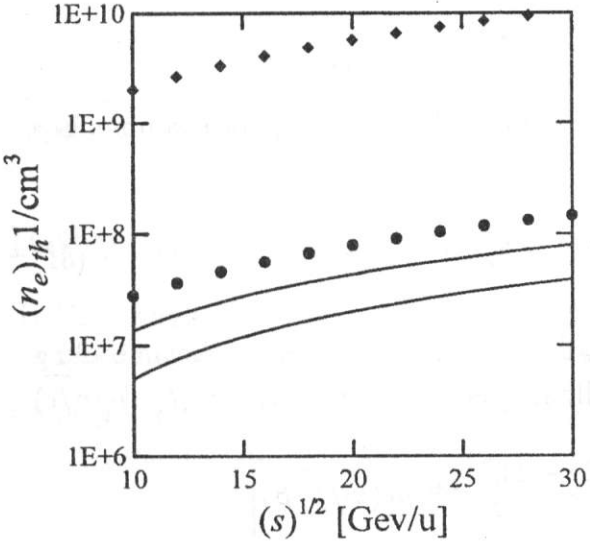

Figure 4: Dependence of $(n_e)_{th}$ on $\sqrt{s}$. Upper solid line – protons, lower – bare uranium ions; full diamonds and full dots show the densities of the proton (diamonds) and bare uranium ion bunches in the cooling section. Optimum luminosity conditions, $L = 10^{33}$ [1/cm^{2}s].

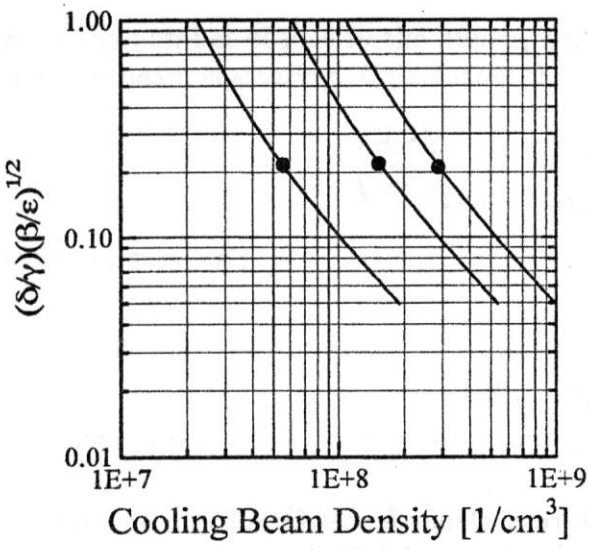

Figure 5: Dependence of the equilibrium bunch momentum spread on the cooling electron beam density. Optimum luminosity conditions (see in Ref.[2]; $L = 10^{33}$ [1/cm^{2}s] per nucleon), from left to right $\sqrt{s}$ =10, 20, 30 GeV/u, full dots – the electron beam density twice exceeds that for the ion bunch at the cooling region [2].

Ref. [2]) shows (see in Fig.5) that its value is about constant $z_{st} \simeq 0.2$ [$\delta_{st} \simeq 0.2\gamma\sqrt{\epsilon/\beta}$; see also in Fig.3] in the energy range $\sqrt{s} = 10 \div 30$ GeV/u.

We may also prove, if the equilibrium between the ion beam cooling and intrabeam scattering does not result in the higher bunch emittances than that corresponding to the space charge, or the beam-beam limit. We write (see in Appendix C of Ref.[2])

$$\begin{aligned}\left(\frac{d\epsilon_x}{dt}\right)_{IBS} &= \frac{K_{IBS}}{\epsilon^2\sigma_s\delta}\left[\overline{\beta}G_x + \frac{\gamma^2 D_x^2}{\overline{\beta}}G_s\right] \\ &= \frac{K_{IBS}}{\epsilon\sigma_s\delta}\int_0^1 \frac{du[g(1-3u^2)+1-(3/2)(1-u^2)]}{1+[(\gamma/\gamma_c)^2-q]u^2} \\ &= \frac{K_{IBS}}{\epsilon\sigma_s\delta}(g-1/2)\int_0^1 \frac{du(1-3u^2)}{1+[(\gamma/\gamma_c)^2-q]u^2}\end{aligned}$$

The integral in the r.h.s of this equation was already calculated. Using, for example, Eqs (25) and (27), we find

$$\left(\frac{d\epsilon_x}{dt}\right)_{IBS} = \frac{K_{IBS}}{2\epsilon\sigma_s\delta}(2g-1)\frac{\overline{\beta}}{\beta}z^2\Phi_{IBS}(z\sqrt{\overline{\beta}/\beta}). \tag{31}$$

Here, $q = 1-(\delta^2\overline{\beta})/(\gamma^2\epsilon)$ Total variation of ϵ_x due to magnetized electron beam cooling and intrabeam scattering is described by the following equation ($\epsilon_x = \epsilon$; $z = (\delta/\gamma)\sqrt{\beta/\epsilon}$)

$$\frac{d\epsilon}{dt} = -\Lambda_0\epsilon\left[\Phi_x(z) - \frac{K_{IBS}\sqrt{2\pi}}{K\sigma_s}\frac{(2g-1)\overline{\beta}}{\delta\sqrt{\epsilon}\beta^{5/2}}z^2\Phi_{IBS}(z\sqrt{\overline{\beta}/\beta})\right],$$

or

$$\frac{d\epsilon}{dt} = -\Lambda_0\epsilon\left[\Phi_x(z) - \frac{\Delta\nu_L\gamma^3}{n_e r_e l}\frac{(2g-1)\overline{\beta}}{\beta^2}z\Phi_{IBS}(z\sqrt{\overline{\beta}/\beta})\right].$$

For the equilibrium conditions ($d\epsilon/dt = 0$) we find

$$n_e = \frac{\Delta\nu_L\gamma^3}{r_e l}\frac{(2g-1)\overline{\beta}}{\beta^2}\frac{z\Phi_{IBS}(z\sqrt{\overline{\beta}/\beta})}{\Phi_x(z)}. \tag{32}$$

Similarly, taking in Eq.(29) $d\delta^2/dt = 0$, we find

$$n_e = \frac{\Delta\nu_L\gamma^3}{2r_e l\sqrt{\beta\overline{\beta}}}\frac{\Phi_{IBS}(z\sqrt{\overline{\beta}/\beta})}{z\Phi(z)}, \tag{33}$$

or

$$2(2g-1)\left(\frac{\overline{\beta}}{\beta}\right)^{3/2} = \frac{\Phi_x(z)}{z^2\Phi(z)}. \tag{34}$$

These equilibrium equations [Eq.(32) and Eq.(33), or (34)] define $(n_e)_{st}$ and z_{st}. Note, that Eq.(mo14) defines the ratio of the equilibrium beam momentum spread to its angular divergency. According to Eq.(34) in the equilibrium this ratio depends on the beam energy and ring focusing only [2]. Numerical solutions of Eq.(34) yield (n_e^* is the cooling beam density calculated to be twice higher than the ion beam density, corresponding to the space charge, or to the beam-beam limit; see in Ref.[2])

$\sqrt{s}$	[GeV/u]	10	20	30
Ion Energy	[GeV/u]	13.6	19.2	23.5
z_{st}		1.78	1.24	1
$(n_e)_{st} \times 10^7$	[1/cm^3]	2.24	5.45	10
$n_e^* \times 10^7$	[1/cm3]	5.6	15.8	29

A comparison of two last rows in this Table shows that the planed cooling beam densities in ENC are about 2, or 3 times higher than that, corresponding the equilibrium between beam cooling and intrabeam scattering. It means that the beam in ENC will be cooled to the space charge (or beam-beam) limit, when z_{th} must be calculated using equation $d\delta^2/dt = 0$ with a given ϵ.

References

[1] Ya.S. Derbenev, A.N. Skrinsky. Part. Accel. 8, p. 1, 1977; see also in Physics Reviews, ser. Soviet Physical Reviews, v. 3, p. 165, 1981.

[2] Conceptual Design Study of the GSI Electron – Nucleon Collider. http://www.gsi.de (Accelerator studies), March, 1997.

Electron beam technique for high voltage electron cooling

Veis M.E., Kuksanov N.K., Malinin A.B., Nemytov P.I., Salimov R.A.

Budker Institute of Nuclear Physics,

630090 Novosibirk, Russia

Abstract

Electron beam cooling is effective method for redusing the emmitance of charge particle beam. For this purpose electron beams whith energy up to tens MeV and current up to some Amperes are neccesary. The possibility of designe of installation for generation and recuperation of energy of such electron beams is discussed.

Kuksanov N.K., BINP, Ac. Lavrentiev 11, Novosibirsk, Russia, 630090.

phone — 3832-35-93-65, fax — 3832-35-21-63, e-mail — kuksanov@inp.nsk.su

Keywords - electron beam, high voltage, accelerating, recuperation.

PASC code: 29.17.+W

The development of experimental investigation related to nuclear physics requires the high quality particle beams. Electron cooling is a method of reducing the beam emmitance. It is especially attractiv in an energy region of antiprotons and ions of some GeV/nuclon. So the energy region of cooling electron beam is about some MeV. Required E.B. current - up to some Amperes. Due to this circumstance BINP in 1985 has started the design of installation for high-voltage electron cooling device. First of all we should check the possibility of forming, acceleration and recuperation of electron beam with Amperes current and energy in Mev scale. This device was also usefull for development E.B. accelerators for industrial applications with a beam power of some Megawatts.

This experiments were described in papers [1] [2]. We repeat briefly its design and main results obtained on this installation. Fig. 1 Shows the general view of device. It is typicall configuration for electron cooling device with recuperation of E.B. energy. Vacuum chamber has U-shape, accelerating and decelerating tubes are placed on vertical parts. It allows to reduce the mechanical strength in tubes and to simplify high-voltage system.

Electrons emmited by cathode obtain the total energy eU_0. The beam is turned on 90° in equipotential space, passes through stright part of pipe and turned additionally on 90° . Passing through deccelerating tubes electrons reduce their energy and hit the collector. Collector has positive potential in comparision with cathode. Reflected electrons are moved back and accelerated up to eU_0. But for this electrons the direction of centrifugical drift is opposite and they are passing to the walls of vacuum chamber or to speciall target.

The high-voltage power source is designed on the base of rectifier of ELV-accelerator for industrial application. It has maximum voltage 1 MV and power 20 kW. Recuperation rectifier is connected beetwen cathod and collector. It has maximum voltage 5 kV and power up to 20 kW. All high-voltage elements are placed inside of common gas system wich combined the

vessel for rectifiers and vessels for accelerating and deccelerating tubes.

Longitudinal magnetic field is provided by conical, toroidal and cylindrical solenoids. It has the additional windings for correction of centrifiginal drift and other disturbunce of trajectory. Main parameters of device are as follows:

Voltage of H/V rectifier	1 MV
Voltage of recuperation rectifier	5 kV
Magnetic field	900 Gauss
Stability	1 %
Larmor radius	5 sm
Acceleration tube length	115 sm
Deceleration tube length	150 sm
Aperture diameter	10 sm
Cathode diameter	1 sm
Vacuum	$10^{-6} \div 10^{-5}$

Following results were obtaned:

Beam energy	1 MeV
Beam current (continuous)	1 A
Beam current (maximum)	1.7 A
Current loses (minimal)	$2 \cdot 10^{-4}$
Current loses (usually)	10^{-3}
Collector potential	3 kV
Time of continuous operation	1 hour

This data and expirience allow to promote both the poject of installation for electron cooling in

energy region 4 - 30 Gev/nuclon and d.c. electron accelerator with energy of 1 MeV and power up to 500 kW. Configuration diagram of the proposed installation for high voltage electron cooling is shown in Fig. 2. Main elements of the installation are the following: a high-voltage rectifier, accelerating and decelerating tubes, recuperation rectifier. They are placed inside a tank filled with SF6 gas under a pressure of 12 bar. For the installation with the energy higher than 7 MeV an additional electrode is supposed to be used to reduce its overall dimensions. Fig. 3 shows a sectional view of the accelerating tubes and high-voltage terminal. The tubes are located in solenoid which creates magnetic field up to 1000 Gy. Power consumed by the solenoid is 8 kW/m. The high-voltage rectifier and solenoid are transformer supplied. The recuperation rectifier, ion pumps, injector control unit, collector cooling system are located in the high-voltage terminal. Power of the recuperation rectifier is 10 kW.

Alternative designes of installation for an energy of 5, 7, 10 and 15 MeV were examined. Main parameters of the variants considered are presented in the Tabl. 1.

The installation tank overall dimensions were determined meeting a condition of providing the electric strength. When choosing a configuration the following considerations were taken into account. In a case when the installation column ends with a sphere electrode, the electric field strenght at the electrode surface is determined from the relation $E = 2\frac{U}{r_1} = 4\frac{U}{r_2}$, where r_1 and r_2 are radiuses of inner and outer electrodes, U is a voltage of a high-voltage gap. Hereinafter the equations for the electric field intensity are given at an optimal relation of the electrodes radiuses. In a case when a tandem arrangement is used the high-voltage electrode has a cylinder form, and field $E = \frac{U}{r_1} = 2.718\frac{U}{r_2}$. In the latter case the tank radius is 1.47 times less and the area is 2.17 times less than in the variant with a sphere electrode. As far as installation lengths differs more than twice, the tank volume at the tandem arrangement is slightly smaller. Besides, in the case the rectifier and solenoid are spaced apart through the

length, it allows to provide their separate supplying and independence of energy and magnetic field adjustment.

As a practice shows the long accelerating tubes operate reliably at an acceleration rate no more than 1 MeV/m. The same gradient is close to maximal one for a high-voltage cascade generator. So the installation total length is determined on this basis. The tank diameter is determined from a gas insulation electric strength of about 200 kV/cm. Presence of gaps between the high-voltage rectifier sections and accelerating column leads to 20÷30% increase of the maximal electric field intensity as compared to the case with a smooth cylinder. Thus, the tank and column diameters should be chosen meeting the condition of 150÷160 kV/cm intensity at a surface of the smaller cylinder. At a voltage of more than 7 MV it is advantageous to use an additional electrode at an intermediate potential. In this case the intensity is determined from the relation $E = 0.423\frac{U}{r_1} = 1.917\frac{U}{r_2}$, and it is 1.4 time less than that of the variant without an electrode at the same outer radius. The following data were used to estimate the solenoid power consumption. The solenoid sectional view is shown in Fig. 4. Diameter of the accelerating tube in an outer edge of the electrodes is 220 mm. Considering that a potential difference between the electrode and coil is up to 20 kV and that it is necessary to locate a shielding ring protecting the tube from an alternating magnetic field component, the coil inner diameter chould be no less then 250 mm. The inner diameter is determined from the column dimensions, it is 425 mm. The section step is 40 mm, the coil height is 30 mm. To obtain the magnetic field of 0.1 T it is necessary to provide 3200 A·turns for every coil. At a filling factor 0.7, the power in coil will be 103 W at 20°C, and 136 W at a maximal operation temperature of 100°C. Considering losses in the shielding rings and rectifier, the power given off in the solenoid is 8 kW per meter (for two acceleratig tubes).

The solenoid is supposed to be cooled by an SF6 gas flow. A diagram of the cooling system

is presented in Fig. 5. The output at 10°C heating should be 1500 m^3/hour for the 15 MeV installation. At the the gas flow rate of 1.5 m/s, a convective heat transfer factor is about 80 $W/(m^2 \cdot °C)$, this is enough for heat removing from the solenoid side surface. The collector is cooled by an additional cooling loop on the heat tube priciple.

When estimation the power consumption we took into account consumptions of the solenoid, recuperation rectifier, high-voltage rectifier and 85 % efficiency of the facility.

The total view of cooling facility is presented at Fig.6.

These data are the estimation parameters, they should be improved at a more detailed consideration.

References

[1] Salimov R.A., Veis M.E., Kuksanov N.K, Meshkov I.N, Smirnov B,N and other, High voltage electron cooling device, Proc. 13 International confernce accelerators conference, Novosibirsk, 1987.

[2] Salimov R.A., Veis M.E., Korabelnikov B.M and Kuksanov N.K, Electron beam with energy 1 MeV in recuperation regime, Proc. EPAC, Rome, 1988.

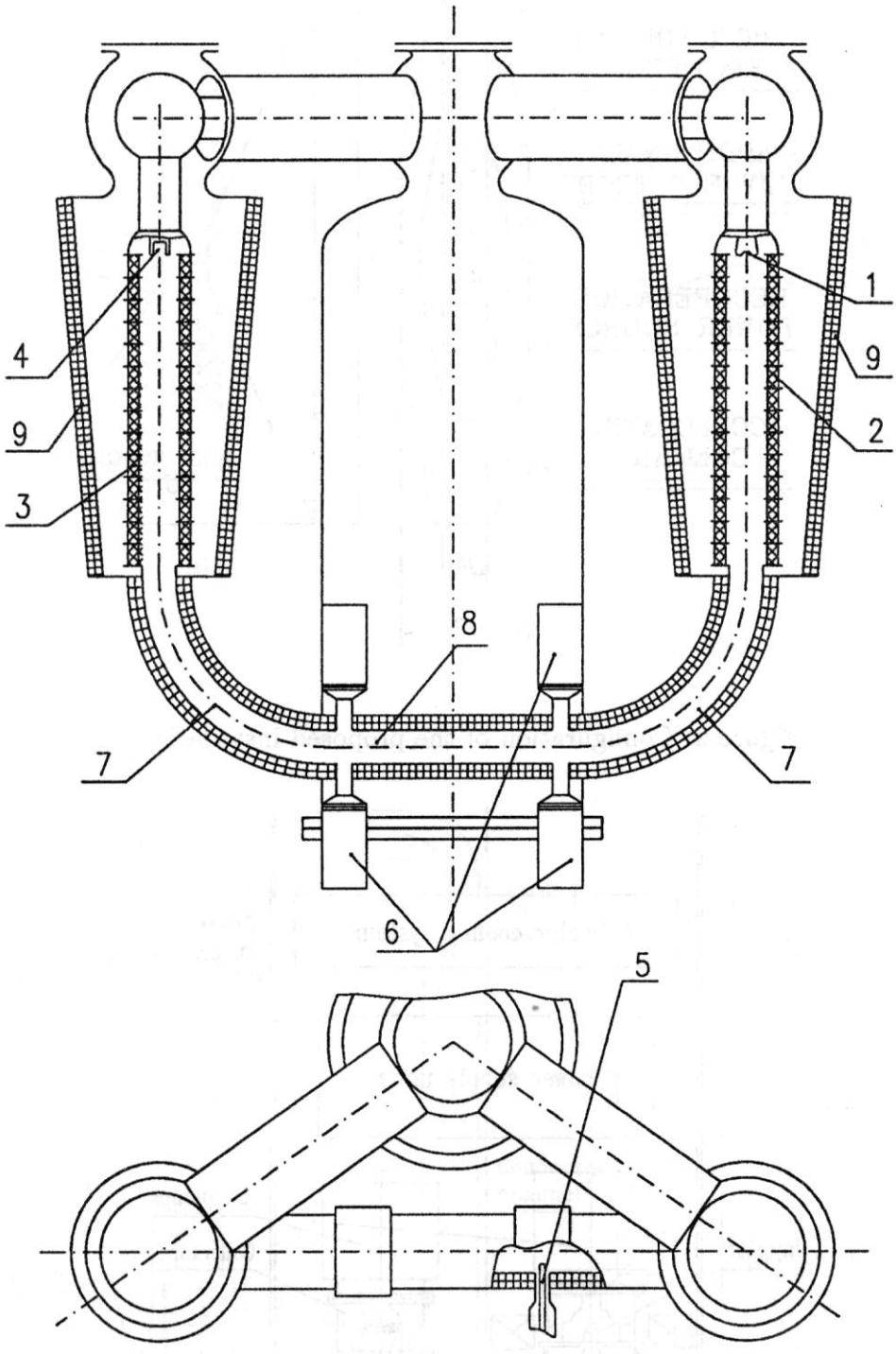

Figure 1: High voltage electron cooling device.

1 - cathod, 2, 3 - accelerating tubes, 4 - collector, 5 - reseiver, 6 - ion pumps, 7, 8, 9 - solenoids parts.

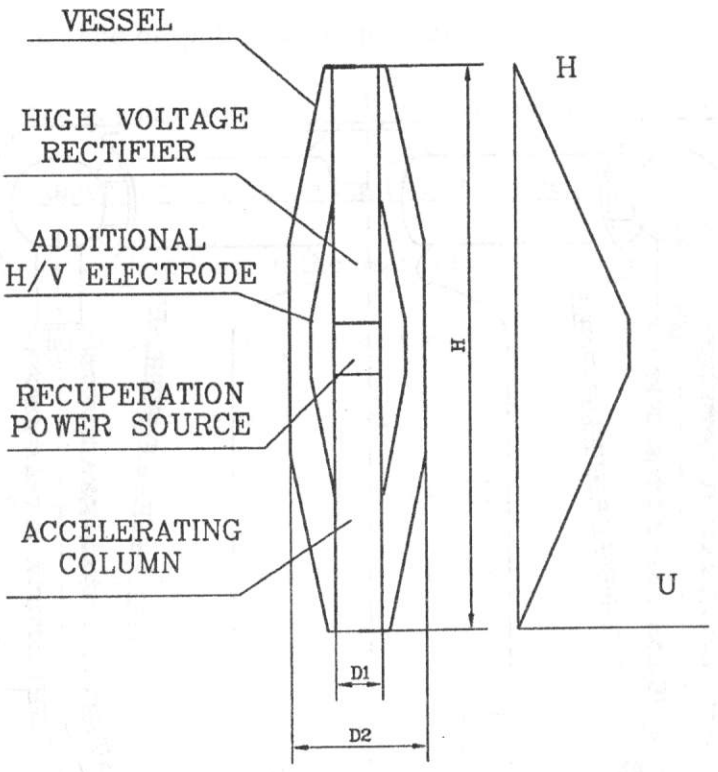

Figure 2: Configuration of the proposed installation.

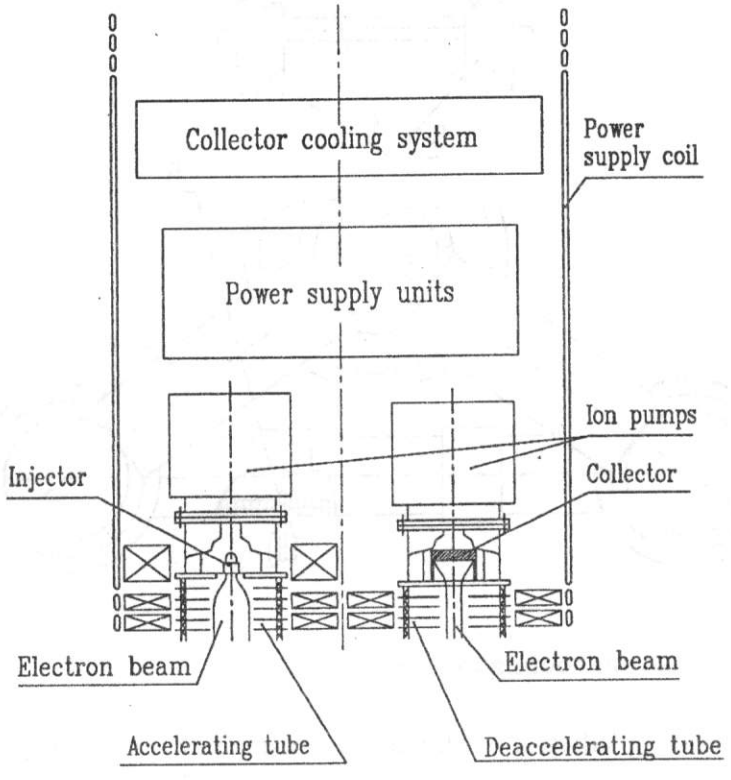

Figure 3: Sectional view of the accelerating tubes and high-voltage terminal.

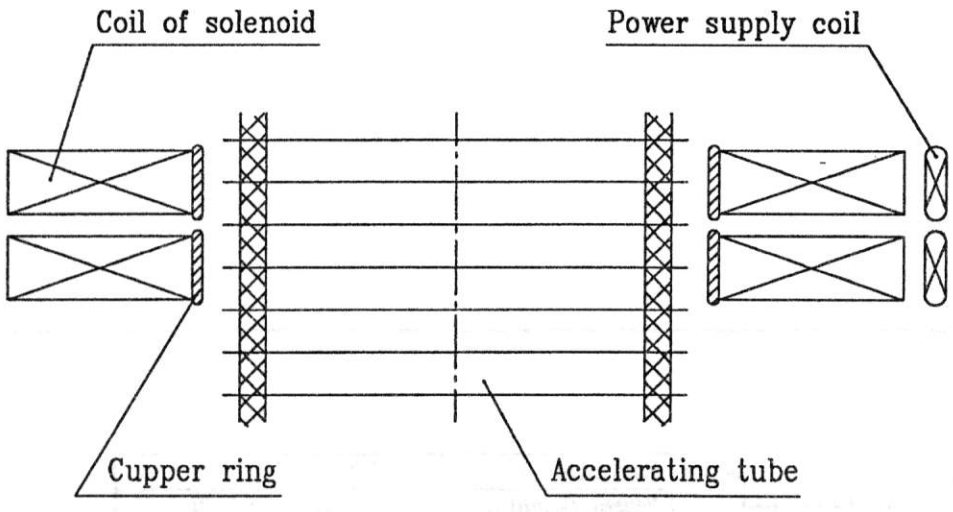

Figure 4: The solenid sectional view.

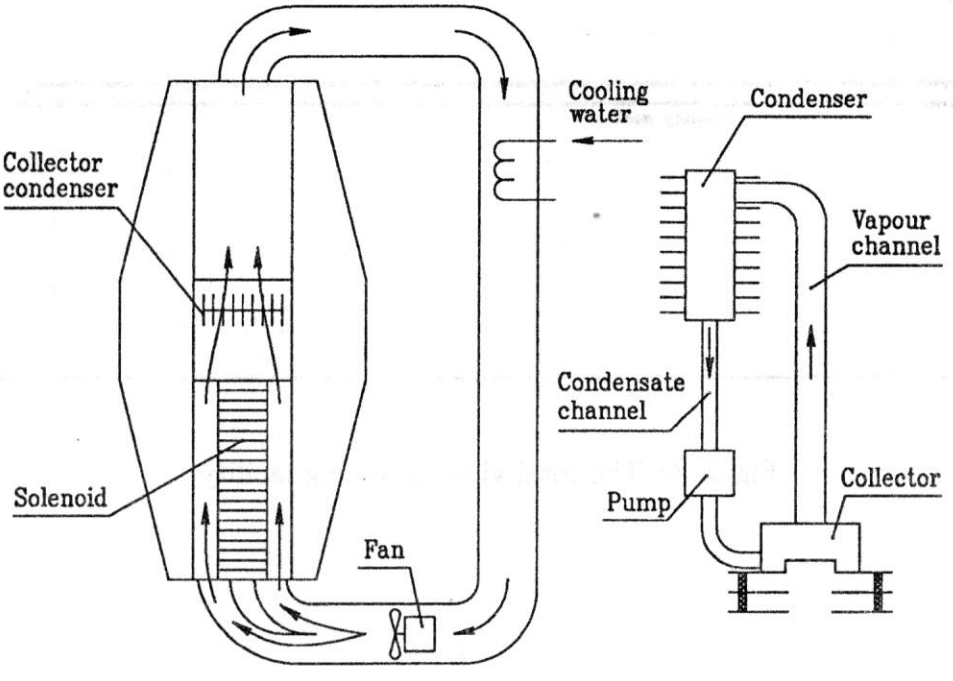

Figure 5: Cooling system of the solenoid.

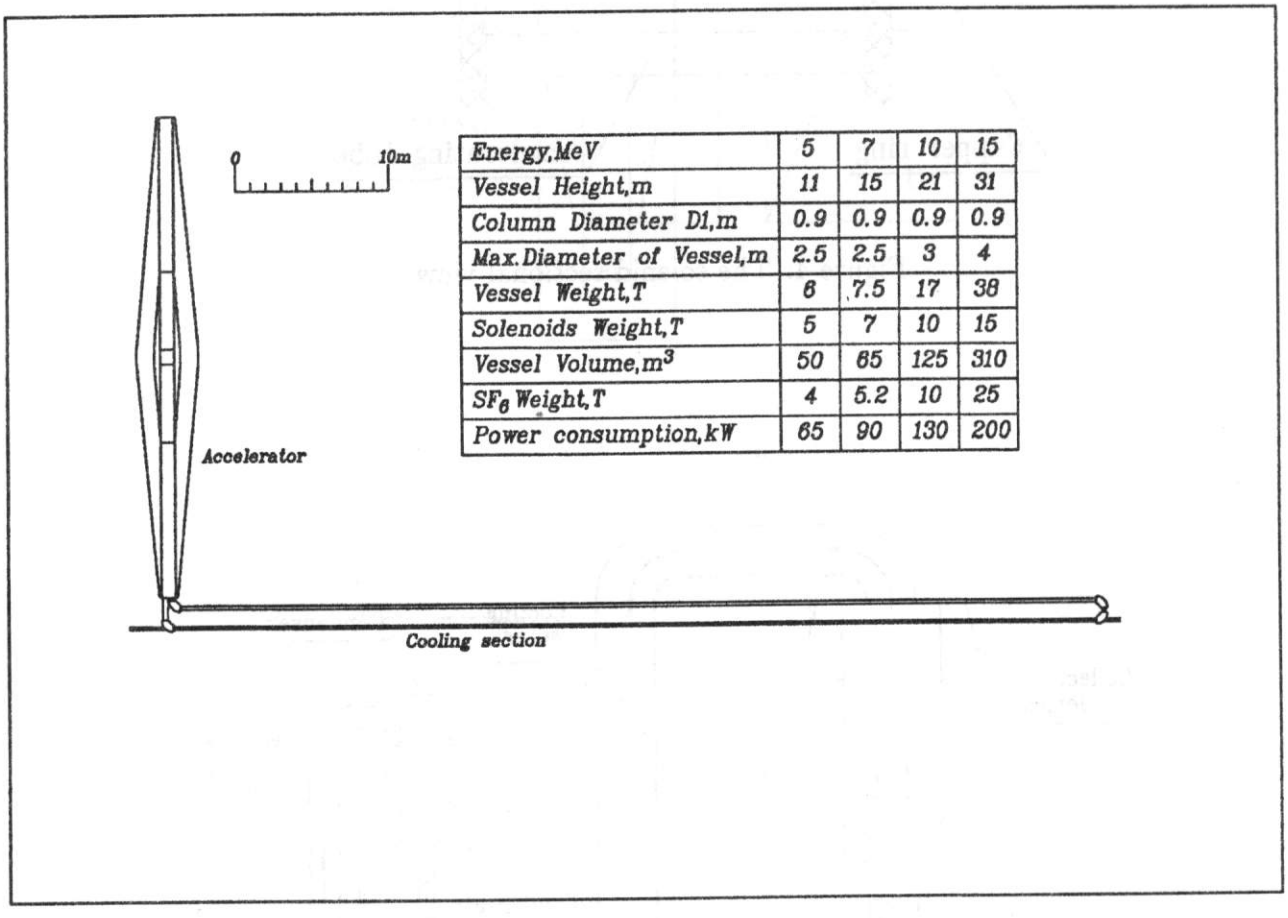

Energy,MeV	5	7	10	15
Vessel Height,m	11	15	21	31
Column Diameter D1,m	0.9	0.9	0.9	0.9
Max.Diameter of Vessel,m	2.5	2.5	3	4
Vessel Weight,T	6	7.5	17	38
Solenoids Weight,T	5	7	10	15
Vessel Volume,m^3	50	65	125	310
SF_6 Weight,T	4	5.2	10	25
Power consumption,kW	65	90	130	200

Figure 6: The total view of cooling facility.

Table 1: Main parameters of installations.

Energy of electrons,	MeV	5	7	10	15
Height of tank H,	m	11	15	21	31
Diameter of column D1,	m	0.9			
Maximal diameter of tank D2,	m	2.5	2.5	3	4
Mass of tank,	tonnes	6	7.5	17	38
Mass of solenoid,	tonnes	5	7	10	15
Volume of tank,	m^3	50	65	125	310
SF6 mass,	tonnes	4	5.2	10	25
Power consumpsion,	kW	65	90	130	200

Linac—based electron cooling device

N.S.Dikansky, V.V.Parkhomchuk, V.M.Petrov, V.G.Shamovsky,
A.N.Smirnov, P.D.Vobly, V.N.Volkov.

The electron beam for electron cooling is traditionally obtained by direct electrostatic acceleration. But for the higher electron energies (above 5 MV), the difficulties in implementing sharply increase and set natural limits for such method in use.

That is why it is interesting to consider alternative ways for obtaining a high energy electron beam applicable for the electron cooling. Thus, to obtain the electron cooling at the collider ENC for GSI storage ring, it is necessary to have an electron beam with an energy of 15 MV, a current of up to 1A, an energy spread of $\frac{\Delta\gamma}{\gamma} \sim 10^{-4}$, and $\frac{\Delta P_\perp}{P_\parallel} \sim 10^{-4}$ spread in a transverse momentum.

As the ion beams cooled at GSI are bunched with a σ_z of 10 cm, and the bunches follow each other at a 60 MHz frequency, the cooling electron beam can be bunched as well.

The usual source of bunched electron beam of such energy and intensity is a linear accelerator. The main problem for using the linear accelerator for our purposes is a way to meet high precision requirements to the energy and momentum spreads of beam.

For the sake of definiteness, let us consider a device, one of possible rough drawing of which is given in Fig.1. The version of linear accelerator under consideration consists of six identical units, each unit consists of four 60 MHz frequency resonant cavities with a 700 KV voltage, one 180 MHz frequency resonant cavity, and one 300 MHz frequency resonant cavity (2 of these 6 units are shown in the figure). A rough drawing of the main 60 MHz resonant cavity is given in Fig.2. The supposed characteristics of the resonant cavities are given in Table 1.

Table 1.

N	1	2	3
Frequency of a cavity (MHz)	60.0	180.0	300.0
Voltage at a gap (kV)	700.0	466.0	56.0
Amount of cavities	24	6	6
Shunt resistance (ohm)	$2.4 \cdot 10^6$	$3.5 \cdot 10^6$	$15 \cdot 10^3$
Q-factor	$15.5 \cdot 10^3$	$33 \cdot 10^3$	$14 \cdot 10^3$
Power dissipated by one cavity (kW)	104.0	31.0	1.5
Total power dissipated by all the cavities (kW)	2500	181	9
Power consumed by electron beam in one cavity (kW)	70.0	-47.0	5.6
Total power consumed by electron beam in all the cavities (kW)	1680	-287	34

The bunched electron beam of 0.5 - 1 MV energy is injected to the linear accelerator from an electrostatic preinjector. The whole cavity system as well as the preinjector is immersed in a longitudinal 0.5 T magnetic field, created by a superconducting solenoid.

The main factors, affecting the energy and momentum spreads of the electron beam in this linear accelerator, are the following:

1. The time dependence of the accelerating RF voltage in the accelerating gap during the passage of a short electron bunch.

2. The influence of a space charge field on the energy spread of particles.

3. The influence of inhomogeneity of the longitudinal magnetic field and of the electric field transverse components of the cavity on an increment in transverse momentum of particles.

4. The influence of the wake field upper harmonic of the cavity on the motion of particles.

We shall briefly consider each of these factors.

1. The way to obtain the rather constant RF voltage in a cavity during the passage of a short bunch through the accelerating gap is well known. For this one needs only to add the required quantity of upper harmonics of a necessary amplitude to the main RF harmonic. In order to meet a requirement of $(\frac{\Delta\gamma}{\gamma})_{gap} \sim 10^{-4}$ for every section of the accelerator, one need only to add both the third harmonic with a relative amplitude of 0.167 and the 5th one with a relative amplitude of 0.02 to the leading harmonic. The additional correcting cavities of 180 and 300 MHz frequencies, shown in Fig.1, are used for this purpose.

2. When the short bunch passes through, the particles which are at a distance s from its center are affected by the longitudinal component of the space charge force. Let us suppose that the density distribution of bunch particles is parabolic in form.

$$n(s) = \frac{3}{4} \cdot \frac{N}{\sigma_x} \cdot (1 - \frac{s^2}{{\sigma_x}^2})$$

Then once the bunch passed the distance l, the particle being at a distance s from the bunch center has an additional longitudinal momentum.

$$\frac{\Delta P_{\|}}{P} = \frac{3}{2} \cdot \frac{N r_e g}{{\sigma_x}^3 \gamma^3 \beta^2} \cdot ls$$

Here: $g = 1 + 2ln(\frac{a}{b})$,
N is the number of the electrons in the bunch
a is the radius of the beam
b is the radius if a vacuum chamber
r_e is the classical electron radius of 2.810^{-13} cm.

At high energies ($\gamma \sim 10$) this value is negligibly small ($\sim 10^{-5}$) when the bunch passes the distance of 100 m. But at low energies ($\gamma \geq 1$) the value $\frac{\Delta P_{\|}}{P}$ will be equal to 10^{-3} just after the bunch passes 1 m. But, as the phase dependence of the longitudinal

momentum increment is a linear one at a chosen special form of the density distribution of bunch space charge, this effect can be easily corrected.

Here it is pertinent to note the following. At a first glance it would seem that the accelerator operating in a range of rather short wave lengths of about $1 \div 10$ cm is more attractive, as its overall dimensions are relatively small as well as its cost. But as $\frac{\Delta P_{\parallel}}{P} \sim {\sigma_z}^3 \sim {\omega_0}^3$, where ω_0 is a main frequency, it is obvious that the difficulties, related to the effect of space charge on the accelerator particle dynamics, sharply increase with an increase in the accelerator working frequency and become insuperable. Besides, there are much more problems connected with the necessity to obtain super short electron bunches at a stage of their injection to accelerator and to significantly elongate the accelerated bunch. In this connection it is seen that we should use the minimum RF frequency. So the accelerator working frequency is chosen considering the reasons just listed.

3. The particle can acquire an additional transverse momentum, when it moves in the inhomogeneous electrical field of the cavity, and effected by small inhomogeneities of the longitudinal magnetic field.

It can be shown that in the case of small disturbances the transverse momentum increment of a particle can be compensated by a special correcting magnetic lens. This lens creates an additional disturbance of longitudinal magnetic field of the required amplitude. It should be located at a point determined by a phase of a Larmour motion. Fig. 3 shows the possibilities to compensate the transverse momentum increment of a particle moving in the inhomogeneous electrical field of the cavity. There are shown trajectories of particle motion in the transverse momentum space for the case of absence of such compensation (b) and for the case of presence of a correcting lens (c). Fig.3(a) presents strength component distributions of the cavity electrical RF field and of the leading magnetic field along the direction of particles movement.

The precise adjustment of all the correcting lenses positioned after every resonant cavity is a delicate and labour-consuming work. Besides, errors in production and alignment of the cavities lead to an increase in the transverse momentum of particles. This casts some doubt upon the real ability to obtain the accelerated electron beam of required characteristics and hence upon the serviceability of the proposed device. But there is one rather elegant way to avoid these difficulties. Let us assume the bunch moves along the system of cavities, acquiring the transverse momentum component increment at the accelerating gaps for some reasons. Assume there is a special correcting lens at the accelerator outlet (for some cases, when the total value of transverse momentum is sufficiently small, its role is played by the electrical field inhomogeneity of the last cavity).

Let us consider an ideal case, when the particle motion disturbances caused by cavity fields are in one plane, for example X-Z (Z is the direction of the particle motion). Here we can always eliminate the increment of particle transverse momentum, acquired during the acceleration. For this we need to properly choose the value and phase of the disturbance created by the correcting lens.

Obviously for the case of one-dimensional disturbances, we can always eliminate the

residual increments of particle transverse momentum, acquired during the acceleration, by a proper choice of these two parameters. To show the efficiency of the described method we have simulated the simplest model. We supposed that the disturbance in the transverse motion of particles was due to a random error in the cavity angle alignment in a plane (X–Z) (Z is the direction of particles motion; the value of a standard deviation in our calculations was adopted as 0.01). We calculated the particle transverse momentum (at the accelerator outlet) depending on the value of the leading longitudinal magnetic field. The results are presented in Fig.4(a) and Fig. 4(b). It is seen that this value is close to zero at a specific b. The extension of the described method to the case of non-one-dimensional disturbances of the particle transverse motion is obviously out of principal difficulties. This correction method was successfully used for electron cooling at INP.

4. The wake fields of upper harmonics for the current with a peak amplitude of 1A, and a bunch length of 10 cm following each other at a frequency of 60 MHz were calculated for the main 60 MHz resonant cavity. Relatively small dimensions of the cavity provide a low beam–imposed voltage at an accelerating interval. Fig.4(a) shows the spectrum of upper axial symmetrical modes in the cavity, which are excited by the beam. The values of both active and reactive components of the imposed RF voltage are given in Fig. 4(b) and 4(c), respectively. As is evident, the imposed voltage values are small. Moreover, the reactive component of the imposed voltage, contributing significantly to the amplitude, linearly depends on phase, and this value can be easily corrected when needed.

So, the results of the above estimations show, that there are reasons to hope to obtain the electron beam parameters required for electron cooling. This will enable to extend the use of electron cooling of heavy particles in a several Gev range energies per nucleon.

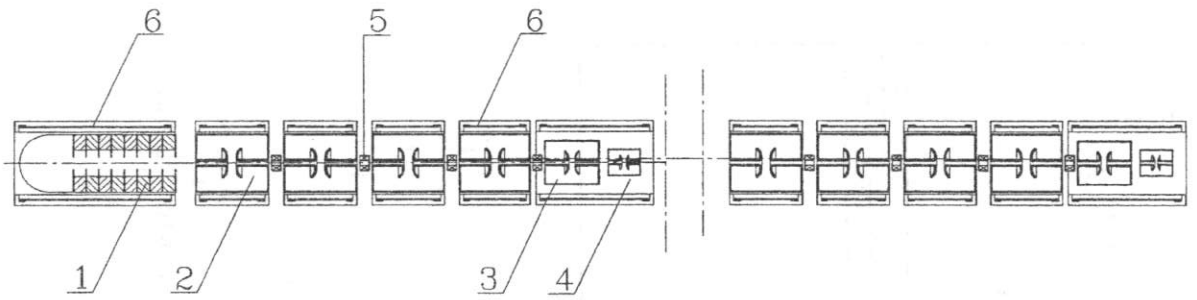

Fig.1 General view of LINAC

1–preinjector,
2–main cavity (F=60MHz),
3–correcting cavity (F=180MHz),
4–correcting cavity (F=300MHz),
5–correcting magnet lens,
6–superconducting solenoid

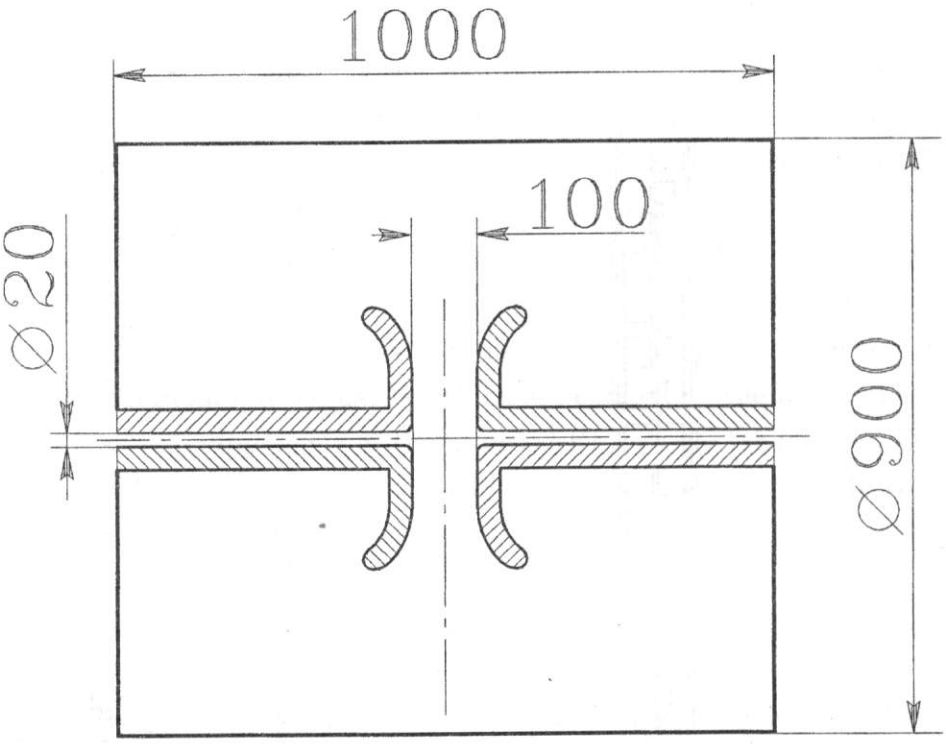

Fig.2 General view of main cavity,
(F=60MHz, U=700kV)

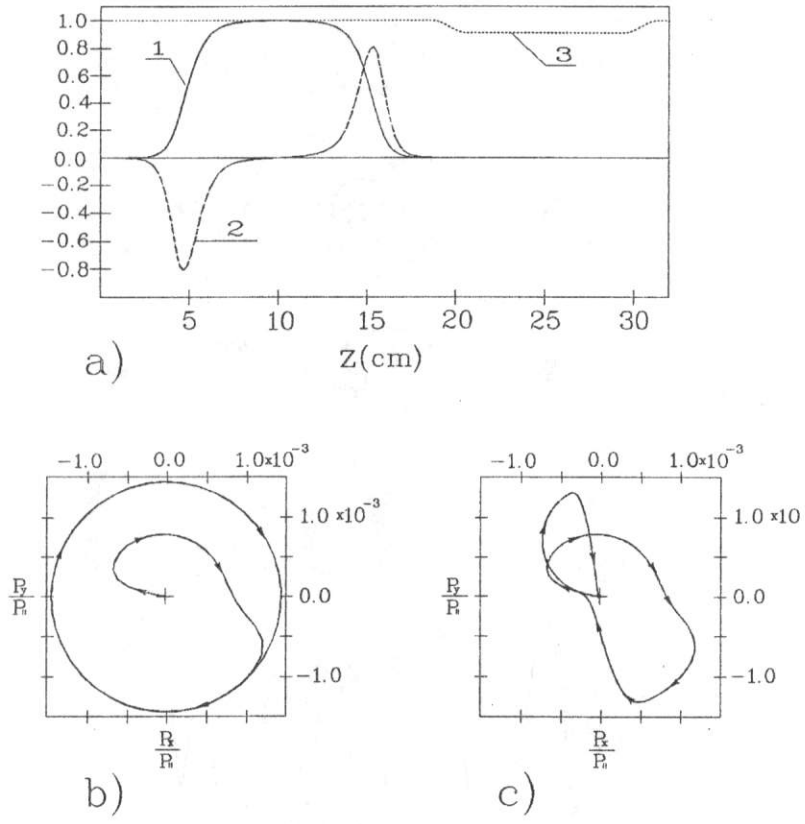

Fig. 3 Correction ot the influence of inhomogenity in cavity electric field on the transverce motion of electron.

a) distribution of fields
   1–longitudinal electric field of cavity
   2–radial electric field of cavity
   3–longitudinal magnetic field
b) trajectory of the particle motion in a transverse momentum spase (correcting lens is absetnt)
c) trajectory of the particle motion in a transverse momentum space (correcting lens is present)

Gun and collector for FNAL recirculation experiment

G.F.Kuznetsov, A.N. Sharapa and A.V. Shemyakin
Institute of Nuclear Physics, 630090 Novosibirsk, Russia

The gun and collector developed for the FNAL recirculation experiment are presented. Results of their tests at the INP test bench are described. The electron beam of 0.5 A current is formed, accelerated up to 50 kV and its energy is recuperated in the collector with the relative current loss less than 10^{-4}. A simple formula for an estimation of the collector secondary emission coefficient is suggested.

1 Introduction

The present paper is related to the high voltage electron cooling project being under development at FNAL [1]. Contrary to the existing electron cooling devices, a beam confinement by a longitudinal magnetic field is not used here. The beam is accelerated and decellerated inside Pelletron accelerator.
The characteristic feature of the chosen scheme is a strict current loss limitation at the acceleration, transportation and deceleration of a beam. The relative value of the loss should be less than 10^{-4}, which is to put heightened requirements to the gun and collector.
The first stage of experiment supposes to achieve a reliable recirculation of 500 mA, 2 MeV electron beam. The electron gun and collector intended for this stage were developed, produced and tested at BINP (Novosibirsk, Russia). [1]
This paper describes the gun and collector, suggests the model for the determination of secondary electron flow from the collector and presents experimental results of the gun and collector test, performed at INP.

[1] In frames of the Accord No RU/03533872/60221 between FNAL and BINP.

Preprint submitted to Elsevier Preprint *23 April 1997*

2 The electron gun

Requirements to the electron gun are shown in Table 1.

Table 1
Requirements to the electron gun

electron energy at the gun exit	up to 50	keV
beam current	from 0 to 500	mA
beam diameter in the Pelletron acceleration column for the whole range of the beam current	less than 25	mm
part of electrons in the halo	less than 10^{-4}	

There are two groups of problems for the gun optics design. The first one is related to characteristics of the main part of beam (first three items in the Table 1). From this point of view, the range of possible solutions for the gun optics is rather wide, and they can be tested by a trustworthy computer simulation.

The second problem is connected with electrons the movement of which dramatically differs from the one of the main beam (a beam "halo"). Causes can be very different. For instance, such a halo can be created by scattering at a residual gas, by emission from a side surface of the cathode, by an influence of the heater current etc.. Such electrons go to the column electrodes and initiate the breakdowns. For a DC operation, the breakdowns start from the current loss of tens microamperes. The goal to minimize the share of electrones in the halo was the main one at the gun development.

It is difficult to simulate all effects which could produce the halo. The basis for the choose of the gun geometry was our experience and qualitative consideration. The final conclusion is that the smaller is the cathode diameter the better, and the minimum diameter is determined by the cathode emission ability. For the current of 500 mA, the cathode STD134 which diameter is 3.4 mm was choosen. The gun drawing is shown in Fig. 1.

One of the most important sources of the halo is an emission from a cathode side surface. Traditionally, an electrode with zero potential (Pierce electrode) is placed around the cathode to shape the beam. It is difficult to make a thermal gap between the cathode and a Pierce electrode less than few tenth of millimiter. Electrons are emitted from the cylindrical part of the cathode, go away from the gap and create the beam halo. For guns with small diameter cathodes, as simulation shown, this parazite emission can be up to one percents of the beam current. To suppress this emission, an approach described in [2] was used. The "Pierce electrode" is isolated from the cathode and a negative potential is applied to it so that a zero equipotential touched the cathode edge is formed. This electrode can be used also to control the beam

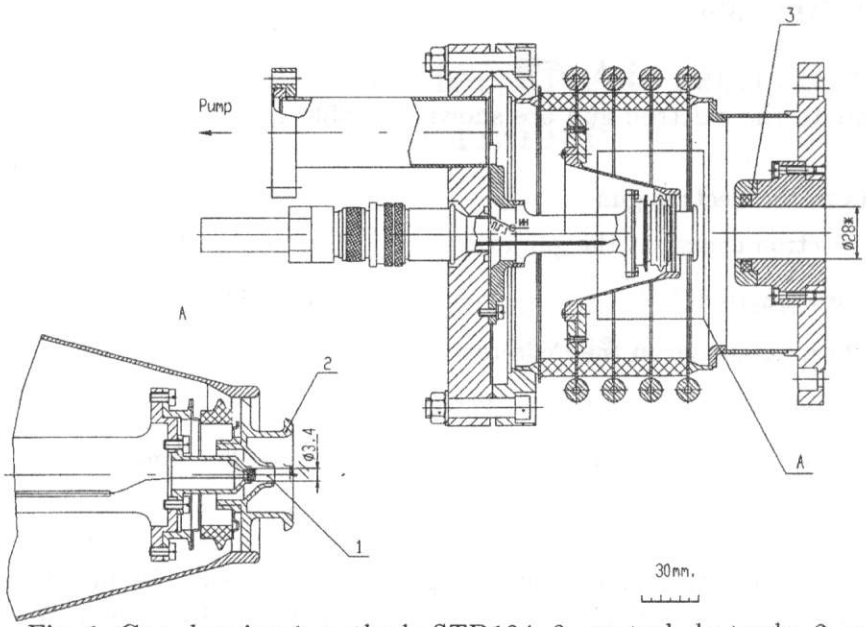

Fig. 1. Gun drawing.1- cathode STD134, 2- control electrode, 3- anode.

current, and we will denote it the control electrode.
Also, the current can be regulated by the cathode emission ability varying at the heater current change. Both methods give similar simulated dependences of the beam size on its current. Note, that all simulation in this work were made by SuperSAM code [3]. Evidently, the smaller is the beam size in the

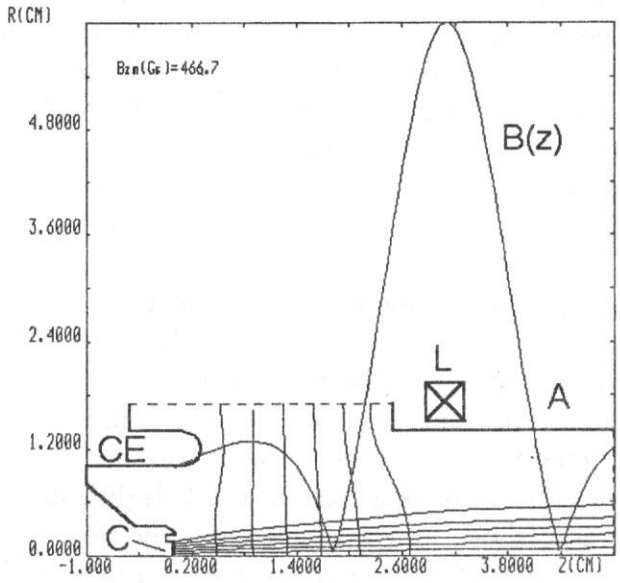

Fig. 2. Sample of a gun simulation.
The anode potential $U_a = 35kV$, potential of the control electrode U_{ce} is equal to the cathode one, the beam current $I = 0.5A$. The gun works in the space charge limited regime. C- cathode, CE- control electrode, L- permanent magnet lens, A- anode

accelerating column, the more tolerant is the accelerator operation to align-

ment errors and to perturbations (for instance, to external magnetic fields). Because of this, the second gun version, which differs from the first one only by a magnet lens inside the anode, was developed and tested. The lens is a permanent magnet ring with the maximum magnetic field at the axis of 460 Gs. An example of simulated beam trajectories in this gun is shown in Fig.2. The maximum beam size in the column is twice less than one for the first gun version.

A pecularity of the gun with the lens is a possibility to operate at zero control electrode voltage. Simulations show, that an electron movement inside the thermal gap is determined by the magnet field of the lens. As result, trajectories of electrons, emitted from the side surface, differ slightly from ones of the main beam, i.e. the electrons do not form a halo.

Characteristic features of the gun and some results of the simulation are listed in Table 2.

Table 2

Characteristic features of the gun

cathode diameter	3.4 mm
cathode current density:	
average	up to $5 A/cm^2$
homogenity	10%
current regulation	by a negative voltage at the control electrode or by the heater current
control electrode voltage	
shut off the gun	$-0.06 \cdot U_a$
calculated maximum beam	
diameter in the column:	
without any lens in the anode	16 mm
with the permanent magnet lens	8 mm

3 Test bench

Tests of the gun and collector were made at the test bench shown in Fig. 3 in a DC regime. The gun generates the beam of energy $e \cdot U_a$, where e is the charge of electron and U_a is the anode potential. Further, electrons are accelerated up to the drift tube potential U_t, decellerated in two steps (down to the collector anode potential U_{ca} and to the collector one U_c). In front of the collector a suppressor electrode is mounted. A decrease of its potential $U_s < U_c$ supresses a secondary electron flow from the collector.

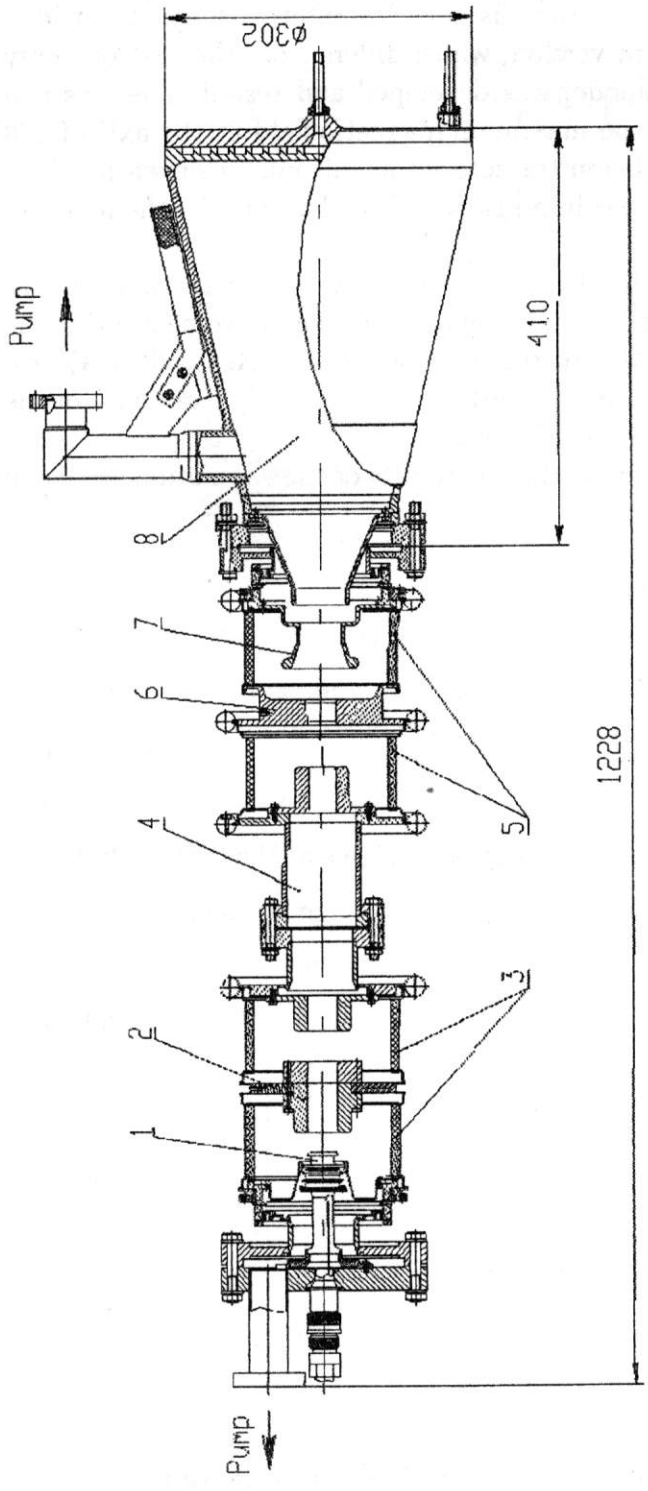

Fig. 3. Test bench drawing.
1- gun, 2- gun anode, 3,5- high voltage isolators, 4- drift tube, 6- collector anode, 7- suppressor, 8- collector.

The reduction of this flow was one of the most comlicated problems of the test. For measurements of the beam halo, a special collector regime with a

very low part of electrons escaped from the collector was used. This regime is not appropriate for the long operation of the collector because of thermal problems and is not described here.
The maximum drift tube voltage is 50 kV. The current loss δI is measured as a sum of currents to the anode , drift tube and collector anode. The pressure near the cathode is between $1 \cdot 10^{-6}$ and $1 \cdot 10^{-7}$ mbar with the beam on.
In the most experiments, a permanent magnet lens was mounted on the drift tube to provide an optimum beam focussing to the collector. Correction coils located at the ground potential near the drift tube were used to change the beam position in the transverse directions.
At Pelletron, an acceleration field of the column forms a strong enough focussing electrostatic lens at the gun exit. To model an influence of this lens in our test, the focal distance of the magnet lens in the anode is reduced, or, for the first gun version, a large enough ratio of the drift tube and anode potentials is used. For the last case, estimation shows, that the electrostaitic lens in Pelletron at $U_a = 50kV$ and an acceleration rate 17 kV/cm corresponds to $U_t/U_a = 4$ in the test.
The electron flight time in the test bench is about the one in Pelletron from the gun to a fist magnet lens. Correspondingly, deviations of disturbed electron trajectories from the ones of the main beam are approximately the same in the test and in the Pelletron. Therefore, the halo particles, which will reach the Pelletron column electrode, should produce the current loss at the test bench.
Of course, it is impossible to completely model in the test the beam behavior in the experiments at Pelletron. The main goal of the work was to check the results of the computer simulation.

4 Experimental results of the gun measurements

The main result of the gun measurements is as follows:
-the halo is practically absent, if the side surface emission is suppressed;
-the beam behavior is in accordance with result of the computer simulation.
At the optimum tuning the current loss is less than 1 μA up to the beam current of 500 mA and is close to the precision of measurements (Fig.4).
Here the beam current is regulated by the control electrode voltage. The same behavior was found for the regulation by the heater power.
The dependence of the current loss on the transverse beam displacement (Fig.5) shows a sharp beam edge, i.e. the beam halo is absent.
The transverse beam displacement gives a possibility to analyze the current dependence of the beam size. The current loss as a function of the beam current for different beam position is shown in Fig.6. The beam diameter is low at the low current, when the cathode emitted surface is small, and at the current

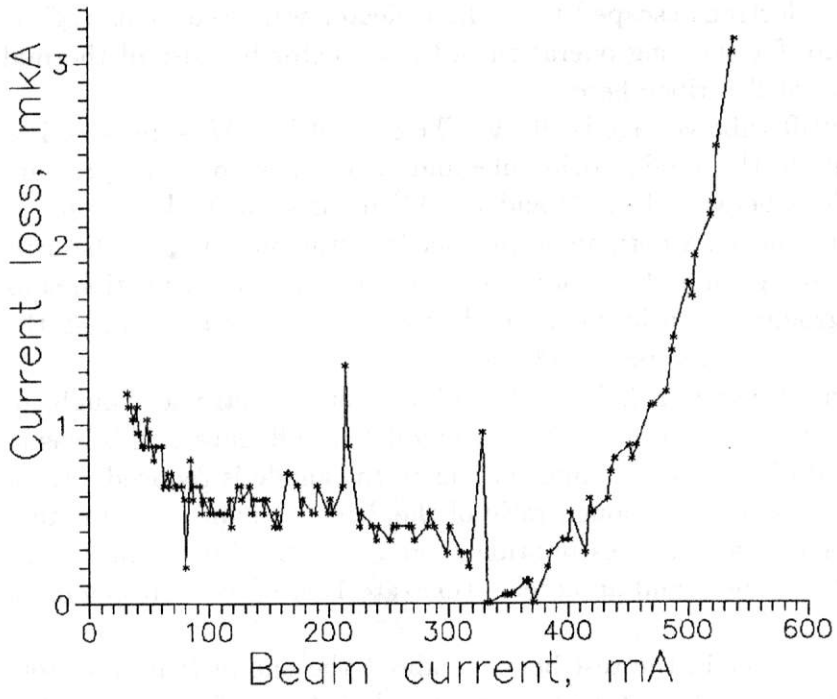

Fig. 4. Current loss as a function of the beam current.
$U_a = U_t = U_{ca} = 50kV, U_{coll} = 3.5kV$.

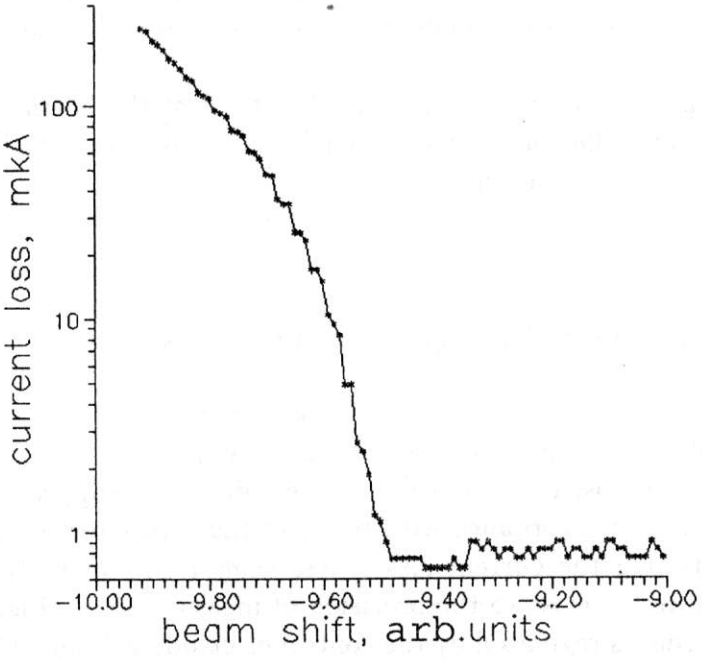

Fig. 5. Current loss as a function of the beam displacement.
$U_a = U_t = U_{ca} = 35kV, U_{coll} = 3.5kV, I = 200mA, U_{ce} = -0.7kV$. 1 unit corresponds approximately to the beam shift of 2 mm.

of 200 mA. Simulation made for the last regime indicates the zero equpotential touched the cathode edge.

Results presented above are obtained for the gun with the magnet lens in the anode. The gun without the lens provides the low current loss also, if the

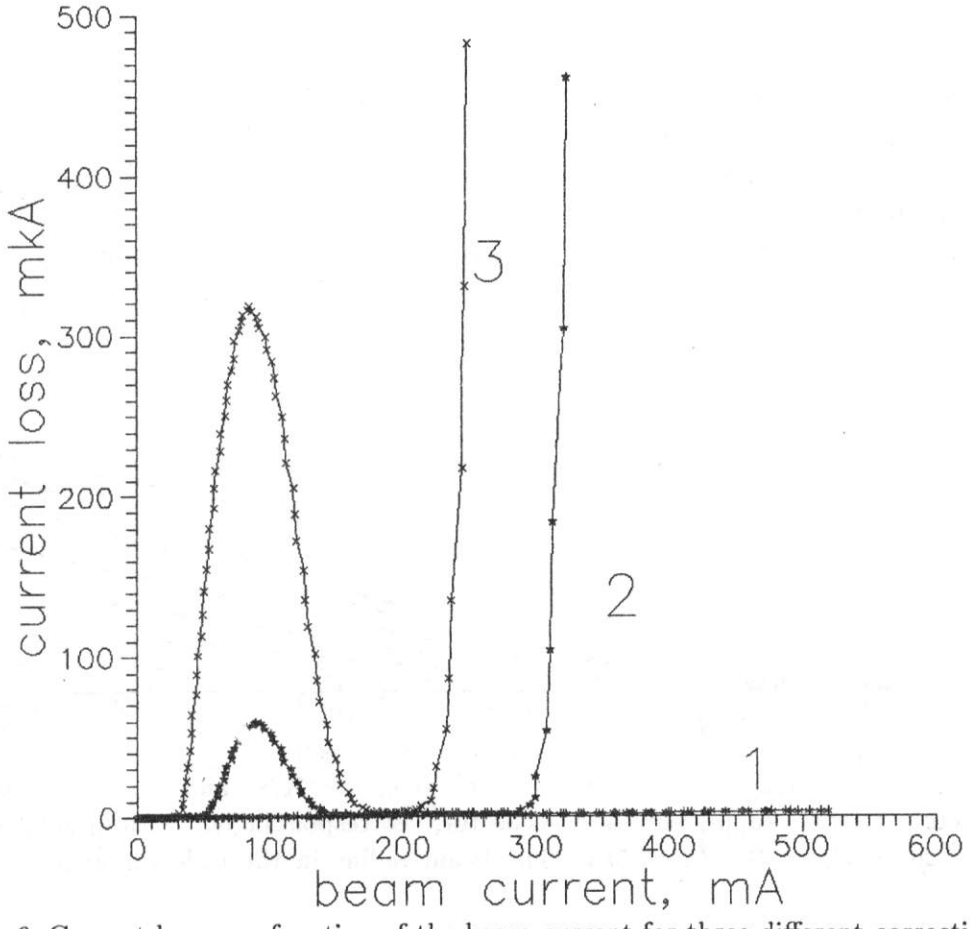

Fig. 6. Current loss as a function of the beam current for three different correction coil currents.
$U_a = U_t = U_{ca} = 35kV, U_{coll} = 3.5kV$. The curve 1 corresponds to the optimum correction, the estimated maximum shift of the beam in the drift tube for the curves 2 and 3 is aproximately 6 and 8 mm, correspondingly.

electrostatic lens at the gun exit is strong enough, $U_a/U_t < 0.3$. For higher relative values of U_a, the $\delta I(I)$ dependence becomes similar to the curves 2,3 in Fig.6, i.e. there is a range of the beam current, where the current loss is high for any tuning.
In this set of measurements the current loss increases dramatically for control electrode potentials close to the cathode one. The bounary value of the control electrode voltage is $U_{ce} = -0.003 \cdot U_a$. This value corresponds in the computer simulation to the beginning of the cathode side surface emission.
At the anode and tube potentials simulated the electrostatic lens at the accelerator column entrance ($U_a = 10kV, U_t = 40kV$), the maximum current with low current loss is 70 mA. According to the "3/2 low", the current in the accelerator at $U_a = 50kV$ will be 770 mA.
So, the both versions of the gun generate the beam with the part of electrones in the halo less than $2 \cdot 10^{-6}$, matched with the Pelletron accelerator column in the beam current range from 0 to 500 mA.

5 The electron beam collector

As in the case of the gun, two problems should be solved at a collector design. First, it is necessary to transport the primary beam inside the collector and to provide a proper power density distribution at the irradiated surface. It is a simpler part of the work, because the trajectories can be simulated by computer. An example of simulation for the collector under discussion is shown in Fig.7. Second problem, which is a prediction and a decrease of the current

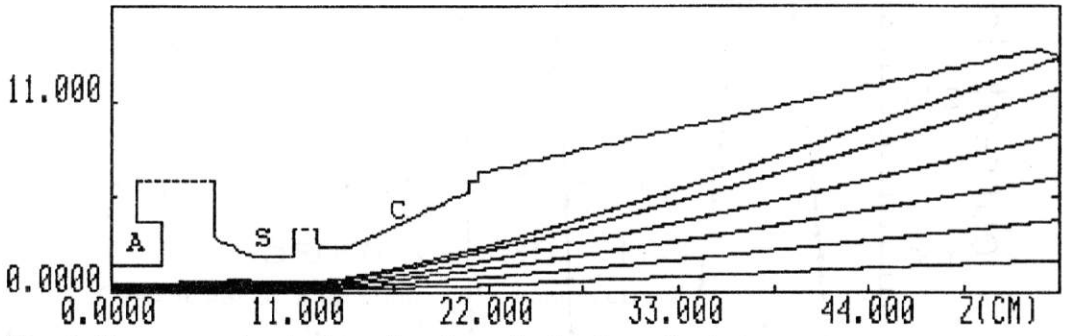

Fig. 7. Computer simulation of trajectories in the collector.
The beam current is 500 mA. The symbols A,S and C label the collector anode, suppressor and collector, correspondingly, with potentials $U_a = 50kV, U_s = 2kV, U_c = 5kV$. The beam radius in the collector anode is 5 mm.

loss due to the secondary electron flow from the collector, is considerably more complicated.
To describe the efficiency of the secondary electron capture by the collector, the notion of the collector secondary emission coefficient [4] can be used:

$$\sigma_{col} = \frac{\Delta I}{I} \tag{1}$$

where δI is a current of secondary electrons escaped from the collector. For systems with a longitudinal magnetic field high enough, the main mechanisms used for detaining secondary electrons are a magnetic mirror and a potential barrier before the collector. In [4], a simple half-empiric formula for the estimation of collector secondary emission coefficient in this case is obtained:

$$(\sigma_{col})_{magn} = k \cdot (\frac{U_m}{U_c})^2 \cdot \frac{H_c}{H_0}, \tag{2}$$

where U_m, U_c are potentials, and H_0, H_c are magnetic field strengths in the area of potential barrier and collector surface respectively, k is a coefficient depending on the collector material and the surface condition. The estimation

(2) is in a good agreement with the results of measurements [5] for $\sigma_{col} \ll 1$, where k about 0.1 was found.

In a sufficiently strong magnetic field the electron trajectories are "freezed" in the field lines. Because of this, $(\sigma_{col})_{magn}$ in (2) is determined by a magnetic field configuration and does not depend on the collector geometry. For the collector without any guiding magnetic field, its geometry may be a determining factor. It is easy to calculate a value of σ_{col} for the equipotential collector of a simple geometry (Fig.8), in which all electrons of the primary beam fall on the collector surface approximately perpendicularly. In such a collector, a share of the secondary electrons escaped from the collector is the same for all points of the exposed surface.

A secondary electron, which initial kinetic energy and angle are E and θ,

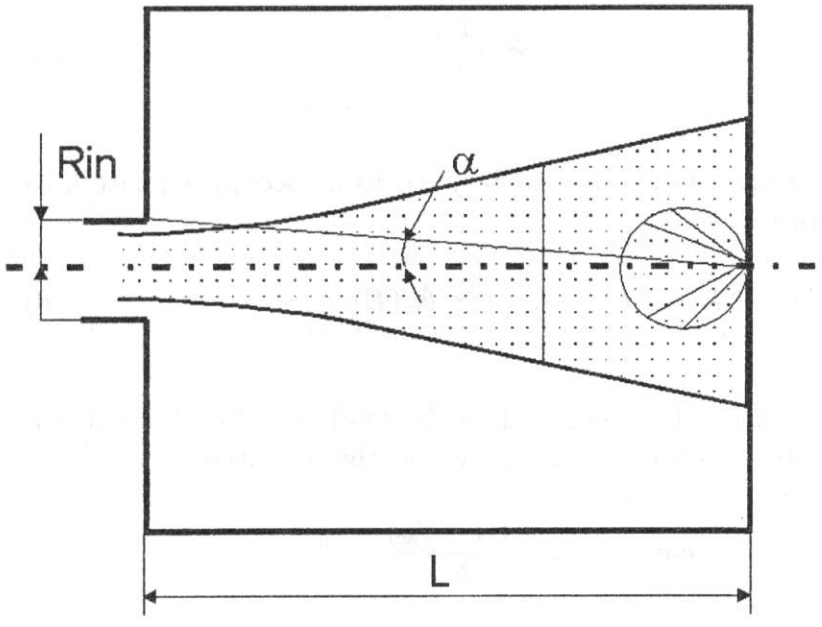

Fig. 8. The collector model.

goes out of the collector, if it is located in the region of the phase plane (θ, E) under the line 1 in Fig.9a

$$\theta < \alpha = \arctan(\frac{R_{in}}{L}), \tag{3}$$

where R_{in} and L are the input hole radius and length of collector. At the

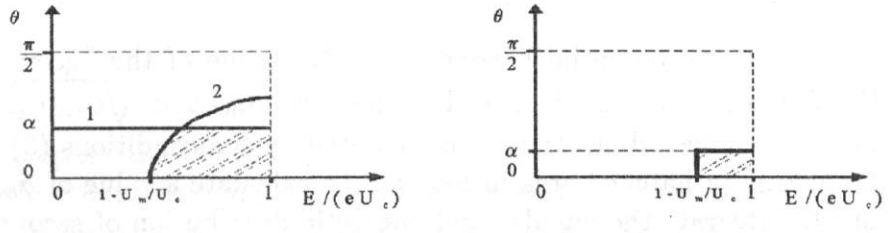

Fig. 9. The phase space of secondary electrons.

cosine angular distribution of secondary electrons,

$$(\sigma_{col})_{geom} = \sigma_0 \cdot \sin^2(\alpha) \approx \sigma_0 \cdot (\frac{R_{in}}{L})^2, \tag{4}$$

where σ_0 is a full coefficient of the secondary emission. In the collector potential range of practical interest, (0.5 - 5 kV), σ_0 is of order 1 (0.4 - 0.8).
The potential barrier efficiency can be estimated from the measurement results presented in [4]. These data show the fraction of secondary electrons overcoming the potential barrier in a flat electric field. The dependence is close to the parabolic one:

$$(\sigma_{col})_{pot} = k \cdot (\frac{U_m}{U_c})^2 \tag{5}$$

and $k \approx 0.1$. In this case, escaped secondary electrons occupy a phase area under the curve 2 in Fig.9a:

$$E > e(U_c - U_m), \theta < \theta_m(E). \tag{6}$$

The maximum angle $\theta_m(E)$ is determined by the condition, that the longitudinal component of the electron velocity is zero at the potential U_m:

$$\cos^2(\theta_m) = \frac{e(U_c - U_m)}{E}. \tag{7}$$

Note, that the formula (5) is valid only for $U_m \ll U_c$. In this case, k is approximately equal to the backscattering coefficient.
The formula (5) is appropriate to the "open" collector when $R_{in} \approx L$. Such a collector is of limited interest, because it is impossible to obtain a low loss ($dI/I < 1 \cdot 10^{-4}$) for large enough values of the collector perveance U_m [6]

$$P_{col} = \frac{I}{U_c^{\frac{3}{2}}}. \tag{8}$$

The collector with the potential barrier and a low value of the "geometric factor" R_{in}/L is much more effective. For the case $R_{in}/L < \sqrt{U_m/U_c}$, the phase space of the escaped electrons is intercepted by the conditions (3) and (6) simultaneously (a hatched area in Fig.9a). To calculate a value of σ_{col}, it is necessary to integrate the angular and energetic distribution of secondary

electrons $\rho(\theta, E)$ over this area:

$$\sigma_{col} = \int_0^{\alpha} 2\pi \cdot \sin(\theta) d\theta \int_{\frac{e(U_c - U_m)}{\cos^2(\theta)}}^{U_c} \rho(\theta, E) dE, \tag{9}$$

where $\rho \cdot d\Omega \cdot dE \cdot I$ is a current of secondary electrons, whose angle and energy are in the intervals $(\theta, \theta + d\theta)$ and $(E, E + dE)$ correspondingly. In a case of practical interest,

$$(\frac{R_{in}}{L})^2 \ll \frac{U_m}{U_c} \ll 1, \tag{10}$$

the result of calculation by (9) is influenced weakly by specific details of angular and energetic distribution, because the escaped electrons occupy a small part of the phase space, where the phase density is approximately constant. The collector geometry cuts the secondary beam which is close to the parallel one and contains α^2 part of all secondaries. The potential barrier reflects all electrons, whose energy differs from the energy of primary electrons by more than eU_m. Consequently, the phase area of escaped electrons is a rectangle (Fig.9b). In such a case, the share of these electrons is equal simply to the product of the density in this area ρ_0 to the phase volume, and the expression (9) is reduced to

$$\sigma_{col} \approx (\rho_0 \cdot \pi \cdot eU_c) \cdot \alpha^2 \cdot \frac{U_m}{U_c} \approx k_1 \cdot (\frac{R_{in}}{L})^2 \cdot \frac{U_m}{U_c}. \tag{11}$$

In this formula, the only term characterizing secondary emission properties of the material is the coefficient k_1. This value is of the same order as the backscattering coefficient, $k_1 \approx 0.1$.
Besides, this coefficient can be estimated from the results of experiments with the magnetized collector and the flat retarding electric field (formulae (2) and (5)). It can be shown, that in both cases the flow of escaped secondary electrons is also a product of the same phase density ρ_0 to the corresponding phase volume. Such an estimation gives $k_1 = 2 \cdot k$. Finally, the formula for the collector secondary emission coefficient is

$$\sigma_{col} \approx 2 \cdot k \cdot (\frac{R_{in}}{L})^2 \cdot \frac{U_m}{U_c}. \tag{12}$$

Lets compare the efficiency of collectors with and without magnetic field. From the comparison of (2) and (12) it is seen that the magnetic mirror ratio H_c/H_0 is an analog to the geometric factor $(R_{in}/L)^2$. At the equipotential

regime ($U_m/U_c = 1$), the secondary electron fluxes are equal, if

$$\frac{H_c}{H_0} = 2 \cdot (\frac{R_{in}}{L})^2. \tag{13}$$

The potential barrier efficiency is higher in a magnetized collector. The reason is in different types of angular distribution of the electrons reaching the barrier. As shown in [4], in the magnetized collector this distribution turns to be of a cosine type, whereas in collectors without any magnetic fields, with the condition (9), the electrons have small spread of angles.

6 Experimental results of the collector measurements

The experiments on determination of the collector secondary emission coefficient were carried out at the test bench given in Fig.3. As it is shown above, the beam halo is very low and the current loss is practically equal to the current of secodaries from the collector, $\delta I = \Delta I$.

6.1 Equipotential collector

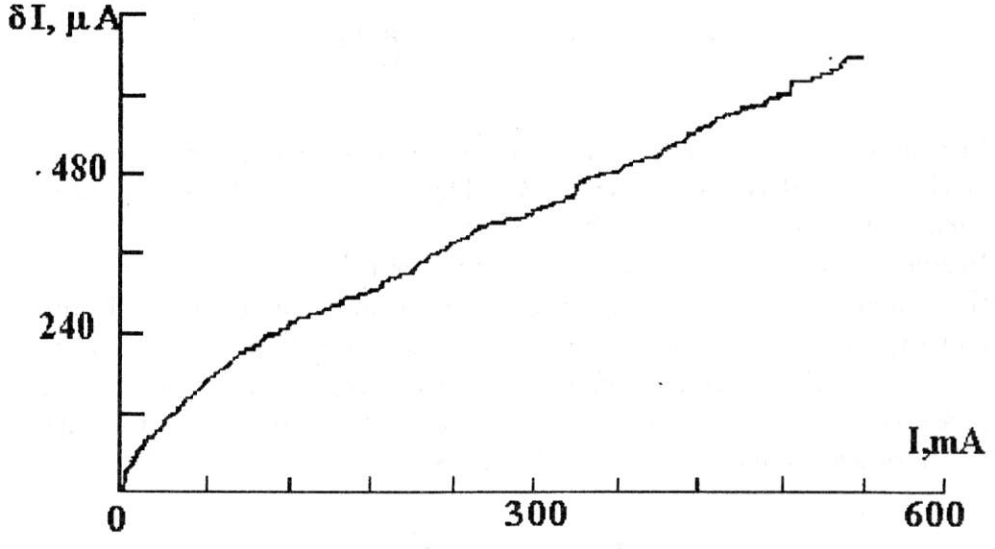

Fig. 10. Current loss as a function of the beam current in the equipotential collector. $U_s = U_c = 4.2kV$, collector anode potential $U_{ca} = 35kV$.

Fig.10 presents the current loss as a function of the beam current for the case of equal collector and suppressor potentials $U_s = U_c$. As simulations show,

in such a regime for all the currents from 0 to 500 mA the beam falls on a collector bottom, and the ratio R_{in}/L is approximately the same for all points of the collector surface.
Measured value of σ_{col} is changed from $5 \cdot 10^{-3}$ at small currents to $1.2 \cdot 10^{-3}$ at $I = 500mA$. The last value is in accordance with the estimation (4), because $(R_{in}/L)^2 = 2.5 \cdot 10^{-3}$ for this collector. σ_{col} at low currents is noticeably higher than that predicted by the formula (4). It is possibly connected with the generation of tertiary electrons. Their contribution to the loss in the equipotential collector may be of the order of the secondary electron contribution. Decreasing σ_{col} at increasing current is related to the formation of a potential barrier inside the collector, reflecting slow electrons.

6.2 Collector with a potential barrier

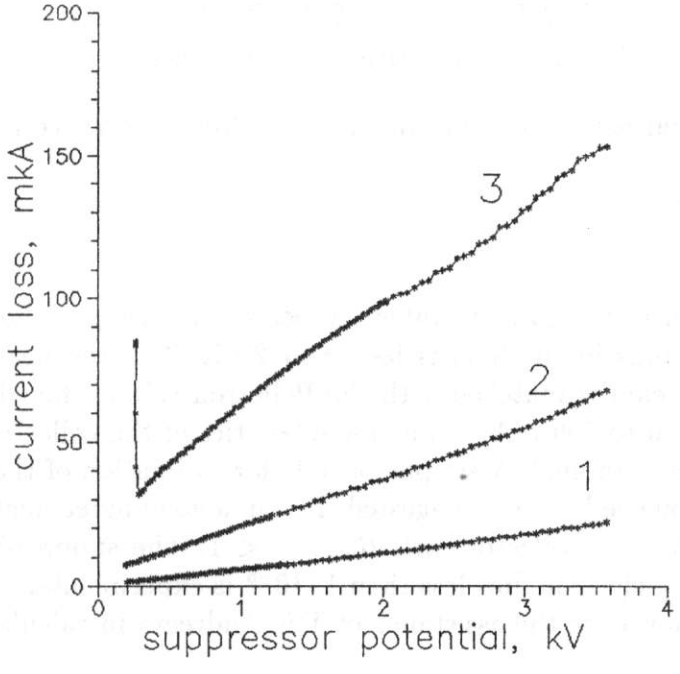

Fig. 11. Current loss as a function of the suppressor potential.
$U_c = 4.4kV, U_{ca} = 35kV$. The beam current for curves 1,2,3 is 50, 200 and 500 mA, correspondingly.

The current loss as a function of the suppressor electrode potential U_s is given in Fig.11. This function is close to a linear one according to (12), with k about 0.1. Minimum values of σ_{col} measured for different perveances of the collector are shown in Fig.12. The optimum for the suppressor potential was chosen for each point of this curve. The value of σ_{col} increases with the perveance. The reason is an increase in the optimum value of the ratio U_s/U_c with the perveance.

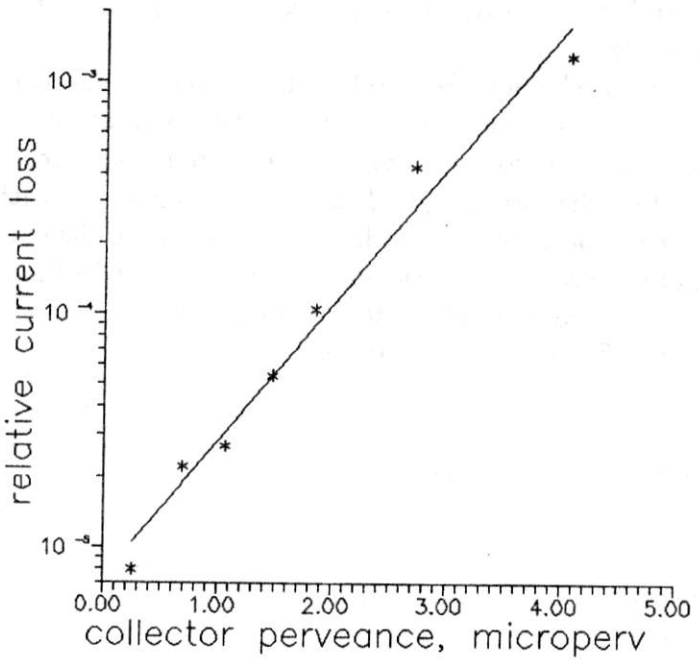

Fig. 12. Relative current loss as a function of the collector perveance $P_{col} = \frac{I}{U_c^{\frac{3}{2}}}$.

7 Conclusions

The produced and tested gun generates the beam practically without a halo. The part of electrons in the halo is less than $2 \cdot 10^{-6}$ at the beam current of 500 mA. The beam is matched with the Pelletron column for all currents in the range from 0 to 500 mA. Main characteristics of the collector without magnetic field are examined. A simple formula for estimation of the collector secondary emission coefficient is suggested. It is in a good agreement with σ_{col} value measured for the collector with $R_{in}/L << 1$. The suppression of the collector secondary electron flow less than $1 \cdot 10^{-5}$ is experimentally obtained.
The authors acknowledge the assistance of T.N.Andreeva in calculations.

References

[1] MEB E-Cool Design Report 1992, Indiana University Cyclotron Facility (October 1992); S. Nagaitsev, Electron Cooling for the Fermilab Recycler, in Proc. of the 1996 Workshop on Beam Cooling and Instability Damping (18-26 June 1996, Dubna), to be published in Nucl.Instr. Methods, **A**

[2] I.N.Meshkov, A.N.Sharapa and A.V.Shemyakin, Generation of an electron beam with the limit low phase volume, Jour. of Tech. Phys., v.59 (1989) p.146 (in

russian)

[3] D.M. Myakishev et al., Proc. XV Int. Conf. on High Energy Acc., Int. Mod. Phys. A, **2B** (1993) 915.

[4] Sharapa A.N. and Shemyakin A.V., Nucl.Instr. Methods, **A351** (1994),295

[5] Sharapa A.N. et al., Proceedings of Workshop on Beam Cooling and Related Topics, Montreux, Switzerland, 4-8 October 1993, edited by J.Bosser, Geneva, 1994, p.249.

[6] Sharapa A.N., Nucl.Instr. Methods, **A329**, (1993), 551.

Programs for Gun and Collector Simulations Developed at INP

A.V.Grudiev, D.G.Myakishev, M.A.Tiunov, V.P.Yakovlev

Budker Institute of Nuclear Physics, Novosibirsk, Russia

The two codes for electron gun and collector simulation developed at BINP are described. The SAM code is based on the boundary integral equations method. The SUPERSAM code is based on the finite elements method. The codes are well tested on the problem of creation of high power RF source units. For the purpose of electron cooling system design new features were added to the codes.

Key words: electron gun; collector; electron cooling.

1 Introduction

At present time the two codes SAM [1] and SUPERSAM [2] for simulation of axisymmetric DC electron guns and collectors have been developed and are actively used at INP. The first version of SAM code was appeared at 1986. The SAM code is based on the method of boundary integral equations. The SUPERSAM code was developed at 1991 and is based on the finite elements method. For the purpose of electron cooling system design the model of particle emission from the cathode with non-orthogonal magnetic field was added to codes. The possibility of transverse temperature calculation was added to SAM code. At present time there are versions of codes for PC/DOS and VAX/VMS.

2 SAM code

The SAM code was developed for calculation of DC electron guns and of elements of electron optic systems with the axial symmetry. SAM is a package of computer codes which permit to solve the following problems:

- Calculation of high-voltage insulators and other electrostatic systems;

Preprint submitted to Elsevier Preprint *27 March 1997*

- Calculation of magnetic systems with DC coils, permanent magnets and ferromagnetics (without saturation effects);
- Calculation of electron guns and electron optic systems.
- Calculation of electric and magnetic fields in the system with small distortion of axial symmetry without space charge effects.

Calculation of electrostatic and linear magnetostatic problems is based on the boundary integral equations method with three-order spline interpolation of the boundary solutions. The main advantage of this method is that electric fields are calculated with the same accuracy as potentials because the analytical derivation of integral equation kernel is used.

To describe the beam dynamics in the gun the quasilaminar current tubes model is used. The space charge and beam current distribution are described using a set of meshes with rectangular cells in the cylindrical coordinates covering only the expected area of the beam particle motion.

The following methods are used to increase the accuracy of calculation:

- An analytical separation of the kernel singularity.
- An analytical separation of the solution singularities on the electrode, dielectric and magnetic edges and in the points where dielectric joints to the metal is also performed. The power of singularity in the last case is determined automatically.
- For calculation of scattered magnetic field with good accuracy the Tozony regularization is used.
- The mesh dimensions are chosen to be matched with the beam envelope. The current tubes have the finite section, which varies with the change of the beam radius.

The good illustration of SAM possibilities is simulation and design of magnetic system and electron guns of the high-power 7 GHz Magnicon amplifier [3]. DC power of the electron beam is about 100 MW. One of the Magnicon design problem which was solved with SAM code is to form and transfer through magnetic biasing system an electron beam with diameter not greater than 3 mm, what is necessary for the maximum efficiency obtaining. The calculated and measured data are presented in the Table 1.

A high voltage diode gun on the basis of 120 mm diameter oxide cathode is used in the Magnicon as an electron injector. The main problem of the electron gun design is to receive a maximum beam area convergence (more than 1000) and minimum value of electric field on the focusing electrode (vacuum breakdown). The geometry of the gun and calculation results are shown on the Figure 1.

Table 1
Design and measured parameters of electron source for X-band Magnicon.

	calculations	measurements
Beam voltage[kV]	430	436
Beam current[A]	233	236
Microperveance	.83	.82
Electrostatic beam area compression	1500	1000
Beam diameter[mm]	2.2	2.5
Beam area compression	2900	2300

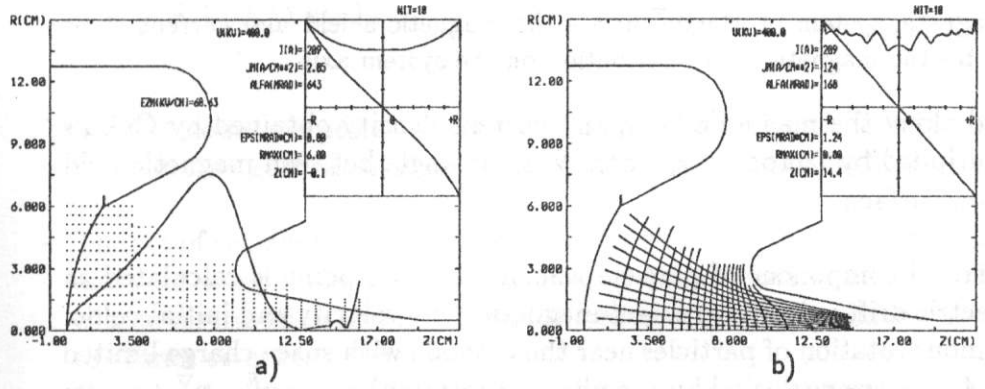

Fig. 1. Electron gun of Magnicon: a - gun geometry, space mesh and axis field distribution; b - results of simulation.

The SAM code was also used for design of Magnicon magnetic system. The geometry of the system and the results of simulations and experiments are shown on the Figure 2. One can see that Tozony regularization significantly improves accuracy of calculation.

The two problems of electron gun simulation arise during electron cooling system design:

- calculation of emission from cathode with arbitrary shape immersed to magnetic field;
- calculation of Larmour rotation temperature and drift motion temperature of particles in the beam.

To solve the first problem the following start model is used in SAM code: the start conditions on the gap δ from the cathode (at start point) are calculated in the adiabatic approximation $\omega_{L0} \cdot t_0 \gg 1$, where $\omega_{L0} = \frac{e \cdot H_0}{mc}$ is the Larmour frequency and t_0 is the transit time of electron on the gap δ. This condition may be rewritten in the form $\delta \gg R_{L0}$, where $R_{L0} = \frac{v_0}{\omega_{L0}}$ is the full Larmour radius of particle and v_0 is the particle velocity at start point. In this approximation we assume the projection of particle start velocity to the plane (r,z)

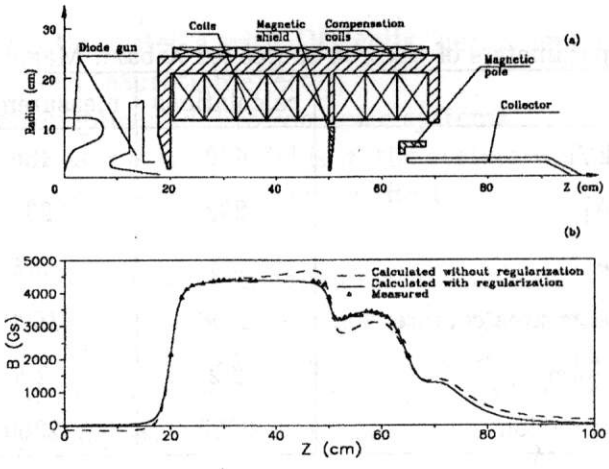

Fig. 2. Magnetic system of Magnicon: a - the magnetic shield and current wires geometry; b - the magnetic field distribution on the system axis.

is oriented along the magnetic field, and current density obtained by Child's law is multiplied by factor $\sin\theta$, where θ is the angle between magnetic field and emitter surface.

The azimuthal component of particle velocity at start point is calculated as sum of electric drift velocity, gradient magnetic drift velocity and initial velocity of Larmour rotation of particles near the cathode with space charge limited emission [4] (we are neglected by the phase of rotation) $v_{\theta 0} = v_d^E + v_d^\nabla + v_L$ or:

$$v_{\theta 0} = c \cdot \frac{\vec{E}_0 \times \vec{H}_0}{H_0^2} + \frac{mc(2v_{\|0}^2 + v_{\perp 0}^2)}{2eH_0^3} \cdot (\vec{H}_0 \times \vec{\nabla} H_0) + \frac{4\pi j_0 c}{\omega_{L0} H_0} \cdot \frac{\vec{E}_0 \times \vec{H}_0}{E_0 H_0},$$

where j_0 is the current density on the cathode.

The new useful possibility of SAM is the calculation of transverse temperature of the beam particle in the gun. In this case the following procedure is used. At any moment we can consider transverse to magnetic field component of velocity as a sum of the following components: $\vec{v}_\perp = \vec{v}_L + \vec{v}_d^E + \vec{v}_d^\nabla$, where $\vec{v}_L$ is the local value of the Larmour rotation velocity, $\vec{v}_d^E$ and $\vec{v}_d^\nabla$ are local values of drift velocity and gradient magnetic drift velocity (see previous formula). Knowing calculated velocities $\vec{v}_\perp$ and $\vec{v}_d^E$ and $\vec{v}_d^\nabla$ we can extract $\vec{v}_L$. The temperatures of Larmour rotation and drift motion are calculated as $T_L = mv_L^2/2$ and $T_d = m\left(v_d^E + v_d^\nabla\right)^2/2$.

On the Figure 3 the results of calculation of the gun for GSI SIS electron cooling device which was developed in group of A.Sharapa are shown. The voltages on electrodes are 6 and 35 KV, the beam current is 0.824 A, magnetic field is 1000 Gs. For this variant the output temperatures of Larmour rotation and drift rotation are equal to $3 \cdot 10^{-3}$ eV and $2.8 \cdot 10^{-2}$ eV correspondingly.

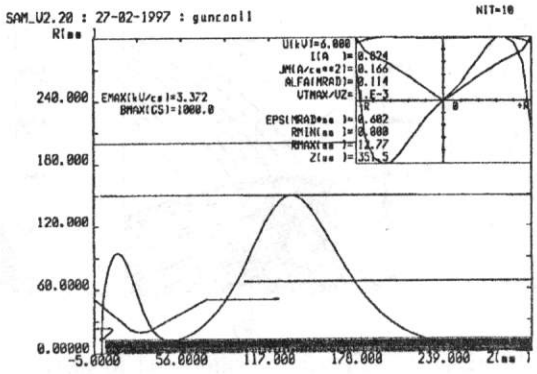

Fig. 3. The results of simulation of GSI SIS electron cooling device gun.

3 SUPERSAM code

The SAM code is a power tool for electron gun simulation, but the accuracy of the electron gun calculation by SAM is limited by two factors:

- The set of rectangular meshes is not matched well with the spherical cathode and with complicated shape beam envelope, that provides errors in the space charge distribution and fields near the cathode and it is difficult to describe the inner structure of beam.
- The quasilaminar model of current tubes permits to calculate only the beam with $|V_r/V_z| < 1$.

To avoid these difficulties and increase the accuracy of evaluation we have made a new computer code SUPERSAM, which used FEM. The SUPERSAM code is based on eight-nodes second order isoparametric elements. The current pipe model is used to describe the space charge effects. The charge density of current pipes is expanded on finite-element basic functions to obtain the smooth charge distribution over the beam. This model permits to calculate collectors with reflected particle trajectories. External magnetic field can be defined on axis and then expanded to FEM mesh by paraxial approximation or it is possible to transfer magnetic field from SAM to SUPERSAM directly.

The use of FEM with curve mesh for the evaluation of axisymmetric electron guns has the advantage over FDM and the boundary integral equations method, because the finite elements mesh permits:

- to describe better the curve surfaces of gun electrodes, particular the cathode surface;
- to investigate non-pierce optics and effects of cathode edges.
- to conform with the beam envelope, which reduces the calculation aberration on the edge of the beam. It is especially important for evaluation of the guns with a high beam area compression.

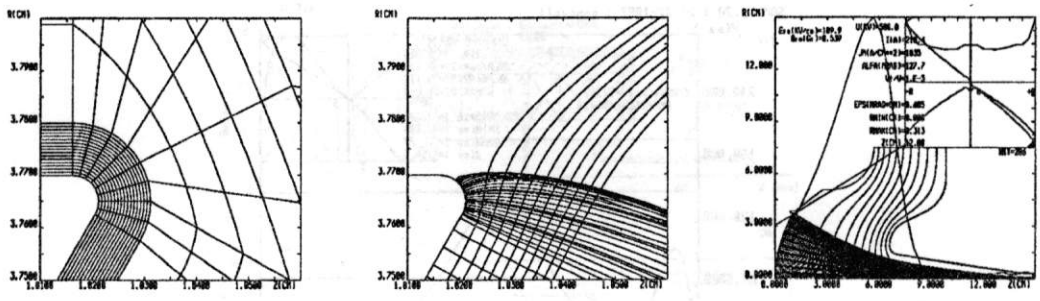

Fig. 4. The result of simulation of emission from cathode edge for Magnicon gun: a - finite element mesh near the cathode edge, b - particle trajectories and equipotentials, c - total view of gun.

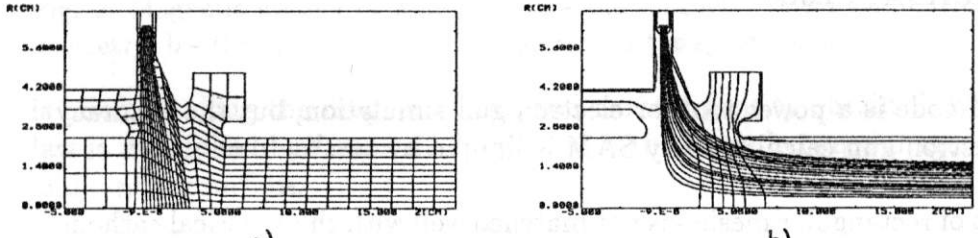

Fig. 5. The result of simulation of the hollow cathode gun for electron cooling device without toroids: a - finite element mesh; b - equipotentials and trajectories of particles.

The features of SUPERSAM code permitted to use it for optimization of the electron gun for Magnicon. The following examples shows the possibility to investigate the influence of emission from the cathode edge. The first picture on the Figure 4 shows the finite element mesh near the cathode edge, the second one shows the behavior of beam near the cathode edge, the last picture shows the whole view of the gun.

For the purpose of electron cooling system design the following modification of SUPERSAM code was made. To describe correctly the emission from cathode with magnetic field the new emission model was added to code. Accordingly [5], we used the model of plane diode with homogeneous magnetic field with angle θ to emitter surface. This model permits to calculate the gun with cathode of arbitrary shape immersed to the arbitrary magnetic field. The emission model which is used in SAM is the particular case of this model.

On the Figure 5 the result of simulation of hollow cathode gun for electron cooling device without toroids (bending magnets) is present. This gun was designed by the group of A.Sharapa. The voltage of electrodes is 1 and 8 kV, the beam current is about 0.2 A.

The SUPERSAM code can be also used for precise collector simulations. The curvilinear finite element mesh permits to describe the complicated collector

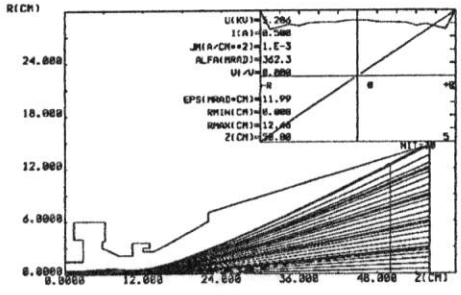

Fig. 6. The result of simulation of the collector for FNAL recirculation experiment.

shape with good accuracy. The used current pipe model permits to calculate the reflected trajectories. One of the examples is the collector for FNAL recirculation experiment, which was designed by the group of A.Sharapa. The beam current is 0.5 A, the initial beam voltage is 50 kV, the beam voltage on the collector is 5 kV. The result of simulation of one variant is shown on Figure 6.

4 Conclusion

The two codes for calculation of axisymmetric DC electron guns and collectors have been developed in INP. The codes use different numerical methods which permit to use these codes for solution of the different problems where each method has own advantages. These codes are enough power tools for electron gun simulation and are actively and successfully used in INP.

References

[1] B.M.Fomel, M.A.Tiunov, V.P.Yakovlev, SAM - an interactive code for evaluation of electron guns (Budker INP 96-11)

[2] D.G.Myakishev, M.A.Tiunov, V.P.Yakovlev, Code SuperSAM for calculation of electron guns with high beam area convergence. *Proc.XV ICHEA*(Hamburg, 1992), Int.J.Mod.Phys. A (Proc. Suppl.) 2B (1993) Volume II, pp.915-917.

[3] Y.V.Baryshev et al., A 100 MW electron source with extremely high beam area compression. Nuclear Instruments & Methods in Physic Research A 340 (1994) 241-258.

[4] Д.Д. Рютов, Об угловых характеристиках электронного пучка, получаемого в бесфольговом диоде. Препринт ИЯФ 83-146, 1983

[5] В.А.Астрелин, И.А.Котельников, С.Л.Синицкий, Отрицательное дифференциальное сопротивление электронного диода в магнитном поле. Журнал технической физики, Т.59, в.4, 1989.